Simulating diluted bitumen spills in boreal lake limnocorrals - Part 1: Experimental design and responses of hydrocarbons, metals, and water quality parameters

Corresponding author: Jules Blais

Department of Biology

University of Ottawa

20 Marie-Curie

Ottawa, ON, Canada K1N 6N5,

Tel: +1 (613) 562-5800 ext. 6650

Email: jules.blais@uottawa.ca

Total Word Count (excluding abstract, captions, acknowledgements and references): 13968

Simulating diluted bitumen spills in boreal lake limnocorrals - Part 1: Experimental design and responses of hydrocarbons, metals, and water quality parameters

Jose Luis Rodriguez-Gil[1, 2, 5], Sawyer Stoyanovich[1], Mark L. Hanson[2], Bruce Hollebone[3], Diane M. Orihel[4], Vince Palace[5], Robert Faragher[3], Fatemeh S. Mirnaghi[3], Keval Shah[3], Zeyu Yang[3], Tyler Black[2], Jeffrey Cederwall[4], Johanna Mason[4], Samuel Patterson[4], Lauren Timlick[2], Jonathan Séguin[1], Jules M. Blais[1]

[1] Department of Biology, University of Ottawa, Ottawa, ON, Canada K1N 6N5

[2] Department of Environment and Geography, University of Manitoba, Winnipeg, MB, Canada R3T 2N2

[3] Emergencies Science and Technology Section, Environment and Climate Change Canada, Ottawa, ON, Canada K1V 1H2

[4] Department of Biology and School of Environmental Studies, Queen's University, Kingston, ON, Canada K7L 3N6

[5] International Institute for Sustainable Development - Experimental Lakes Area, Winnipeg, MB, Canada R3B 0T4

Type of manuscript: Original Article

Abstract

Large-scale, in-lake enclosures (limnocorrals) were used to simulate spills of diluted bitumen (dilbit) in a boreal lake. In this study we use these simulated spills, which covered a range of sizes (oil:water ratio) representative of the upper 25% of onshore crude oil spills in north America (2008-2019), to assess the fate of dilbit-derived hydrocarbons and metals as well as the impacts of the spills in standard water quality parameters. The systems were monitored over 70 days following the application of dilbit amounts ranging between 1.5 – 179.8 L into 10-m diameter, ~100 m^3 limnocorrals. The concentration of total petroleum hydrocarbons (TPH) in the water column increased rapidly over the first two weeks reaching a plateau that ranged between 200 µg/L and 2200 µg/L for the lowest and highest treatment respectively. The concentration of total polycyclic aromatic compounds (PACs) also increased over the first two weeks, prior to a slow decrease until day 70. The maximum measured concentrations in the highest treatment were 2858 ng/L for the sum of all 46 quantified PACs, 2716 ng/L for alkylated PACs and 154 ng/L for the 16 EPA priority PAHs. The concentrations of PACs in the sediment increased continuously over the study in the three highest treatments with maximum observed concentrations of 189 ng/g for ΣPAC_{46}, 169 ng/g for ΣPAC_{alk}. No significant treatment-related changes in the 16 EPA priority PAHs were observed in the sediment. Of the 25 metals quantified in the water column, only manganese, molybdenum, and vanadium displayed a significant treatment effect with increases of 280, 76 and 25% respectively in the total fraction. These results can help us understand and predict the fate of oil-derived contaminants following a spill and characterize the exposure of freshwater organisms living within them. These results should help inform the risk assessment of future dilbit transportation projects.

Keywords: ***Dilbit, Oil spill, PAH, Freshwater, Mesocosms, boreal lake.***

Abbreviations

CLWB – Cold Lake Winter Blend (diluted bitumen)

Dilbit – Diluted bitumen

FFC – Far-Field Control

GC-FID – Gas Chromatography Flame Ionization Detector

GC-MS – Gas Chromatography Mass Spectrometry

IISD-ELA– International Institute for Sustainable Development Experimental Lakes Area

NFC – Near-Field Control

PAC – Polycyclic Aromatic Compound

PTFE – Polytetrafluoroethylene

TPH – Total petroleum hydrocarbons

1 Introduction

Research on oil spills has traditionally been heavily weighted towards spills occurring in coastal and marine areas, and in particular those of traditional crude oils (Lee et al., 2015; Murray et al., 2018). Certainly marine transportation constitutes the main means of transborder movement of petroleum products and, historically, its nature (i.e. large tanker vessels) has often led to large volumes of oil spilled in a particular event (e.g. the Exxon Valdez, or Prestige) (Murray et al., 2018; Transport Canada, 2013). The Exxon Valdez oil spill in 1989 represented a turning point in our scientific understanding and regulatory approaches towards oil spills. Nevertheless, the majority of active oil production sites are landlocked and require some form of land-based transportation from production sites to refineries or marine transportation hubs for long-range shipment (Furchtgott-Roth and Green, 2013; IEA, 2018). Additionally, a reduced capacity for dilution (when compared to marine systems) and increased clean-up complexity can increase the vulnerability of onshore systems to an oil spill (Lee et al., 2015). Despite this, there is a paucity of research addressing the potential impacts of in-land oil spills and, in particular, spills on freshwater systems (Lee et al., 2015; NASEM, 2016).

Unconventional oils present different composition and physical properties than more commonly studied conventional crudes (Lee et al., 2015). These differences make our knowledge on the fate and environmental impacts of spills of conventional crudes not directly applicable to spills of unconventional products. This became clear in 2010 when the Enbridge Line 6B pipeline ruptured and spilled ~3 million L of diluted bitumen (dilbit), an unconventional oil, into the Talmadge Creek and Kalamazoo River, a Lake Michigan tributary (Kalamazoo River Trustees, 2015). The unique properties of the mixture and the high flow of the river caused a large portion of the oil to sink, rendering traditional recovery techniques ineffective. The result was a long and highly intrusive clean-up (Kalamazoo River Trustees, 2015; USEPA, 2016).

In recent years, multiple high-level reports have highlighted the need to increase of our preparedness for spills of unconventional oil products and, in particular, those taking place in-land and affecting freshwater aquatic systems (Crosby et al., 2013; Lee et al., 2015; NASEM, 2016). These reports also emphasized the need for research conducted under field conditions that can address the risk of these spills at the ecosystem level. Currently most of our understanding about oil spills comes from small-scale laboratory/tank studies or from post-spill damage assessments and monitoring of impacted sites, also known as “spills of opportunity”. Small-scale laboratory or tank studies are unable to replicate the

multitude of physical and biological factors affecting the fate and behaviour of oil in a real-world spill, nor are they able to assess its impacts at ecological scales or those resulting from indirect effects. On the other hand, data collected from actual spills often suffer from the lack of baseline or reference data needed to assess the nature and size of the effects caused by the spill. Furthermore, the quantity and quality of data collection at the onset of the spill and in the early hours and days after, is often limited by other priorities such as focus on containment and clean-up instead of research efforts (Gros et al., 2014). These research limitations have hampered our ability to understand and predict oil behaviour, fate, and effects in real aquatic environments in those early stages.

A growth in demand and higher oil prices in recent years has resulted in increased extraction and transportation of unconventional oil reserves (e.g. oil sands and oil shales), a trend that is expected to continue over the next decade (IEA, 2018). Canada is home to the third largest crude oil reserve in the world holding 10.3% of the global reserves (NRCAN, 2014). Most of this oil (97%) is found in the Alberta/Saskatchewan oil sands, which are estimated to hold 166.3 billion barrels of oil in the form of bitumen (NRCAN, 2014). Oil production in the oil sands area nearly doubled between 2010 and 2018 (CAAP, 2019). Transportation of this bitumen to upgraders, refineries, and marine transportation hubs requires an intricate network of land-based systems, which can include pipelines, railways, and roads. The high viscosity of the bitumen extracted from the oil sands makes it difficult to transport as extracted. In particular, it is too viscous to effectively flow through pipelines. In order to facilitate its handling, bitumen is often mixed with other lighter petroleum products, such as natural gas condensates to achieve target physical properties (e.g. a lower viscosity) (ECCC, 2013).

In addition to oil, Canada is also home to nearly two million freshwater lakes, which in some areas, such as the boreal region, can account for up to 20% of the surface area (Schertzer, 1997; Slota, 2013). With increasing rates of dilbit extraction, and a growing need to transport this oil to markets, the likelihood of a spill affecting one of these ecosystems will continue to increase over the next decade.

In this context, the “Boreal lake Oil Release Experiment by Additions to Limnocorrals” (BOREAL) project set to address some of these research needs. In particular our project aimed to specifically address four research priorities set in the Lee et al. (2015) report that calls for research to better understand the effects of oil spills in sensitive poorly understood areas, such as freshwaters; research at the population, community and ecosystem levels; controlled field research in different ecosystems and conditions and; research to be used in the update of risk assessment protocols. In order to directly address those research

needs, the BOREAL project took advantage of the opportunity provided by the IISD-Experimental Lakes Area (IISD-ELA), a unique facility in Northern Ontario (Canada) consisting of 58 boreal lakes set aside for scientific research and available for experimental manipulation. After a pilot study conducted in 2017 using small land-based microcosms (Cederwall et al., 2020; Stoyanovich et al., 2019), in the summer of 2018 we conducted a large-scale, in-lake limnocorral study that would simulate a series of variable-volume spills of dilbit (1.5 - 180 L) in a typical boreal lake ecosystem. These simulated spills were designed to represent a worst-case-scenario of a direct spill into a water body lasting 70 days with no clean-up or remediation techniques applied.

The specific objectives of this manuscript are: (1) to describe the experimental system and basic water quality parameters measured in the experimental limnocorrals throughout the study as well as any observed treatment effects on these measures; (2) to describe the temporal trends of major oil-derived hydrocarbon groups in the water column and sediment of the limnocorrals as well as their relationship with the amount of oil applied; and (3) to describe the temporal trends of oil-derived metals in the water column of the limnocorrals as well as their relationship with the amount of oil applied. A companion paper in this issue (Stoyanovich et al., submited) provides data on dilbit's physical fate and behaviour. These two publications are the first two of a series of BOREAL project-related articles with future work covering other aspects including detailed oil chemistry, fate modelling, ecological-level effects, fish toxicity, and contaminant bioaccumulation.

2 Materials and Methods

2.1. Field site, experimental limnocorrals, and environmental protection measures

Our experiment was carried out in Lake 260, one of 58 experimental lakes at the IISD – Experimental Lakes (IISD-ELA) Area near Kenora, Ontario (49°40′N, 93°44′W). Lake 260 is a typical Canadian Shield oligotrophic boreal lake. The lake has a surface area of 330,000 m^2, a volume of 2,000,000 m^3, a mean depth of 7 m, and a maximum depth of 16 m. Lake 260 has been the site of previous high-profile research on estrogens (Kidd et al., 2007; Kidd et al., 2014) from which it has been deemed completely recovered prior to the start of our study (Blanchfield et al., 2015). As a result of its active research past, an extensive dataset of baseline data was available for the lake.

A total of nine 10-m diameter, open-bottom enclosures (limnocorrals) were installed in a sheltered bay on the north-west shore of lake 260 (Figure 1). The limnocorrals consisted of a curtain of polypropylene

sheeting (woven Novathene®, Curry Industries, Winnipeg, Manitoba, Canada) which was suspended from a floating vinyl-wrapped Styrofoam decagonal ring (Dow, Midland, Michigan, USA) and sealed to the sediment. The limnocorral curtains were sealed to the bottom sediment with a double layer of sandbags sitting on top of a flare of limnocorral curtain to enable a full water seal from the lake. The sandbags were installed by a team of commercial divers to ensure proper placement and maximize the seal. The limnocorrals were installed at an average depth of 1.5 m (nominal volume of 117.8 m^3). Each limnocorral was outfitted with an external floating platform that provided a safe area to work, collect samples, and take measurements of limnological parameters. The formation of an oil slick and/or sheen was expected after treatment. In order to be able to collect samples and deploy instruments while minimizing equipment damage and fouling, extensive clean-up between sampling, and artificial disturbance of the oil, an oil slick-free section of the surface of the limnocorral was needed. To achieve this, a partition was installed that extended 30-cm deep from the water surface. This partition was constructed of the same polypropylene sheeting as the limnocorral walls and supported by a length of vinyl-wrapped Styrofoam, and it was installed between two non-consecutive vertices of the decagon (Figure 2). To provide additional shelter from the oil, the oil-free partition was placed in the south-east direction, which was chosen because it opposed the prevailing winds in the area. The placement of the floating platforms was chosen to match this oil-free partition.

With the same objective of facilitating sampling while minimizing artificial disturbance to the oil, each limnocorral was outfitted with a central sampling column consisting of a vertical 75-mm drinking-water quality PVC pipe attached to a concrete base (Figure 2). There were three 45-degree angle downward-facing y-connectors were installed at 30 cm below the water surface ("top"), mid-way through the water column (~0.75 m deep, "middle") and 30 cm above the sediment (~ 1.4 m deep, "bottom"). Individual lengths of 6-mm internal diameter high density polyethylene (HDPE) tubing were run from the sampling platform and through the bottom of each limnocorral to end at each of the three ports on the center sampling column. The downward-facing y-connectors helped reduce the likelihood of oil or other debris entered the tubing as they sunk into the sediment. An additional line of 9.5-mm linear low-density polyethylene (LLDPE) tubing (DeeTag Ltd., London, Ontario, Canada) was also run to the middle port to be used for zooplankton sampling. This line was outfitted with a funnel at its mouth to limit zooplankton avoidance and increase sampling efficacy. At the sampling dock, the end of all tubing runs was secured inside of a covered plastic container to minimize contamination. Tubing was labelled and colour-coded to

facilitate identification of the desired sampling depth. The three pieces of 6-mm HDPE tubing were connected to short lengths (~15 cm) of silicon tubing for their use with a peristaltic pump.

Each limnocorral was outfitted with a temperature and visible light intensity logger (HOBO Pendant MX, Onset, Bourne, MA, USA) secured on the south-facing side of the sampling column at a depth of 60 cm. A number of additional implements or devices were installed or deployed in the limnocorrals for specific endpoints (e.g., time-lapse cameras, insect emergence traps, periphyton strips). These will be described in detail in future publications dealing with these aspects of the study.

Immediately after the limnocorral curtains were sealed to the sediment (June 31st, 2018), and prior to oil addition (July 20th, 2028), any trapped fish inside of the limnocorrals were removed via minnow cage traps, seine nets, and gill nets to ensure the limnocorrals began the experiment with a similar biological composition. A known number of fish were added on 11th July (Day 21).

The safety of our team and the surrounding environment were a top priority during the study. Environmental protection and health and safety plans were specifically developed for this project and are available upon request. As part of the environmental protection plan a number of layers of protection were implemented to minimize the likelihood of an accidental oil release from the experimental limnocorrals into the surrounding lake and downstream environments. The limnocorrals provided a first layer of protection. As a secondary containment, the limnocorrals were surrounded by containment floating boom. A boat gate, which remained closed except for when in use, allowed for boat access to the limnocorral area. Additional sections of floating containment boom were installed in the northern section of the lake to protect a lake trout sensitive spawning area, as well as the outflows of the lake in the unlikely event of a dilbit release bypassing the previous two barriers. An underflow dam was also installed in the stream serving as outflow of the lake as a fourth level of containment.

The work conducted for this project was approved by the IISD-ELA Research Advisory Board and the Ontario Ministry of the Environment and Climate Change under the provisions of specific regulation concerning work at IISD-ELA. Additional permits and insurance were acquired as required.

2.2. Meteorological data collection

A portable weather station (Campbell scientific, CR300 series) was installed in one of the islands surrounding the NW bay of Lake 260, immediately south-east from the limnocorrals (Figure 1). The portable station recorded, temperature, wind direction, wind speed, precipitation, and relative humidity.

The IISD-ELA is also the site of an Environment and Climate Change Canada's meteorological stations located ~5 km from the limnocorrals; this station provided additional meteorological data. Data from an extended network of rain gauges spread through the IISD-ELA were also used. The water level at the lake was also monitored hourly with a calibrated logger.

2.3. Experimental design and selection of treatment levels

Our study aimed to assess the fate, behaviour, and effects of dilbit spills in freshwater aquatic systems. In order to be able to better understand the underlying phenomena driving our observations, as well as to provide data that was applicable to spills of variable size, a regression design with seven treatments evenly distributed in a logarithmic space was chosen for this study (Liber et al., 1992). Two additional limnocorrals were used as controls. One of these controls was placed within the boomed area among the treated limnocorrals (Near-Field Control, NFC), while the other was placed outside the boomed area, approximately 50 m north in the same bay (Far-Field Control). The FFC, spatially separated from the other limnocorrals, would serve to inform on aspects related to any potential aerial deposition of oil-derived contaminants. With the exception of the FFC, the rest of the treatments were randomly allocated to the 8 limnocorrals located inside the boomed area.

The volume of oil applied to the treated limnocorrals was selected based on practical considerations (such as oil availability) guided by empirical data on crude oil spills in North America during the 2008-2019 period. Spill data were compiled from the U.S. Department of Transportation (USDOT, 2019) and the National Energy Board of Canada (NEB, 2019). Data from both databases was merged and filtered for the specified time range, and for information regarding onshore spills of crude oil. The US data include information on whether surface water was impacted during the spill. Analysis of the data considering all onshore crude oil spills or just those causing an impact on surface water (only US data) were conducted and compared.

Cumulative probability distributions (SI Figure 1) were generated for the compiled spill volume data by fitting a lognormal distribution as described in (Rodríguez-Gil et al., 2018) via maximum likelihood estimation (MLE) with the fitdist function in the R package fitdistrplus (Delignette-Muller and Dutang, 2015; R Development Core Team, 2020). The fitdist function calculates the probability plotting position using Hazen's rule, with probability points of the empirical distribution calculated as (1:n - 0.5)/n, where n is the total number of data points (Delignette-Muller and Dutang, 2015). Table 1 summarizes the upper centiles of the distributions of each dataset.

To assist with the experimental design, the oil-to-water ratios (v:v) that would be expected if these spills occurred in a lake similar to Lake 260 (~2 million m^3) were calculated. From these, 7 nominal oil:water ratios (equally spaced in a logarithmic scale) were selected spanning from 1:100,000 to 1:1,000 (oil:water, v:v). The nominal volumes of dilbit required to achieve these oil-to-water ratios in the limnocorrals, as well as final applied volumes and resulting final oil-to-water ratios (on day 0) are presented on Table 2.

2.4. Product selection and oil application

Cold Lake Winter Blend (CLWB) dilbit was selected for this study based on its production and transport amounts, being one of the most transported dilbits by pipeline in Canada (ECCC, 2013). The winter blend was selected due to its higher percent of diluent content (ECCC, 2013), which was considered a worst-case-scenario from the point of view of our toxicity endpoints due to the known acute toxicity of diluent components.

CLWB was added to the water's surface of the treated limnocorrals on June 20th, 2018 (hereafter, Day 0) between 8:30am and 10:00am CST. Detailed description of the application procedures is presented in Shah et al. (2019). Briefly, CLWB was pumped from a boat into the surface of the treated limnocorrals using a diaphragm pump at a rate of approximately 7.5 L min^{-1} through 127 mm-diameter tubing. Cans, hoses, pumps, and other items used for the application of the oil to each limnocorral were weighed before and after addition to determine the mass of dilbit added. We then estimated spill volumes from the mass of CLWB added and its density measured at 15 ºC (0.9215 g mL^{-1}).

2.5. Limnocorral volume and water exchange determinations

Tritium, in the form of tritiated water, was used as a tracer to determine the initial volume of the limnocorrals as well as the characterization of any possible water exchange between the limnocorrals and the lake. On June 14th, 2018 (6 days prior to oil application) a spike of 92,500,000 Bq of Tritium (10 mL of a 925 x 10^6 Bq L^{-1} solution of tritiated water in distilled water) was added to each limnocorral. This concentration was chosen to maximize our ability to quantify the tracer for the whole duration of the study based on expected losses and the limit of detection of the analytical method. The initial tritium activity concentrations in the limnocorrals were ~7 times lower than the current Canadian Quality Guideline value for drinking water of 7000 Bq L^{-1} (Health Canada, 2007), and were not expected to cause any biological effects in the limnocorrals.

Samples were collected following the sampling schedule in Figure 3. A total of 50 mL of water were collected in a 50-mL polypropylene centrifuge tube via peristaltic pump (Spectra Field-Pro, flowrate ~1 L min^{-1}) from the middle port of the central sampling structure (depth ~0.75) of each limnocorral. Samples were stored in the dark until analysis at the University of Ottawa A. E. Lalonde AMS Laboratory. Samples were mixed with scintillation cocktail and the tritium activity was measured by liquid scintillation counting of the decay events in a low-background Quantulus liquid scintillation counter.

In order to determine the initial volume of the limnocorrals at the time of tritium application, a linear regression was fitted to the activity values of the three first sampling times (day 3, 7, and 9 post tritium application). The intercept of this regression (activity at the time of tritium application) was corrected to account for a precipitation event (27-mm) that occurred in the morning of June 15th and resulted in additional dilution. No other precipitation was registered during the first nine days after tritium application. The resulting tritium activity was used to determine the volume of water in the limnocorral from the known activity of the initial spike.

The rate of water exchange between the limnocorrals and the lake was determined by comparison of the measured tritium activity throughout the study to the theoretical value that would be expected from a theoretical mass balance of the system if the only inputs and losses of tritium would come from precipitation, evaporation, and isotopic decay. Similar approaches have been followed in previous limnocorrals work carried out at the IISD-ELA (Orihel et al., 2006). Detailed description of the approach used is provided in the supplemental Information (SI Section 1). Briefly, the daily theoretical tritium activity for each limnocorral was subtracted from the measured tritium activity to isolate the change solely due to water exchange (e.g., water exchange through gaps in the limnocorral sandbag seal, perforations in the curtain, and/or water diffusion through the sediment bed). Once the water exchange losses were isolated, these values were fit to a first order exponential decay model to determine the rate of water exchange on each limnocorral.

2.6. Sample collection

The limnocorrals were actively monitored from the moment the curtains were sealed (June 31st, 2018, day -20), through August 29th, 2018 (day 70). The schedule of samples collected is presented in Figure 3. This list only represents samples collected during the BOREAL project which were used to produce the data presented in this paper. Many more samples and matrices (including biological samples) were collected but are the focus of subsequent publications.

2.6.1. *Water samples*

All water samples were collected from the centre of each limnocorral through the central sampling structure. Sampling followed the schedule in Figure 3.

Water for basic water quality was collected from the middle depth (~0.75 m) via peristaltic pump (Spectra Field-Pro, flow rate ~1 L min^{-1}) into a 4-L amber bottle after rinsing three times with water from the limnocorral.

Water samples for hydrocarbon analysis were collected from the top and bottom sampling ports (depth of 0.3 m and 1.2 m) via peristaltic pump (Spectra Field-Pro, flow rate ~1 L min^{-1}). After discarding ~1L of limnocorral water to rinse the tubing, water was collected into a pre-weighted 1-L certified clean amber glass bottle (Thermo Fisher, Mississauga, Ontario, Canada) with PTFE caps. Water samples were collected with no headspace to prevent the loss of volatile compounds. Samples for metals were collected on the same dates, but from the middle sampling port (~0.75 m) and into a 50-mL polypropylene centrifuge tube. For the purposes of the samples intended for hydrocarbon analysis 4 limnocorrals were selected for intensive sampling. These were the NFC and the 1.5, 18.1, and 179.8 L treatments (lowest, medium, and highest treatment). Samples from these limnocorrals were collected in triplicate in order to assess the variability within limnocorrals as well as whether there were any differences in concentration between the surface (top sampling port, ~ 30 cm depth) and the bottom (sampling port ~ 1.4 m depth) of the water column.

Samples for water-column metal analysis were collected from a subset of 4 limnocorrals (FFC, 1.5 L, 18.1 L and 179.8 L).

2.6.2. *Sediment samples*

Our ability to sample the sediment of the limnocorrals following traditional methods (e.g., sediment coring or Ekman/ponar samplers) was limited due to our need to limit the artificial disturbance of the oil slick/sheen layer as well as to limit resuspension of sediment particulate into the water column, which could have artificially induced oil sinking. Additionally, we needed a method to allow for measuring the partitioning of oil-derived (petrogenic) hydrocarbons from the water column into the sediment with minimal contamination from sinking oil.

With these limitations in mind, we chose the sediment jar method. Prior to oil addition, a series of 250-mL pre-cleaned glass jars were filled with sediment collected from the bottom of each limnocorral. In

order to minimize contamination from sinking oil, we deployed jars on the sediment surface of each limnocorral immediately under the oil-free partition. Individual jars were then retrieved from the bottom of each limnocorral through the partition at -1, 1, 2, 8, 15, 22, 28, 42, and 70-days post dilbit addition (Figure 3). Upon retrieval, the jars were capped and stored refrigerated in the dark until analysis.

2.7. Analytical methods

2.7.1. Hydrocarbons

The collected water and sediment samples were analysed to determine the concentrations of Total Petroleum Hydrocarbons (TPH) (largely n-C9 through n-C40), as well as 46 individual Polycyclic Aromatic Compounds (PACs) (including 25 alkylated PAC homologues and other unsubstituted PACs). We report data on the sum of the 46 individual PACs (ΣPAC_{46}), the sum of the alkylated PACs (ΣPAC_{alk}), as well as the sum of the 16 EPA priority Polycyclic Aromatic Hydrocarbons (ΣPAH_{16}). SI Table 1 lists all the individual compounds included on each of these summary groups. Method reporting limits are provided in SI Table 2.

Water samples for hydrocarbon analysis were processed on the day of collection. Sample extraction methodologies are described in detail in Shah et al. (2019). Briefly, samples were spiked with surrogates (20 ppm o-terphenyl, 20 ppm C24D50 and 1ppm deuterated PAHs - manufactured by SPEX CertiPrep Labs, NJ, USA) and extracted with 50 mL of dichloromethane (DCM) for 16 hours at 8 rpm on a roller apparatus (DWK Life Sciences Wheaton™ Bottom-Drive R2P 2.0 Roller Apparatus). The extracts were then removed and dried by passage through sodium sulfate and stored in the dark in 125 mL pre-cleaned amber glass jars at 2 ºC. Most samples were analysed at the Oil Research Laboratory of the Emergencies Science and Technology Section -Environment and Climate Change Canada (ECCC), with a subset of the samples analysed at the Fisheries and Oceans Canada Specialized Lab Analysis. Inter-laboratory tests were carried out in advance of this study to ensure comparability of analytical results. No meaningful differences were found between test samples provided to both laboratories and as such, comparison of data from either source was deemed appropriate. Upon arrival at the analytical laboratories, extracts were concentrated via rotary evaporation, solvent exchanged to hexane and then evaporated to a volume of 1 – 2 mL prior to instrumental analysis. Extracts for PAC analysis went through an additional step of silica column fractionation. Details on the column fractionation and instrumental methods are provided in SI

section 2. Triplicate lab blanks were run on ultra-pure Milli-Q water and PAH concentrations were blank corrected.

Sediment samples were stored in the dark at -4°C until arrival at the analytical laboratory at ECCC. Once in the analytical laboratory, the top 5 cm of the sediments in the jars were removed, homogenized and dried with sodium sulphate, spiked with deuterated PAH surrogate and then Soxhlet extracted with DCM for 16 hours. The extracts were then treated the same way as the water samples following the instrumental methods described in SI section 2.

2.7.2. Metals

A total of 25 metals were measured in a subset of water-column samples from 4 limnocorrals (FFC, 1.5 L, 18.1 L and 179.8 L). These metals were quantified in the total (unfiltered) and dissolved (filtered) fractions. On the day of collection 15 mL of the 50 mL collected for metal analysis was filtered using a 0.45 µm digiFILTER™ (SCP Science, Clark Graham Baie D'Urfé, Quebec) for dissolved metal analysis while the remaining water sample (35 mL) was designated for total metals. Samples were preserved using 70% nitric acid (1% of total volume) after filtering and stored at 4 °C. Samples were submitted to the Geochemistry Laboratory at the University of Ottawa for analysis using ICP-MS.

2.7.3. Basic water quality

Physicochemical parameters (pH, temperature, dissolved oxygen, and conductivity) were measured on-site using a hand-held probe (HQ Series probe, Hach, Loveland, CO). A total of 25 water quality parameters (NH_4^+, NO_3^-, NO_2^-, total dissolved nitrogen, total dissolved phosphorus, particulate phosphorus, suspended carbon, suspended nitrogen, dissolved inorganic carbon, dissolved organic carbon, major anions and cations, alkalinity, soluble reactive silica, and turbidity) were analysed by the IISD-ELA chemical analysis lab following standard methodologies described in Stainton et al. (1977) . Sample processing and preservation was carried out on the day of collection, and water samples requiring suspended and dissolved fractions were filtered through pre-ashed Whatman GF/C glass microfiber filters.

2.8. Data and statistical analysis

All data were processed in R version 4.0.2 (R Development Core Team, 2020) employing tidy data approaches (Wickham, 2014; Wickham et al., 2019). Figures were created using ggplot2 (Wickham, 2016).

A regression design was chosen for this study to facilitate the analysis of treatment effects. For this purpose, general linear models were fit to explore the relationship between the different measured variables, the volume of oil applied, and time as well as the interaction between time and oil volume. For this, only data from samples collected after the oil application were considered. In addition to this complete model, individual regressions between each parameter and the volume of oil applied were fit for each individual sampling day. Due to the spacing of the treatment levels (equally spaced in a logarithmic space) these daily regressions were fit using the log of the volume of oil applied. Control treatments were not included in these daily regressions. Compliance with the required assumptions was accomplished visually by inspecting the residuals of the model.

Because only three treatments plus a control were considered for the quantification of metals in the water column, a regression approach was considered inappropriate their statistical analysis. For this endpoint, treatment effects were assessed using analyses of variance (ANOVA) followed by a Tukey's HSD (honestly significant difference).

3 Results and discussion

3.1. Weather data, limnocorral volume and water exchange determinations

A summary of weather parameters measured at the experimental site over the study period is provided in SI Table 3. The full temporal progression of these variables is presented in SI Figures 2 and 3.

Limnocorral volumes estimated from the added spike of tritiated water ranged from 90.7 to 106.5 m^3 (Table 2). From these limnocorral volumes and the actual amount of oil applied, the final oil:water ratios in the limnocorrals (on day 0) ranged from 1:71,353 to 1:505 (oil:water, v:v). These ratios would be equivalent to hypothetical spill sizes from 28 to 3,963 m^3 of dilbit, would they have occurred on a generic boreal lake with a volume of 2 million m^3 (same size as L260). This would cover a range of spills between the 73rd and 9th centile of the distribution of on-shore pipeline crude oil spills (2008-2019) for those causing an impact on surface waters (94th – 99th centiles for all on-shore spills) (SI Figure 1). For comparison, the Kalamazoo River event (the largest on-shore spill in North America in the studied 2008-

2019 range that resulted in impacts to surface waters) spilled 3,275 m^3 (USDOT, 2019). Our study, thus, covered the upper ¼ of all recent spill scenarios, including the worst-case-scenario.

As part of the theoretical tritium model, a water budget was conducted for each limnocorral using precipitation and evaporation data. Based on this water budget 15.8 m^3 of water were loss to evaporation from each limnocorral, during the study, an average of 16% of the limnocorral volume. This estimate is consistent with a cumulative 177 mm drop in lake level observed over the duration of the study (SI Figure 2, bottom panel) (due to low precipitation in the summer of 2018, the lake stopped receiving inflows and became disconnected from its surface outflows, making evaporation the driving mechanism of volume change over most of the study period).

After installation, the integrity of the limnocorrals and their seal to the sediment was visually assessed, and structural checks were carried out throughout the study. No gaps, ruptures, or holes were detected at any point during the study. The concentration of tritium in the limnocorrals continued to be monitored throughout the study to determine any possible water exchange between the limnocorrals and the lake. Our results show discrepancies between the theoretical (SI Figure 4) and measured (SI Figure 5) tritium levels in all limnocorrals, but to varying degrees. Table 3 summarizes the loss rates of tritium due to water exchange with the lake (k_{leak}). The estimated half-life of tritium in the limnocorral (the portion due to exchange with the lake only) is also presented, providing a clear representation of the rate at which this exchange was taking place. This table is extended in SI table 4

While the loss rates are generally similar among limnocorrals, three limnocorral, namely the 18.1 and 81.8 L treatments and to a lesser extent the FFC, showed higher exchange rates, with half-life values for the loss of tritium due to exchange as low as 20 days (18.1L treatment). At this rate, a one-half of the water contained in the limnocorral could have been exchanged ~ 4 times over the duration of the study.

3.2. Hydrocarbons in the water column

3.2.1. Total petroleum hydrocarbons

Total petroleum hydrocarbon concentrations (TPHs) were not statistically different between samples collected from each of the two sampling ports (top and bottom) in each of the four intensive limnocorrals (SI Table 5), suggesting the water columns were fully mixed throughout the study. We therefore treated samples from either depth as replicates. A clear treatment-dependent increase in TPH concentration is observed (Figure 4 panel a), starting after oil application and continuing for a number of weeks after

448 which concentrations reached a maximum that remained relatively constant for the duration of the study.
449 The treatment-dependent nature of this relationship is clearly displayed in SI figure 6. SI figure 6 also
450 helps highlight some aspects of the dynamics of the concentration change. Initially, TPH levels in all
451 treated limnocorrals increased to their respective maximum levels, peaking at around day 15. After that,
452 the lower treatments started displaying a slow decrease in TPH levels, while the highest treatments
453 remained at the same level or showed small increases (179.8 L treatment). This behaviour resulted in a
454 stronger relationship between TPH and treatment as the study progressed. It is also obvious from this
455 figure how the 18.1L limnocorral, which had the highest water exchange rate with the lake, recurrently
456 displayed lower TPH levels than what would be expected based on the observed regression. To a lesser
457 extent, the 81.8L treatment, which had the second largest water exchange rate followed this trend. A
458 summary of the parameters of each of these sampling-day-specific regressions are provided in SI Table 6.
459 Figure 4 panel b presents a surface plot of the linear regression of TPH concentration against time and the
460 volume of oil applied (as well as their interaction) (a summary of the model fit is presented in SI Table 7).
461 The 18.1 L and 81. 8L treatments were excluded when fitting this model. This figure facilitates the
462 estimation of the TPH concentration that would be expected to occur in the water column after a dilbit
463 spill of a particular size and a certain spill duration. Maximum levels found ranged between 200 µg/l for
464 the 1.5L treatment and 2200 µg/L in the 179.8 L treatment, with background levels around 50 µg/L.
465 These results are comparable to what we observed in our 2017 mesocosm pilot study (Cederwall et al.,
466 2020; Stoyanovich et al., 2019) where exposures to CLB-W at 1:8000 and 1:800 oil:water ratios resulted
467 in maximum TPH levels of 293 and 1,191 µg/L respectively after 11 days.

468 The observed concentrations are well within the ranges reported by Lee et al. (2015) for concentrations of
469 TPHs able to cause effects in freshwater organisms, where physiological effects are observed in fish
470 between 5 and 200 µg/L, embryotoxic effects between 100 and 1000 µg/L and finally fish mortality is
471 reported in the range between 70 and 11,000 µg/L. Based on these reported ranges, any of the above-
472 listed effects could be expected in our limnocorrals. While these ranges are informative, the specific
473 toxicological profile would depend on the specific composition of that TPH fraction. The polycyclic
474 aromatic compounds (PACs) are presented in the next section, and detailed analysis of the oil-derived
475 hydrocarbons will be provided in upcoming publications, some which will also analyse the effects of the
476 observed exposures on specific biological receptors as well as the system as a whole. As part of the
477 response to the Enbridge Line 6B spill into the Kalamazoo river, the US EPA measured TPH (TPH by
478 GC, Extended range) in the water-column between July 31st, and August 31st 2010 (EPA, 2010).

Maximum concentrations of TPH along the Talmadge Creek, the Kalamazoo River, and Morrow Lake were 850 µg/L with only 7% of the samples being above the limit of detection (100 µg/L). The average TPH concentration for all quantified samples was 568 µg/L. In our study, concentrations above 500 µg/L were only reached in the three highest treatments, around day 7. While the 42.4 L and 81.8L treatments plateaued around 700 g/L, the 2200 µg/L reached in the 179.8L is higher than those observed during the Kalamazoo spill, despite similar oil:water ratios between both scenarios. The higher levels observed in our study are not unexpected, given the extended period of exposure without any clean-up, as well as the lentic nature of our experimental system.

Another relevant comparison is that of the TPH concentrations measured in this study to concentrations previously reported in water-accommodated fractions (WAFs) of various dilbits prepared for laboratory toxicity studies. Madison et al. (2015) reported TPH concentrations (by fluorescence) of ~3,500 µg/L in a 1/3 dilution of a 1:9 oil:water WAF of Access Western Blend (AWB) dilbit, with tested concentrations as low as 100 µg/L in their lowest dilution of the WAF. Slightly lower values are reported in Madison et al. (2017) ranging between 5 - 374 µg/L for a 1/30 and 1/3 dilution, respectively, of a similarly prepared WAF of CLB. Following the same methodologies as the previous two studies, Alsaadi et al. (2018) reported TPH concentrations of 2895 and 2174 µg/L for 1/3 dilutions of 1:9 WAFs of AWB and CLB respectively. Also following similar methodologies Madison et al. (2020) found TPH concentrations of ~200 and ~250 µg/L for 10% dilutions of 1:9 WAFs of AWB and CLB respectively. Philibert et al. (2016), measured TPH concentrations of 2760 µg/L in a 1:10 dilbit WAF, with the lowest tested dilution being a 10% (~276 µg/L). Robidoux et al. (2018) report TPH levels ~ 1000 µg/L and ~1200 µg/L for a 10% dilution of 10 g/L WAFs of AWB and CLB respectively. Finally, McDonnell et al. (2019) observed concentrations of 4,150 and 4360 µg/L for 1/3 dilutions of 1:9 WAFs of AWB and CLB.

Whereas it is hard to directly compare the results from these WAFs to those observed in our study, in general, the range of concentrations tested in the above-mentioned studies, tend to overlap with those measured in this study. WAFs, as commonly prepared (1:10 or 1:9 oil water loading), appear to produce TPH levels only 3 to 10 times higher than the maximum levels measured in this study. This is interesting given that our maximum loading was ~ 50 times lower (1:505) and that the study took place in a low energy system without active mixing. A possible explanation for the small difference in final TPH concentrations might be the increased exposure time (70 days).

3.2.2. *Polycyclic aromatic compounds*

The concentrations of total polycyclic aromatic compounds (ΣPAC_{46}), the sum of the alkylated PACs (ΣPAC_{alk}), as well as the sum of the EPA 16 priority polycyclic aromatic hydrocarbons (ΣPAH_{16}) increased in limnocorrals in a treatment-dependent manner (Figures 5 and 6). A linear regression was fit to determine the relationship between each of these groups of compounds, time, and the volume of oil added (as well as the interaction between time and treatment). The results of these regressions are presented in SI Table 8 and indicate that for all three groups of compounds the effects of oil and the interaction between oil and time were significant ($p < 0.05$), but time alone was not. Alkylated compounds represented the large majority of the 46 different PACs (by mass) measured in the water column. Across all treated limnocorrals and timepoints (after oil application only) the average percent of the ΣPAC_{46} represented by the ΣPAC_{alk} was 91.3 % (± 10.3 SD). Because of this, the temporal progression of the ΣPAC_{46} and ΣPAC_{alk} was almost identical with a rapid increase in water column concentrations over the first two weeks followed by a slow decrease for the rest of the study. ΣPAC_{46} and ΣPAC_{alk} in the 179.8 L treatment increased significantly on the last day of sampling. At the time of the last sampling event, the 179.8 L treatment limnocorral was the only one with visible oil/sheen remaining on the water surface (see companion paper (Stoyanovich et al., submited)). Over the two days prior to this sampling, two rain events were recorded (SI Figure 2). Remobilization of the surface oil/sheen into the water column and resulting dilution of oil-derived hydrocarbons could explain this unexpected increase. Similarly to what was observed for TPHs, the time taken to reach the maximum concentration appeared to also be influenced by the amount of oil added to each limnocorral, with the four lower treatments reaching maximum concentrations of ΣPAC_{46} and ΣPAC_{alk} on day 8, while the three highest treatments reached their maximum a week later on day 15 (ignoring the final increase observed in the 179.8 L treatment). The concentrations of the 16 EPA priority PAHs were markedly lower and much closer to the background levels observed in the control limnocorrals. A treatment effect was still apparent as confirmed by individual linear regressions conducted for each sampling time between the observed concentrations and the volume of oil added (SI Table 9 and SI figures 7 through 9). Peak concentrations of ΣPAH_{16} were reached later than for ΣPAC_{46} and ΣPAC_{alk} with peaks appearing between days 20 and 50.

Figure 6 shows the relationship between the volume of oil added and the maximum concentration of ΣPAC_{46}, ΣPAC_{alk} and ΣPAH_{16} measured in the limnocorrals. SI Table 10 reports the results of the fit of

these regressions. In this study, with a maximum volume of oil applied of 179.8 L (a 1:505 oil:water, v:v), the maximum measured concentrations in the highest treatment were 2860 ng/L for the ΣPAC_{46}, 2715 ng/L for the ΣPAC_{alk} and 153 ng/L for the ΣPAH_{16}. Once again, these results are comparable to what we observed in our 2017 pilot study (Cederwall et al., 2020; Stoyanovich et al., 2019) where exposures to CLB-W at 1:8000 and 1:800 oil:water ratios in in-land mesocosms resulted in maximum ΣPAC_{46} levels of 1,250 and 4,590 ng/L respectively after 11 days. Concentrations in the pilot study appeared slightly higher than in the in-lake study. The pilot study experienced an intense precipitation event on day 8 of the study, while a visible layer of oil was still present. The active mixing induced by this rainfall, could explain these elevated levels.

Direct comparison of ΣPAC_{46} levels to previous literature is limited by the variability of analytical methods employed and the number of compounds included in each method. While data on concentrations of specific PAHs in the water column are available within the US EPA data related to the Line 6B Kalamazoo spill (EPA, 2010), no ΣPAC_{46} or ΣPAH_{16} data are directly reported. The availability of water column data, in general, for the Line 6B spill is limited due, in part, to the initial focus on clean-up efforts, and later focus on monitoring of sediment and biota (Kalamazoo River Trustees, 2015). While not directly comparable due to the different nature of the spilled oil, different exposure scenario, and different matrix, a review of total PAH concentrations in over 16,000 samples of water collected during the Deepwater Horizon (DWH) spill in 2010, shows that 79% of the collected samples had less than 54 ng/L total PAHs (sum of all the two to six ring aromatic hydrocarbons including alkylated PAH), 17% had concentrations of total PAHs between 54 and 1,000 ng/L and 4% showed total PAH concentrations above 1,000 ng/L (Wade et al., 2016). The levels of ΣPAC_{46} observed in our study are generally higher than those measured during the DWH spill. This could be partially due to differences in analytical methodologies (e.g., a smaller number of compounds included in the analytical suit), differences in the composition of the oil, or differences in the exposure scenario. Our simulated spill occurred in low energy, confined systems where virtually unlimited dilution would not be a removal option as it was during the DWH spill. This difference should be kept in mind when assessing the risks posed by oil spills in freshwater systems, lakes in particular. The low energy system, however, might have limited mixing and consequent partitioning of oil-derived hydrocarbons into the water column.

As previously noted, a relevant comparison is that of our measured ΣPAC_{46} concentrations to those previously reported in water-accommodated fractions (WAFs) of various dilbits prepared for laboratory

toxicity studies. Madison et al. (2015) report total PAH concentrations of 1,480 ng/L in a 10% dilution of a 1:9 oil:water WAF of Access Western Blend (AWB) dilbit. Slightly higher values are reported in Madison et al. (2017) ranging between ~2,400 – 80 µg/L for a 1/3 and 1/30 dilution, respectively, of a similarly prepared WAF of CLB. Following the same methodologies as the previous two studies, Alsaadi et al. (2018) report TPH concentrations of approximately 6,264 and 3,019 ng/L for 1/3 dilutions of 1:9 WAFs of AWB and CLB respectively. Also following similar methodologies Madison et al. (2020) report TPH concentrations of ~1,600 and ~3,000 ng/L for 10% dilutions of 1:9 WAFs of AWB and CLB respectively. Philibert et al. (2016), report TPH concentrations of 46,100 ng/L in a 1:10 dilbit WAF, with the lowest tested dilution being a 10% (~4,610 ng/L). Robidoux et al. (2018) report total PAH levels ~ 10,000 µg/L and ~12,000 µg/L for a 10% dilution of 10 g/L WAFs of AWB and CLB respectively. Finally, McDonnell et al. (2019) report concentrations of ~ 14,000 ng/L for 1/3 dilutions of 1:9 WAFs of AWB and CLB. Similar to what was observed for the TPH, the WAF-derived exposures reported in most of these studies are within the range of concentrations observed in our study, indicating that the exposure scenarios currently being tested in laboratory studies are consistent with levels that would be expected to occur in the field.

3.3. Hydrocarbons in the sediment

The concentrations of ΣPAC_{46} and ΣPAC_{alk} in the sediment jars of the three highest treatments increased continuously from the second week until the end of the study while the concentrations of ΣPAH_{16} showed no treatment-related changes (Figure 7). By avoiding direct deposition of sinking oil, these jars were intended to quantify the oil-derived hydrocarbons that would partition into the sediment directly from the soluble fraction present in the water column. The maximum observed concentrations were 189 ng/g for the ΣPAC_{46}, 169 ng/g for ΣPAC_{alk}, and 14 ng/g for ΣPAH_{16} all in the 18.1 L treatment. Similarly, to the water column results, the large majority of the ΣPAC_{46} mass is represented by alkylated PACs with the ΣPAC_{alk}. Similar to the water column, a linear regression was fitted to each of the compound groups to assess the effects of time, treatment and their interaction. The results of these fits are presented in SI Table 11 and indicate a significant effect of time, treatment and their interaction for both ΣPAC_{46}, and ΣPAC_{alk}. In the case of the ΣPAH_{16}, however only time had a significant effect on concentrations measured in the sediments. Individual regressions between the concentrations of the three compound groups and the volume of oil added were fit for each sampling day (SI table 12 and SI figures 10 through 12). In this case, and while an upward trend begins after day 22 for both ΣPAC_{46}, ΣPAC_{alk}, none of the

fitted regressions were statistically significant. Concentrations in the sediment increased after day 15 in the higher treatments. This timing is consistent with water column TPH concentrations reaching their plateau and the peak in water column ΣPAC_{46}, and ΣPAC_{alk}. No plateauing or indication of a decrease in sediment concentrations is apparent, suggesting that sediment concentrations could have continued to increase should the study have continued past day 73.

Bejarano et al. (2012) reported total PAH concentrations (list of compounds included in the analytical methods not reported) measured in 29 samples collected in 2011 from the Kalamazoo River downstream of the spill site. The maximum total PAH concentration measured in these samples was 169,000 ng/g with an average of 37,500 ng/g. Al Isawi (2016) measured ΣPAH_{16} concentrations in sediment samples (upper 15 cm) collected along the Kalamazoo river in 2015 (five years after the spill) and reported levels up to 61,170 ng/g at the point of entry of the spill into the river with concentrations dropping to 2,703 ng/g just half a mile downstream. The sediment concentrations reported in these studies are orders of magnitude higher than those measured in our study. This is especially relevant for the total of EPA priority PAHs for which we did not see any treatment-induced changes in sediment concentration. The main reason for the discrepancy is likely the nature of our samples vs those collected in the Kalamazoo River. Our sediment jars were deployed in a way that minimized deposition from oil droplets and particles with the intention of characterizing only the partitioning taking place directly from the dissolved fraction of the water column. Sediment samples collected in the Kalamazoo river are likely to contain entrenched oil as turbulence and high particulate content in the river resulted in rapid sinking of the oil shortly after the spill.

3.4. Metals in the water column

Of the 25 analyzed metals, only manganese, molybdenum, and vanadium displayed a significant treatment effect. This effect was only apparent in the total fraction for both manganese and molybdenum, but it was significant for both the dissolved and total fractions for vanadium. The temporal progression of the concentrations of the each of the 25 metals is presented in SI Figures 13 through 37. The summary of the statistical tests is presented in SI Table 13.

In the case of manganese levels in the total fraction, only the highest treatment showed to be significantly different from the far-field control (FFC) (based on a Tuckey's HSD test) with a 280% increase from 13.9 to 38.7 µg/L. Similarly, only the concentrations of molybdenum in the total fraction of the highest treatment appeared significantly different from those of the control with a 42 % increase from 0.05 to

0.07 µg/L. In the case of vanadium, the concentrations in both the dissolved and total fraction of the highest treatment appeared significantly different from the FFC with a 25% increase from the dissolved phase (from 0.04 to 0.09 µg/L) and a 62 % in the total (from 0.06 to 0.15 µg/L).

The concentration of manganese in samples collected from the Kalamazoo River in August of 2010 (a month after the spill) was on average 2.5 higher than the values measured in our study at 94 µg/L with maximum values observed at 686 µg/L (EPA, 2010). No data were available for Molybdenum in the US EPA dataset and all collected samples reported values of Vanadium below the limit of detection of 50 µg/L.

The concentration of nine metals in the oil applied in our study is presented in our companion paper (Stoyanovich et al., submited). The concentrations of vanadium in the water column are consistent with the levels in the oil where it displayed the highest concentrations of the nine analyzed metals (137 mg/kg). Molybdenum also showed high concentrations in the applied oil, albeit much lower at 6.41 mg/kg. Unfortunately, manganese concentrations were not measured in the oil used in this study. Interestingly, the second most abundant metal in the applied oil, nickel (60 mg/kg) was not amongst those that showed a treatment effect in its measured water-column concentrations.

Zinc and copper were the only metals to ever exceed a Canadian Council of Ministers of the Environment long-term water quality guideline) (CCREM, 1987). In the case of copper exceedances of the guideline (calculated as 2 µg/L based on the recommended equation and water quality parameters measured in the limnocorrals) occurred only in a couple of samples from the control and the lowest treatment (SI Figure 48). In the case of zinc (SI Figure 21), however, all the measured samples exceeded the guideline (calculated as 3 µg/L) and were in average ~ 33 times higher (~ 100 µg/L). These levels were independent of oil treatment and occurred in all tested limnocorrals. Similar samples collected from the lake itself did not exceed the guideline value with average concentrations 0.9 µg/L (Seguin 2021, in preparation). A clear explanation for these levels is not available at this time, but a possible explanation could have been the use of Zn-plated stainless steel minnow traps in the limnocorrals over the experiment to facilitate fish exposure and retrieval.

3.5. General water quality

Of the parameters routinely assessed using a hand-held probe (conductivity, pH and dissolved oxygen [as mg/L and percent saturation]), Only dissolved oxygen showed a significant treatment effect, while pH

showed a non-significant trend towards lower pH with higher treatment. SI Figures 38 through 41 show the temporal distribution, as well as treatment-dependent trends, of these parameters in the limnocorrals. Conductivity was low and remained relatively stable at around 22 µS/cm with a small increase throughout the study consistent with the evaporative losses observed in the limnocorrals. The pH in the limnocorrals increased from ~ 6 before oil application and remained at around 7.5 for the remainder of the study (measurements performed in the late morning). The dissolved oxygen remained between 7.5 and 8 mg/L for the duration of the study, which represents a level above 80% saturation often exceeding the 100% (measurements performed in the late morning).

SI Table 14 presents the results of the main linear regression between each of these parameters, the volume of oil applied, and time (including the interaction between oil and time). The effect of time was highly significant (p-value < 0.01) for all parameters. The effect of oil addition, and its interactive term with time were only significant for the dissolved oxygen (both as mg/L or saturation). SI tables 15 through 18 summarise the results of individual linear regressions between each of these parameters and the volume of oil applied for each sampling day. A subset of these individual daily fits is also presented in SI Figures 38 through 41. No effect of oil is apparent on the measured conductivity. A decreasing trend of lower pH with higher volume of oil applied becomes apparent starting on day 4. This trend appears on and off throughout the study up to day 29, when it becomes much more apparent with most daily fits showing a significant relationship between oil and pH. A very similar relationship is apparent for the dissolved oxygen data (both as mg/l and percent from saturation), with decreasing DO levels with increasing volumes of oil applied. This effect also becomes more apparent, and statistically significant, at the end of the study. A decrease on pH in the presence of oil could be expected to become more apparent with time as acidic components of the oil (e.g., naphthenic acids, sulphur-containing compounds) partition into the water column. Oil degradation, and particularly photo-degradation, can also lead to the development of organic acids. Dilbit is a highly degraded form of crude oil, and as such, it is usually rich in these degradation products, such as naphthenic acids (Yang et al., 2017). The number of organic acids present in the source oil, together with *in-situ* photodegradation could partially explain the observed changes in pH. Furthermore, indirect effects resulting from changes in primary production or microbial activity due to the impact of the oil in these processes could also lead to treatment-dependent changes in pH. This would be consistent with the parallel changes observed in dissolved oxygen. This possibility will be further studied in future publications dealing specifically with the effects of oil in primary production and microbial communities within the limnocorrals.

A total of 25 water quality parameters were measured throughout the study. SI figures 42 through 64 show the temporal trends of these variables as well as a subset of sampling-day-specific linear regressions between the variable and the volume of oil applied. SI Table 19 reports the parameters of the sampling-day-specific regressions between each of these parameters and the volume of oil applied. Total dissolved and suspended solids remained low (~25 mg/L and ~0.75 mg/L respectively) and show no apparent response to oil. Turbidity also appeared independent from treatment and decreased from ~0.75 NTUs before treatment to ~0.5 NTUs at the end of the study. This decrease is consistent with initial sediment resuspension associated with the installation of the limnocorrals. Increased TSS concentrations are apparent in the NFC throughout the study. Despite our efforts to remove all native fish from the limnocorrals, three white suckers were trapped within this limnocorral at the time of sealing the curtains. Attempts to remove them from the limnocorrals were successful with one sucker, unfortunately, we were unable to remove the other two. Increased TSS in this limnocorral are consistent with the presence of these fish, whose predominantly benthic life would result in sediment resuspension. The amount of particulates in the water column can have an important effect on the formation of oil-particle aggregates (OPAs) (O'Laughlin et al., 2016), the implications of our low particulate levels in the behaviour of the oil are explored further in the companion paper (Stoyanovich et al., submited).

Alkalinity and major ions (Ca, Na, Mg, K, Mn) showed no correlation with treatment and generally increased slightly throughout the study, likely due to the noted evaporative losses. Chloride concentrations were independent of treatment and remained relatively constant at ~ 0.8 mg/L. Sulphate concentrations, on the other hand, displayed a clear concentration-dependent behaviour, with higher sulphate concentrations with increased oil. This relationship became stronger with time (SI Figure 52). CLB Dilbit contains approximately 4% of sulphur by weight (Been and Wolodko, 2011; Conmy et al., 2017; Fingas, 2015), that would represent an addition of up to 6.6 kg of sulphur to the highest treatment limnocorral. Despite its relatively high sulphur concentrations, soluble H_2S is usually low in dilbit (TRB, 2013), with the large majority of the sulphur present as sulphur-containing organic compounds (Been and Wolodko, 2011). If the observed levels were the result of mineralization of these sulphur-containing organics, a delayed response of the sulphate levels would be expected. This delayed effect is apparent in our results. The observed range of sulphate concentrations between the FFC (0.59 mg/L) and the 179L treatment (1.29 mg/L) is, however, relatively small. The NFC shows unusually high values at 1.06 mg/L that diverge from the observed relationship. Remobilization of sediment by the two white suckers in this limnocorral could explain this discrepancy. A combination of an increase in available sulphur, together

719 with indirect effects in microbial activity in the limnocorral's sediments are the most likely explanation
720 for these results. Detailed analysis of the relationship between these data and microbial activity within the
721 limnocorrals will be presented in future publications.

722 When exploring the concentrations of nutrients in the limnocorrals, no significant relationship was
723 observed between treatment and iron levels (SI figure 53), which decreased throughout the study, likely
724 as a result of uptake by periphyton growth in the limnocorral curtains. Our analysis of metals in the
725 source oil (fully described in the companion paper (Stoyanovich et al., submited)) reported 3.7 mg/kg of
726 iron. The lack of a statistically significant relationship between the amount of oil applied and the water
727 column levels could point to limited solubility of the specific form of iron present in the oil, the presence
728 of processes limiting the partitioning of the available oil into the water column, or an iron limitation in the
729 system resulting in quick biological uptake.

730 Similarly, no treatment effect was apparent in the phosphorus concentrations (as TDP or particulate P),
731 which showed a decrease up to around day 50 with a slow increase afterwards. This is consistent with the
732 dynamics of periphyton growth in the limnocorrals, which showed an initial increase and later decrease in
733 biomass, and which will be further explored in future publications. The dynamics of nitrogen throughout
734 the study are less clear and vary with the specific form of nitrogen, but in general, nitrogen concentrations
735 remained relatively constant throughout the study and displayed no correlation with treatment. The
736 slightly different behaviours of phosphorus and nitrogen are consistent with previous observations from
737 long-term manipulation studies conducted at the IISD-ELA indicating a predominant phosphorus
738 limitation in the study lakes (Higgins et al., 2018). Soluble reactive silica levels in the water column
739 followed a similar pattern to that of phosphorus with an initial drop until around day 25 followed by an
740 increase. In this case, however, Si concentrations in water increase proportionally with dilbit treatment
741 volume after day 27 (SI Figure 61). This trend could be due to a treatment dependent reduction in diatom
742 populations in the water column and biofilm and consequent Si release to water. This possibility will be
743 further explored in future publications addressing the effects of oil on biotic components of the system.
744 Suspended carbon remained relatively constant in the water column and showed no relationship with
745 dilbit treatment volume. Dissolved inorganic carbon (DIC) displayed a complex relationship with
746 treatment. Initially, DIC was higher in the high dilbit treatments, but this pattern dissipated after the
747 second week of exposure. Dissolved CO_2 as well as carbonates are common in crude oil and dilbit (TRB,
748 2013). Early dissolution of these components in the water column could explain the increase in DIC in the

high treatment limnocorral. This labile carbon form was likely absorbed rapidly by photosynthetic microbes, explaining the rapid decline in DIC to background levels similar to the control treatments.

Dissolved organic carbon (DOC) concentrations in water were correlated with the volume of added oil (SI Table 19 and SI Figure 64); evidence that petrogenic carbon contributed significantly to the DOC pool. However, this trend was only significant on days 20 and 27. The lack of significance in later sampling events could be due to unusually low DOC concentrations in the 18.1 L treatment. This limnocorral was the one with the highest exchange rate with the lake (Table 2), which could also explain these lower DOC values. An increase in DOC levels with treatment and time is not unexpected given the high organic carbon content of the oil and the increased partitioning of the oil-derived hydrocarbons into the water column over the study period (see following section).

3.6. General considerations

One of the main objectives of this study was to characterize the exposure to oil-derived contaminants occurring after a spill of dilbit into a freshwater lake. This served two main purposes: 1) to put into context any possible effects observed in our study (which will be addressed in future specific publications) and, 2) to serve as a reference for toxicological studies trying to replicate similar exposure scenarios under laboratory conditions. Over the past few years an effort has emerged to standardize the way that exposure solutions are prepared for laboratory test assessing the effects of oil-derived contaminants (Adams et al., 2017). This includes updates to existing guidelines, such as the "Chemical Response to Oil Spills: Ecological Effects Research Forum (CROSERF)" (Barron and Ka'aihue, 2003; Singer et al., 2001). One of the difficulties in this process is defining what scenarios are to be replicated. Data on real world exposure to these contaminants is only available for scenarios that have taken place. Oil spills into fresh waters and lakes in particular have, so far, been a rare occurrence (with a few notable exceptions, like the Kalamazoo river spill), but one that might become more likely under current the current growth and development. The same applies to spills of unconventional crudes, like dilbit. The need for data relevant to these scenarios was noted as a research priority by the Royal Society of Canada report (Lee et al., 2015). Our data provide a range of concentrations that could be expected in a real-world spill, and that can be used to inform the design, development and update of laboratory testing methodologies.

When comparing our data to existing information of previous comparable spills, such as the Kalamazoo river spill, we generally find that for both TPH and PACs our maximum observed concentrations are

779 higher. The confined nature of our exposure system, which minimizes dilution, as well as the length of
780 the spill and lack of clean-up or remediation activities likely explain these differences. Our study length
781 and lack of clean-up was aimed to represent a worst-case-scenario. In most real-world cases, spill
782 response would be initiated within a few hours or a couple of days and a large portion of the oil would be
783 removed before partitioning of its constituents into the water column can take place. Extended spill
784 durations can still take place if they occur in a remote location or if the leak is small and it goes
785 unnoticed. The confined nature of the system, on the other hand, is an intrinsic property of many small
786 and medium-size lakes in Canada. Under these conditions, low volume and limited flow eliminate
787 dilution as a "tool" to reduce exposure like it is commonly the case in marine spills, or even river spills.
788 This main difference makes these systems especially vulnerable to the effects of a spill.

789 The generally low-energy nature of the system, however, could act in the opposite direction. While our
790 measured concentrations were generally higher than those measured in real-world, the lack of energetic
791 mixing resulted in long times needed to reach maximum levels. When compared to wave-tank studies
792 (ECCC, 2013) or laboratory-manufactured WAFs (Alderman et al., 2017; Alsaadi et al., 2018; Lara-
793 Jacobo et al., 2019; Madison et al., 2015; Madison et al., 2017; Madison et al., 2020; McDonnell et al.,
794 2019; Philibert et al., 2016; Robidoux et al., 2018) the concentrations reached in these systems tended to
795 be higher, highlighting the effect of active mixing on the final water-column levels.

796 # 4 Conclusions

797 This study provides a clear picture of the chemical environment following a series of realistic oil spills
798 into a freshwater lake. We show how water-column PAC concentrations tend to increase over the first
799 couple of weeks after the spill to a maximum which is comparable to levels currently being tested in
800 laboratory toxicity studies (Alderman et al., 2017; Alsaadi et al., 2018; Lara-Jacobo et al., 2019; Madison
801 et al., 2015; Madison et al., 2017; Madison et al., 2020; McDonnell et al., 2019; Philibert et al., 2016;
802 Robidoux et al., 2018). We show that, while PAC concentrations in the water column tend to decrease
803 after reaching their maximum, the concentrations of TPH remained relatively constant after reaching a
804 maximum plateau approximately two weeks post spill, highlighting the need to further explore the
805 composition of the TPH and what the ecological effects of those currently understudied compounds (e.g.,
806 oxidation by-products) may be. Our data also show that sediment PAC concentrations did not reach a
807 plateau over the 70-day study, highlighting the importance of this compartment as a sink, and possible
808 future source of exposure to these compounds. Finally, we also show that metal contamination was not as

prominent after the spill, with only three metals showing elevated concentrations in the treated limnocorrals, none of them reaching levels close to current water quality guidelines.

We observed changes in general water quality parameters that could indicate changes in basic limnological and biogeochemical aspects of the system, likely driven by changes in biological elements such as primary producers or microbial communities. These changes will be further explored in upcoming publications.

We hope that the data presented here will aid in informing evidence-based environmental risk assessments for existing and future projects related to land transportation of conventional and unconventional crudes as well as inform the development of refined laboratory testing protocols able to more accurately simulate the chemical environment resulting from an oil spill in a freshwater lake.

5 Acknowledgements

This is contribution No. 3 of the BOREAL study. Funding for this research was provided by an NSERC Strategic Partnership Grant (STPGP 493786-16) awarded to JMB, MLH, and DMO, a grant under the Oceans Protection Program and in-kind contributions from Environment and Climate Change Canada, and in-kind support from the IISD-Experimental Lakes Area. We would like to thank the Canadian Association of Petroleum Producers (CAPP) for kindly providing the diluted bitumen used in this study. A special thank you to Danielle Desrochers (U of Manitoba), and Dalila Seckar (Queen's U) for their contributions to the experimental set up, and to Pauline Gerrard (IISD-ELA) for helping us navigate the administration of this project. We would also like to thank the 4 anonymous reviewers for taking their time to review our manuscript and provide helpful comments that contributed to the improvement of this manuscript. The IISD Experimental Lakes Area field station is in the traditional land of the Anishinaabe Nation in Treaty 3 territory and the homeland of the Métis Nation.

REFERENCES

Adams J, Charbonneau K, Tuori D, Brown RS, Hodson PV. Review of Methods for Measuring the Toxicity to Aquatic Organisms of the Water Accommodated Fraction (WAF) and Chemically-Enhanced Water Accommodated Fraction (CEWAF) of petroleum (CSAS Rep. 2017/064.). In: Canadian Science Advisory Secretariat (CSAS) NCR, Fisheries and Oceans Canada., editor. Fiseries and Oceans Canada, National Capital Region, Canadian Science Advisory Secretariat (CSAS), Ottawa, ON, 2017, pp. xi + 110.

Al Isawi W. Environmental Applications of Chromatography-Mass Spectrometry. Master of Science. Western Michigan University, 2016, pp. 683.

Alderman SL, Lin F, Farrell AP, Kennedy CJ, Gillis TE. Effects of diluted bitumen exposure on juvenile sockeye salmon: From cells to performance. Environ. Toxicol. Chem. 2017; 36: 354-360.

Alsaadi FM, Madison BN, Brown RS, Hodson PV, Langlois VS. Morphological and molecular effects of two diluted bitumens on developing fathead minnow (Pimephales promelas). Aquat. Toxicol. 2018; 204: 107-116.

Barron MG, Ka'aihue L. Critical evaluation of CROSERF test methods for oil dispersant toxicity testing under subarctic conditions. Mar. Poll. Bull. 2003; 46: 1191-1199.

Been J, Wolodko J. Comparison of the corrosivity of dilbit and conventional crude. Alberta Innovates–technology Futures September 2011.

Bejarano AC, Michel J, Williams L. Net Environmental Benefit Analysis (NEBA) relative risk ranking conceptual design, Kalamazoo River system, Enbridge Line 6B Release: Enbridge Line 6B MP 608, Marshall, MI, August 8, 2012; document and appendixes; AR-0963. Scientific Support and Coordination Group (SSCG) to the Federal On Scene Coordinator (FOSC). 2012.

Blanchfield PJ, Kidd KA, Docker MF, Palace VP, Park BJ, Postma LD. Recovery of a Wild Fish Population from Whole-Lake Additions of a Synthetic Estrogen. Environ. Sci. Technol. 2015; 49: 3136-3144.

CAAP. 2019 Crude Oil Forecast, Markets and Transportation. Canadian Association of Petroleum Producers, 2019.

CCREM. Canadian water quality guidelines. Prepared by the Task Force on Water Quality Guidelines. Canadian Council of Resource and Environment Ministers, 1987.

Cederwall J, Black TA, Blais JM, Hanson ML, Hollebone BP, Palace VP, et al. Life under an oil slick: response of a freshwater food web to simulated spills of diluted bitumen in field mesocosms. Can. J. Fish. Aquat. Sci. 2020; 77: 1-10.

Conmy R, Barron M, Santodomingo J, R. D. Characterization and Behavior of Cold Lake Blend and Western Canadian Select Diluted Bitumen Products. EPA/600/R-17/273. U.S. Environmental Protection Agency, Washington, DC, 2017.

Crosby S, Fay R, Groark C, Kani A, Smith JR, Sullivan T, et al. Transporting alberta oil Sands products: Defining the Issues and assessing the risks: Department of Commerce, National Oceanic and Atmospheric Administration, National Ocean Service, Office of Response and Restoration, 2013.

Delignette-Muller ML, Dutang C. fitdistrplus: An R package for fitting distributions. J Stat Software 2015; 64: 1-34.

867 ECCC. Federal Government Technical Report: Properties, Composition and Marine Spill Behaviour, Fate and
868 Transport of Two Diluted Bitumen Products from the Canadian Oil Sands. In: Environment and Climate Change
869 Canada Emergencies Science and Technology, editor, Ottawa, 2013.

870 EPA U. EPA Response to Enbridge Spill in Michigan - Data. United States Environmental Protection Agency.
871 2010. https://archive.epa.gov/region5/enbridgespill/data/web/html/index.html Accesed: 5/12/2020

872 Fingas M. Review of The Properties and Behaviour of Diluted Bitumen. Proc 38th AMOP Technical Seminar,
873 Ottawa, Environment Canada, 2015, pp. 470-494.

874 Furchtgott-Roth DE, Green KP. Intermodal safety in the transport of oil. Studies in Energy Transportation 2013.

875 Gros J, Nabi D, Würz B, Wick LY, Brussaard CPD, Huisman J, et al. First Day of an Oil Spill on the Open Sea:
876 Early Mass Transfers of Hydrocarbons to Air and Water. Environ. Sci. Technol. 2014; 48: 9400-9411.

877 Health Canada. Guidelines for Canadian Drinking Water Quality, Ottawa, Canada, 2007.

878 Higgins SN, Paterson MJ, Hecky RE, Schindler DW, Venkiteswaran JJ, Findlay DL. Biological Nitrogen Fixation
879 Prevents the Response of a Eutrophic Lake to Reduced Loading of Nitrogen: Evidence from a 46-Year Whole-
880 Lake Experiment. Ecosystems 2018; 21: 1088-1100.

881 IEA. World Energy Outlook 2018. International Energy Agency, Paris, 2018.

882 Kalamazoo River Trustees. Final Damage Assessment and Restoration Plan / Environmental Assessment for the
883 July 25-26, 2010 Enbridge Line 6B Oil Discharges near Marshall, MI, 2015.

884 Kidd KA, Blanchfield PJ, Mills KH, Palace VP, Evans RE, Lazorchak JM, et al. Collapse of a fish population after
885 exposure to a synthetic estrogen. Proc. Natl. Acad. Sci. 2007; 104: 8897-8901.

886 Kidd KA, Paterson MJ, Rennie MD, Podemski CL, Findlay DL, Blanchfield PJ, et al. Direct and indirect responses
887 of a freshwater food web to a potent synthetic oestrogen. Philosophical Transactions of the Royal Society B:
888 Biological Sciences 2014; 369: 20130578.

889 Lara-Jacobo LR, Willard B, Wallace SJ, Langlois VS. Cytochrome P450 1A transcript is a suitable biomarker of
890 both exposure and response to diluted bitumen in developing frog embryos. Environ. Pollut. 2019; 246: 501-508.

891 Lee K, Boufadel M, Chen B, Foght J, Hodson PV, Swanson S, et al. Expert Panel Report on the Behaviour and
892 Environmental Impacts of Crude Oil Released into Aqueous Environments. In: Royal Society of Canada, editor,
893 Ottawa, ON. ISBN: 978-1-928140-02-3, 2015.

894 Liber K, Kaushik NK, Solomon KR, Carey JH. Experimental designs for aquatic mesocosm studies: A comparison
895 of the “anova” and “regression” design for assessing the impact of tetrachlorophenol on zooplankton populations in
896 limnocorrals. Environ. Toxicol. Chem. 1992; 11: 61-77.

897 Madison BN, Hodson PV, Langlois VS. Diluted bitumen causes deformities and molecular responses indicative of
898 oxidative stress in Japanese medaka embryos. Aquat. Toxicol. 2015; 165: 222-230.

899 Madison BN, Hodson PV, Langlois VS. Cold Lake Blend diluted bitumen toxicity to the early development of
900 Japanese medaka. Environ. Pollut. 2017; 225: 579-586.

Madison BN, Wallace SJ, Zhang J, Hodson PV, Langlois VS. Transcriptional responses in newly-hatched Japanese medaka (Oryzias latipes) associated with developmental malformations following diluted bitumen exposure. Comp. Biochem. Physiol. D-Genomics Proteomics 2020; 35.

McDonnell D, Madison BN, Baillon L, Wallace SJ, Brown SR, Hodson PV, et al. Comparative toxicity of two diluted bitumens to developing yellow perch (Perca flavescens). Sci. Tot. Environ. 2019; 655: 977-985.

Murray MW, Allan JD, Child M. Potential Ecological Impacts of Crude Oil Transport in the Great Lakes Basin. International Joint Commission, Great Lakes Science Advisory Board Science Priority Committee., Windsord, ON, 2018.

NASEM. Spills of Diluted Bitumen from Pipelines: A Comparative Study of Environmental Fate, Effects, and Response, National Academies of Sciences Engineering and Medicine. Washington, DC: National Academies Press, 2016.

NEB. Incident Data. Government of Canada, National Energy Board, Calgary, AB, 2019.

NRCAN. Energy markets fact book: 2014–2015. Natural Resources Canada, 2014.

O'Laughlin CM, Law BA, Zions VS, King TL, Robinson B, Wu Y. The dynamics of diluted bitumen derived oil-mineral aggregates, Part I. Canadian Technical Report of Fisheries and Aquatic Sciences 2016; 3157: viii + 44p.

Orihel DM, Paterson MJ, Gilmour CC, Bodaly RA, Blanchfield PJ, Hintelmann H, et al. Effect of Loading Rate on the Fate of Mercury in Littoral Mesocosms. Environ. Sci. Technol. 2006; 40: 5992-6000.

Philibert DA, Philibert CP, Lewis C, Tierney KB. Comparison of Diluted Bitumen (Dilbit) and Conventional Crude Oil Toxicity to Developing Zebrafish. Environ. Sci. Technol. 2016; 50: 6091-6098.

R Development Core Team. R: A Language and Environment for Statistical Computing. Vienna, Austria: R Foundation for Statistical Computing, http://www.R-project.org, 2020.

Robidoux PY, Virginie B, Judith L, Marc D. Assessment of acute and chronic toxicity of unweathered and weathered diluted bitumen to freshwater fish and invertebrates. Ecotoxicol. Environ. Safety 2018; 164: 331-343.

Rodríguez-Gil JL, Cáceres N, Dafouz R, Valcárcel Y. Caffeine and paraxanthine in aquatic systems: Global exposure distributions and probabilistic risk assessment. Sci. Tot. Environ. 2018; 612: 1058-1071.

Schertzer WM. Freshwater Lakes. In: Timothy RO, Bailey WG, Wayne R, editors. Surface Climates of Canada. McGill-Queen's University Press, Montreal, 1997, pp. 124-148.

Shah K, Watson K, Hollebone B, Yang Z, Lambert P, Faragher R, et al. The BOREAL Project: The design and Execution of a Controlled Oil Spill Study in a Canadian Freshwater Lake. Proceedings of the Forty-second AMOP Technical Seminar. Environment and Climate Change Canada, Ottawa, ON, Canada, 2019, pp. 276-294.

Singer MM, Aurand DV, Coelho GM, Bragin GE, Clark JR, Sowby M, et al. Making, measuring, and using water-accommodated fractions of petroleum for toxicity testing. International Oil Spill Conference. 2001. American Petroleum Institute, 2001, pp. 1269-1274.

Slota PMA. Evaluation of operational lake evaporation methods in a Canadian Shield landscape. Department of Civil Engineering. Master of Science. University of Manitoba (Canada), Winnipeg, Manitoba, Canada, 2013, pp. 217.

Stainton MP, Capel M, Armstrong F. The chemical analysis of fresh water, 1977.

Stoyanovich S, Rodriguez-Gil J, Hanson M, Hollebone B, Orihel D, Palace V, et al. Simulating diluted bitumen spills in boreal lake limnocorrals - Part 2: Factors affecting the physical characteristics and submergence. Sci. Tot. Environ. submited.

Stoyanovich SS, Yang Z, Hanson M, Hollebone BP, Orihel DM, Palace V, et al. Simulating a Spill of Diluted Bitumen: Environmental Weathering and Submergence in a Model Freshwater System. Environ. Toxicol. Chem. 2019; 38: 2621-2628.

Transport Canada. A review of canada's ship-source spill preparedness and response. In: Panel TSE, editor, 2013.

TRB. Effects of Diluted Bitumen on Crude Oil Transmission Pipelines. Transportation research board special report 311. Transportation Research Board, National Research Council of the Academies, Washington, D.C., 2013.

USDOT. Hazardous Liquid Accident Data, 2010-2017. In: Pipeline and Hazardous Materials Safety Administration, editor. Pipeline Data and Statistics. U.S. Department of Transportation,, Washington, DC, 2019.

USEPA. Federal On-Scene Coordinator Desk Report for the 2010 Enbridge Line 6b Oil Spill in Marshall, Michigan. United States environmental Protection Agency, 2016.

Wade TL, Sericano JL, Sweet ST, Knap AH, Guinasso NL, Jr. Spatial and temporal distribution of water column total polycyclic aromatic hydrocarbons (PAH) and total petroleum hydrocarbons (TPH) from the Deepwater Horizon (Macondo) incident. Mar Pollut Bull 2016; 103: 286-293.

Wickham H. Tidy Data. Journal of Statistical Software; Vol 1, Issue 10 (2014) 2014.

Wickham H. ggplot2 : elegant graphics for data analysis. Cham], Switzerland: Springer, 2016.

Wickham H, Averick M, Bryan J, Chang W, McGowan LDA, François R, et al. Welcome to the Tidyverse. Journal of Open Source Software 2019; 4: 1686.

Yang Z, Hollebone BP, Zhang G, Brown CE, Yang C, Lambert P, et al. Chemical Fate of Photodegraded Diluted Bitumen in Seawater. International Oil Spill Conference Proceedings 2017; 2017: 2286-2305.

962 **Figures**

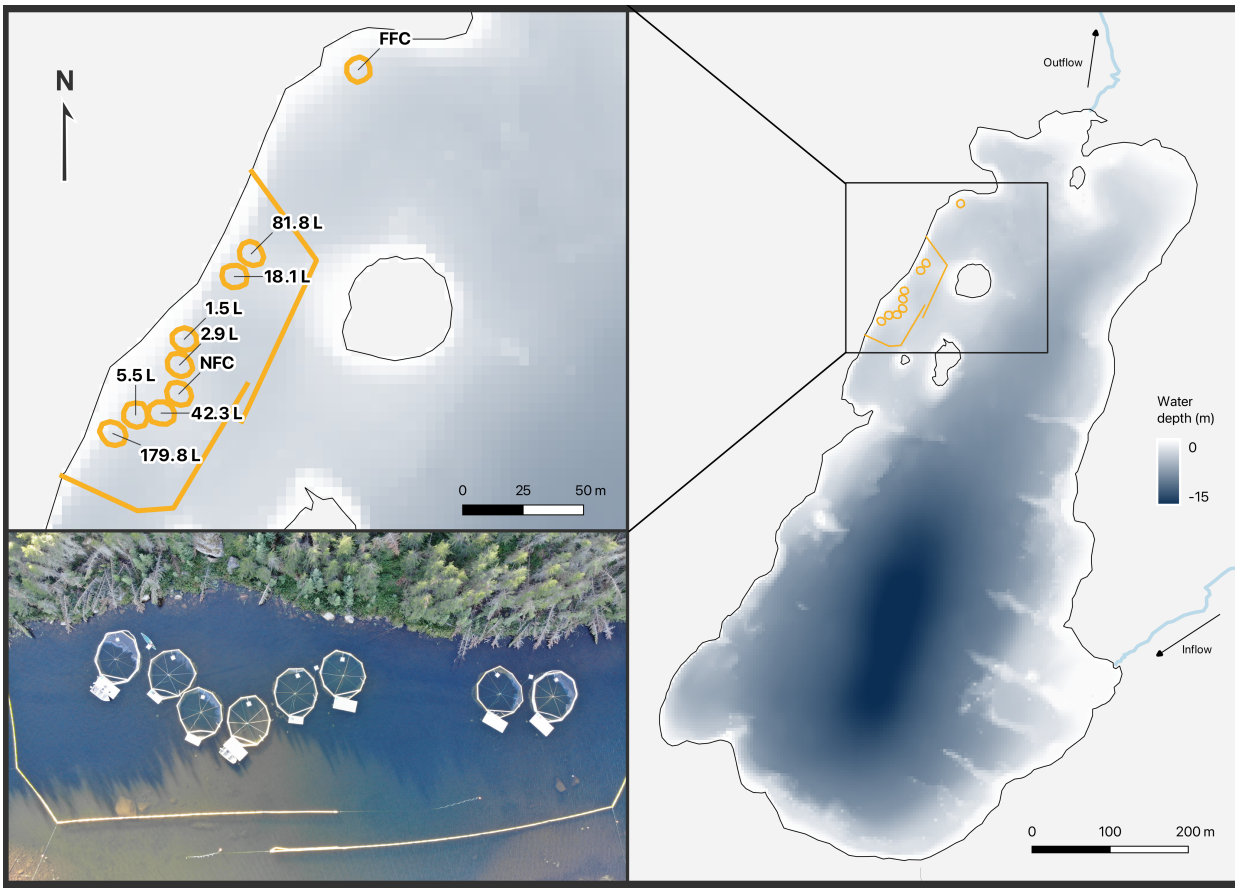

Figure 1: Bathymetric map of Lake 260, location of the limnocorrals, and treatment distribution.

963

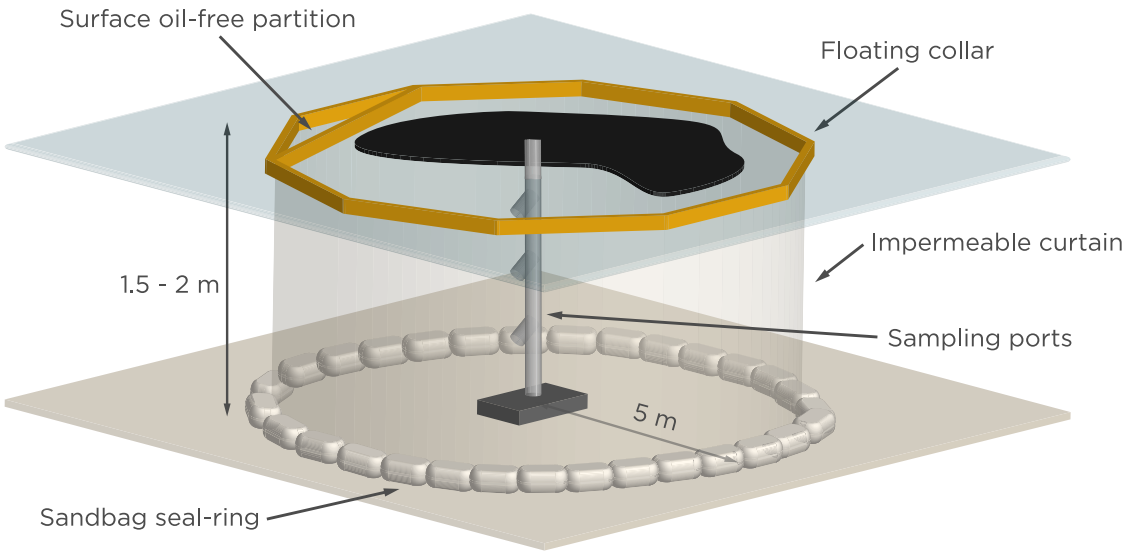

Figure 2: Schematic of a limnocorral and its main components as used in the BOREAL study at the IISD-ELA in 2018.

964

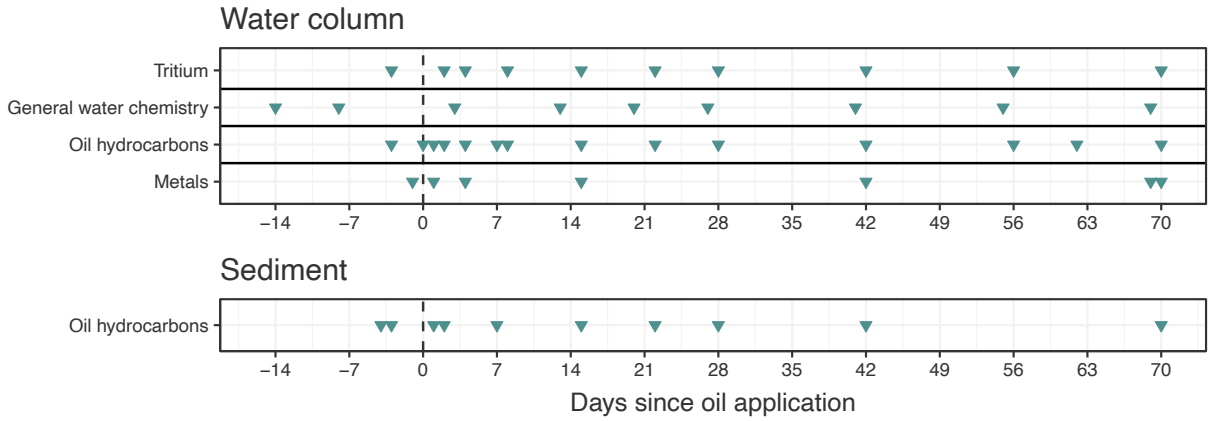

Figure 3: Timeline of sampling events for the different matrices and endpoints assessed in this study. Vertical dashed line represents oil addition (Day 0) on June 20th, 2018.

965

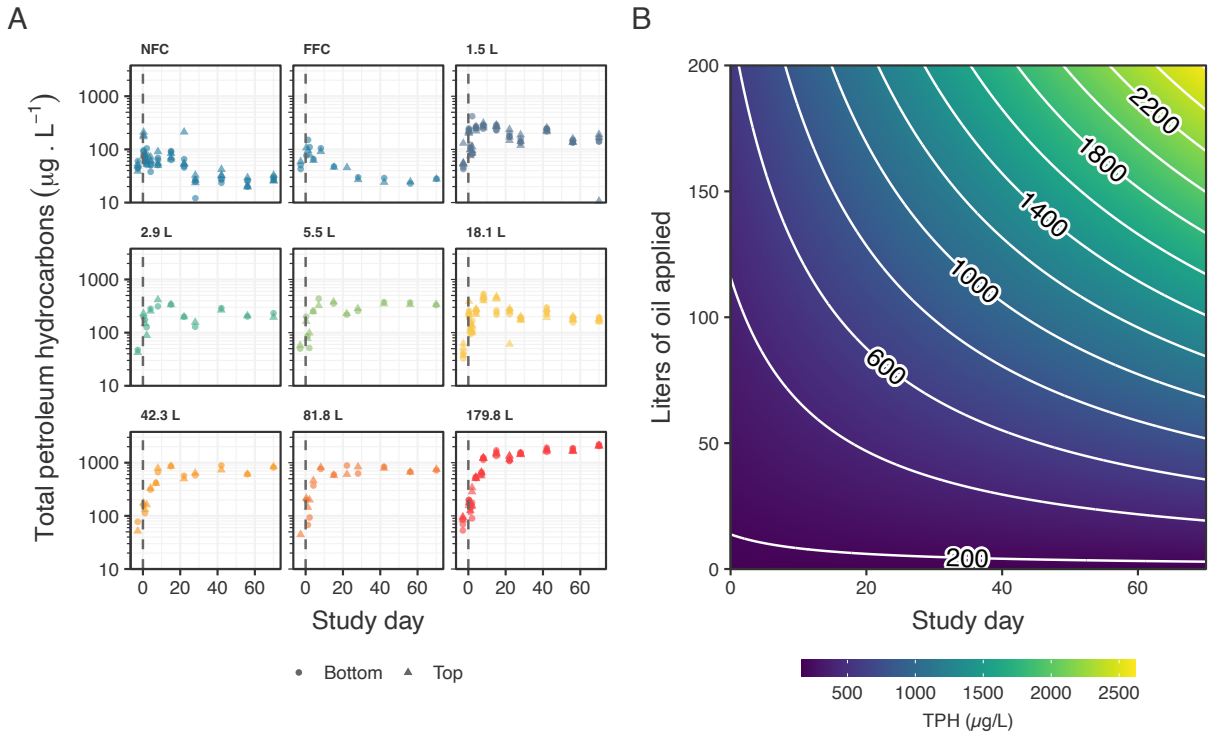

Figure 4: A) Temporal progression of the concentration of Total Petroleum Hydrocarbons (TPH) in the water column of the 9 experimental limnocorrals. Samples collected from the top and bottom sampling ports represented by distinct shapes. B) surface plot of the model fit of the concentration of TPH to time and volume of oil applied.

966

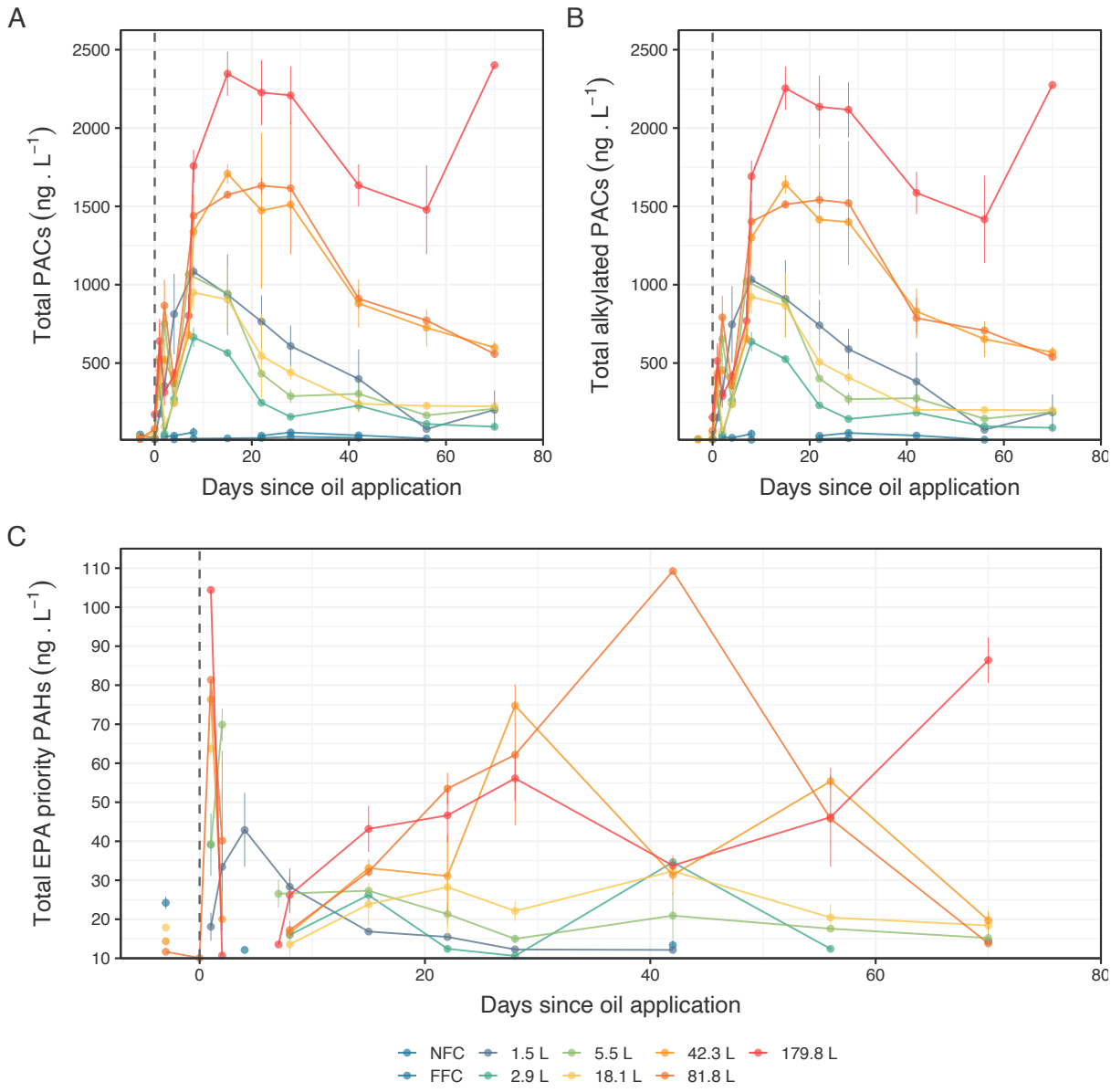

Figure 5: Temporal progression of the concentration of A) Mean total polycyclic aromatic compounds (ΣPAC_{46}), B) Mean total alkylated PACs (ΣPAC_{alk}) and C) Mean total EPA priority polycyclic aromatic hydrocarbons (ΣPAH_{16}) in the water column of the 9 experimental limnocorrals. Error bars represent +/- standard deviation of the mean of all samples (triplicates, when available as well as both sampled depths). Vertical dashed line indicates oil application day. Note different scale on panel C.

967

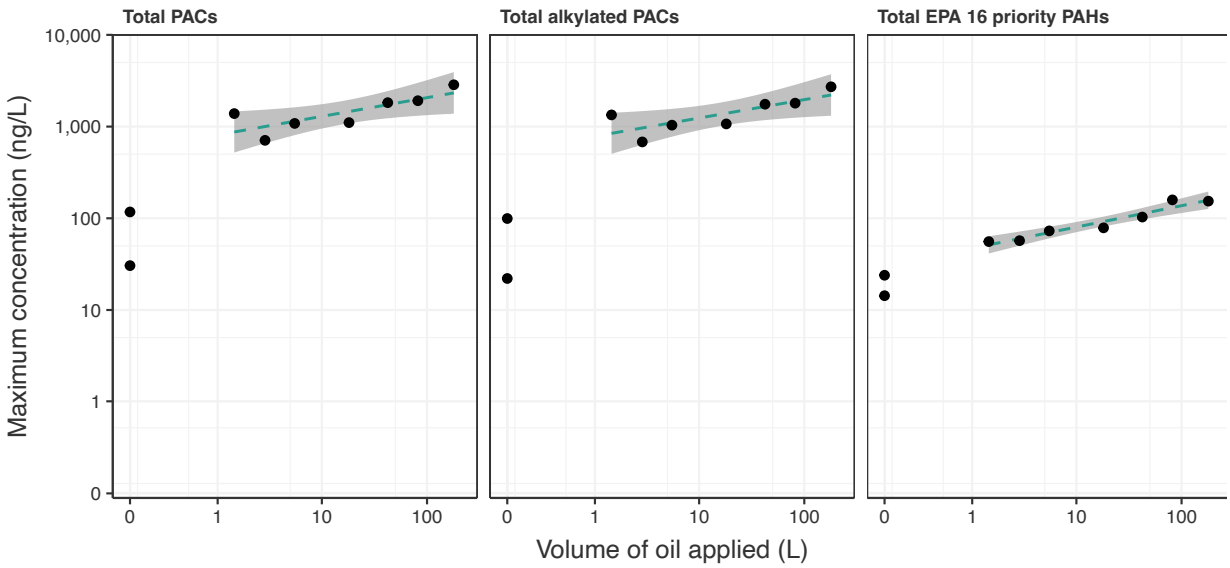

Figure 6: Relationship between the volume of oil applied and the maximum water column concentration of ΣPAC_{46} (left), ΣPAC_{alk} (center) and ΣPAH_{16} (right) measured in the limnocorrals. A liner regression has been fit to the data for the treated limnocorrals. The concentrations measured in the untreated limnocorrals (NFC and FFC) are also presented for reference.

968

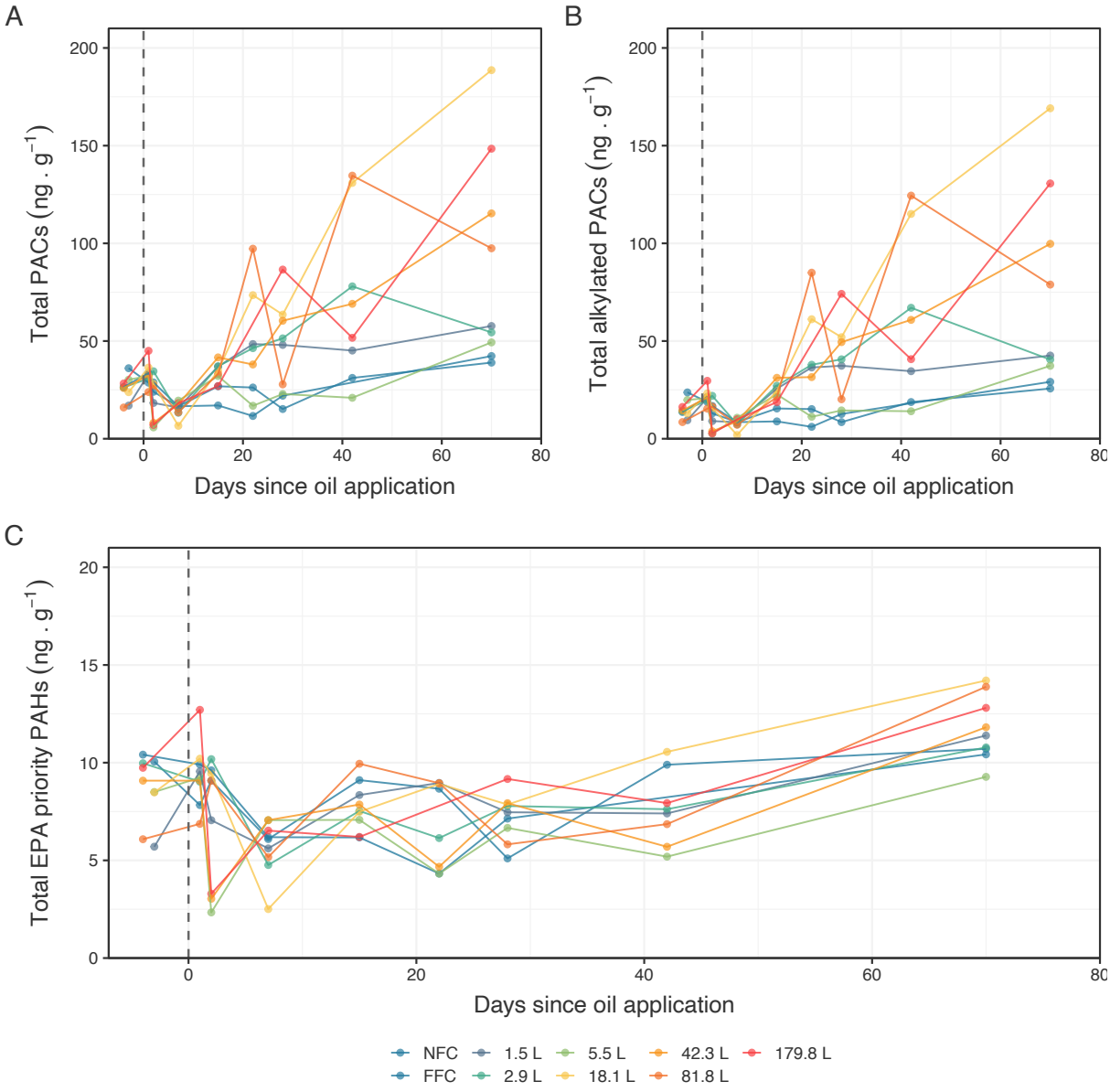

Figure 7: Temporal progression of the concentration of A) Mean total polycyclic aromatic compounds (ΣPAC_{46}), B) Mean total alkylated PACs (ΣPAC_{alk}) and C) Mean total EPA priority polycyclic aromatic hydrocarbons (ΣPAH_{16}) in the sediment of the 9 experimental limnocorrals. Error bars represent +/- standard deviation of the mean of all samples (triplicates, when available as well as both sampled depths). Vertical dashed line indicated oil application day. Note different scale on panel C.

969

Table 1: Upper centiles of the cumulative probability distribution of observed on-shore pipeline crude oil spills in North America (US and Canada) during the period 2008 – 2019. Two subsets are considered; all on-shore spills and on-shore spills that resulted in an impact to surface waters. The maximum volume spilled within those subsets and the name of the spill is also provided.

	Distribution centile and spill volume (m^3)					
	50th	**75th**	**95th**	**99th**	**Max (m3)**	**Location (max)**
All on-shore spills	0.6	3.3	41.3	244.4	3275	North Dakota
On-shore spills impacting surface water	5.5	36.7	566.8	3877.0	3192	Kalamazoo

Table 2: Nominal and actual amounts of dilbit added, limnocorral volumes and resulting nominal and actual oil:water (v:v) ratios.

Nominal dilbit to be added (L)	Actual dilbit added (L)	Limnocorral vol. (m3)	Nominal dilution (v/v)	Actual dilution (v/v)
NFC	NFC	103	0	0
FFC	FFC	93.2	0	0
1.6	1.5	103.8	1 : 100000	1 : 71353
3.45	2.9	97.8	1 : 46377	1 : 34025
7.43	5.5	93.4	1 : 21534	1 : 16939
16.00	18.1	106.8	1 : 10000	1 : 5893
34.47	42.3	106.5	1 : 4642	1 : 2514
74.27	81.8	97.3	1 : 2154	1 : 1190
160.00	179.8	90.7	1 : 1000	1 : 505

Table 3: Rate of exchange of tritium between the limnocorrals and the surrounding lake (K_{leak}) with associated half-life values of tritium in the limnocorrals (due to processes of exchange only). This table is extended with the theoretical and measured rates in SI table 3.

Treatment	K_{leak} (1/day)	Tritium exchange half-life
NFC	-0.0045	154
FFC	-0.00897	77
1.5 L	-0.00457	152
2.9 L	-0.00548	126
5.5 L	-0.00417	166
18.1 L	-0.03491	20
42.3 L	-0.00374	185
81.8 L	-0.01589	44
179.8 L	-0.00343	202

Highlights

- The fate and effects of dilbit spills was monitored in large in-lake limnocorrals
- Total Petroleum Hydrocarbons in water increased in the first week, reaching a plateau
- Sediment Total Polycyclic Aromatic Compounds (PACs) increased over the study
- Water-column PACs increased to a maximum after the first week, decreasing afterward
- V, Mn, and Mo showed a treatment-dependent increase in the water column

Supplementary Information to:

Simulating diluted bitumen spills in boreal lake limnocorrals - Part 1: Experimental design and responses of hydrocarbons, metals, and water quality parameters

Jose Luis Rodriguez-Gil[1, 2, 4], Sawyer Stoyanovich[1], Mark L. Hanson[2], Bruce Hollebone[3], Diane M. Orihel[4], Vince Palace[5], Robert Faragher[3], Fatemeh S. Mirnaghi[3], Keval Shah[3], Zeyu Yang[3], Tyler Black[2], Jeffrey Cederwall[4], Johanna Mason[4], Samuel Patterson[4], Lauren Timlick[2], Jonathan Séguin[1], Jules M. Blais[1]

[1] Department of Biology, University of Ottawa, Ottawa, ON, Canada K1N 6N5

[2] Department of Environment and Geography, University of Manitoba, Winnipeg, MB, Canada R3T 2N2

[3] Emergencies Science and Technology Section, Environment and Climate Change Canada, Ottawa, ON, Canada K1V 1H2

[4] Department of Biology and School of Environmental Studies, Queen's University, Kingston, ON, Canada K7L 3N6

[5] International Institute for Sustainable Development - Experimental Lakes Area, Winnipeg, MB, Canada R3B 0T4

Table of Contents

1 Supplementary methods

1.1. Environmental protection

In order to prevent the spread of the oil around the lake and into the lake outflows and previously identified sensitive areas in the event of the failure of one or several of our limnocorrals (primary containment) a series of additional layers of containment were deployed (Figure 1). For this purpose general purpose (GP) round oil containment boom (Hi-Point Industries, Bishop's Falls, Newfoundland and Labrador) was used. The boom was made of round foam logs covered in Polyvinyl chloride-coated fabric. Deployment of the boom was done with the help of Eastern Canada Response Corporation (ECRC~SIMEC). Secondary containment of the limnocorrals involved controlled gated booming using 800 feet of GP boom and two paravanes (Hi-Point Industries), creating a gated exclusion boom arrangement allowing boat access within the secondary containment for dilbit addition to the limnocorrals and sample collection throughout the experiment. Exclusion booming using 1200 feet of GP boom was also deployed to protect sensitive areas (i.e. lake trout spawning shoals, wetland, and lake outlet) in the case of primary and secondary containment failure.

1.2. Theoretical tritium mass balance

Tritiated water (HTO) was used as a tracer to assess the amount of water being exchanged between the limnocorrals and the lake. In order to accomplish we measured the tritium activity in the enclosures on days 2, 7, 9, 13, 20, 27, 33, 47, 61, and 75 post application of a spike of 92,500,000 Bq of Tritium (10 mL of a 925 x 106 Bq L-1 solution of tritiated water in dis-tilled water). These measured concentrations were then compared to the levels that would have been expected in the systems if the only inputs and outputs were precipitation, evaporation, and isotopic decay.
To develop this theoretical model, precipitation data was compiled from a tipping bucket rain gauge located in the main road leading to the IISD-ELA campsite and adjacent to lake 260 (~ 500 m to the experimental limnocorrals). An activity of 10TU (1.18 Bq L-1) was assumed in the incoming precipitation based on observed trends of measured in Ottawa, Ontario (Michel et al., 2018).
Water budgets were developed using two approaches for the determination of evaporative loses. For ono, data was compiled from a Class A evaporation pan located at IISD – ELA meteorological station (Environment and Climate Change Canada, Rawson Lake station). Given the known limitation of evaporation pan data at low temporal resolution (Granger and Hedstrom, 2011; Slota, 2013), an empirical modelling approach was also included. For this a matlab custom implementation of the Penman-Monteith (Allen et al., 1998) method was used, which estimates evapotranspiration from data on temperature, relative humidity, wind speed, and solar radiation. All the required meteorological data was taken from the IISD-ELA meteorological station. Due to an equipment malfunction data gaps were present in the solar radiation data, which were filled with data from the NASA Prediction Of Worldwide Energy Resources (POWER) project (NASA, 2020). Evaporative losses were assumed to result on isotopic enrichment of tritium in the system. The Inverse of isotopic fractionation factor was assumed to be 0.91 (Calmon and Garnier-Laplace, 2010), i.e. molecules of tritiated water were assumed to be 91% as likely to evaporate as regular water molecules at any given time. Isotopic decay of tritium was also accounted in the calculations with a half-life of 12.32 years (Lucas and Unterweger, 2000).
All data handling was conducted in R version 4.0.2 (R Development Core Team, 2020) employing tidy data approaches (Wickham, 2014; Wickham et al., 2019) Once all data was collected and cleaned

up a custom script was used to calculate the end-of-day tritium activity concentration after all daily sources and losses were accounted for.
Differences in modelled enclosure tritium activity concentrations were negligible between the evaporation pan and those obtained from the Penman-Monteith model. The Penman-Monteith results were used for all following calculations including the final correction of the observed tritium activity concentrations for determination of the water exchange rate.

1.3. Analytical methods

Once concentrated and solvent-exchanged into hexane, the extracts destined to PAC analysis were quantitatively transferred onto a chromatographic column packed with 3 g of silica gel, which was topped with about 1 cm of anhydrous granular sodium sulfate and had been pre-conditioned with 20 mL of hexane, for sample cleanup and fractionation.
Hexane and a hexane-DCM mixture (1:1, v:v) were used to sequentially elute the saturated and aromatic compounds, respectively. These two fractions were concentrated under a gentle stream of nitrogen to appropriate volumes, spiked with internal standards (IS) (including 5-α-androstane, C30 17β(H),21β(H)-hopane and d14-terphenyl for total (GC-detectable) petroleum hydrocarbons (TPHs) and n-alkanes, petroleum biomarker compounds, and polycyclic aromatic compounds (PACs) analysis, respectively), and then adjusted to a volume of 1.0 mL for GC-MS and GC-FID analyses. The saturated fraction was used for analysis of aliphatics (total saturated hydrocarbons, TSHs), n-alkanes, and biomarker terpanes and steranes; the aromatic fraction was used for analysis of aromatic hydrocarbons (TAHs), alkylated homologous PACs and other unsubstituted PACs.
The concentration of Total Petroleum Hydrocarbons (TPH) (largely n-C9 through n-C40) was determined on an Agilent 7890A gas chromatograph equipped with a flame ionization detector (FID) using Agilent OpenLAB ChemStation for data collection. Chemical separation was achieved using a DB-5HT fused silica column (30 m × 0.25 mm i.d., 0.10 μm film thickness) and hydrogen (1.3 mL/min) as a carrier gas. The injector and detector temperatures were 290°C and 300°C, respectively. The temperature program used for TPH determination was 40°C for 2 min, ramp at 20°C/min to 340°C, and held for 20 min.
Forty-six individual Polycyclic Aromatic Compounds (PACs) (including 7 alkylated PAC homologous groups and other unsubstituted PACs) were quantified using an Agilent 7890A GC equipped with an Agilent 5975C mass selective detector (MSD). The GC separation employed a DB-5MS capillary column (30 m × 0.25 mm i.d. × 0.25 μm film thickness). Samples (1.0 μL) injected into the GC in splitless mode (injector temperature at 290°C) with 1.0 mL/min of helium as carrier gas. The MSD operated in select ion monitoring (SIM) mode. For the analysis of alkylated PACs, the column temperature was held at 60°C for 2.0 min, and then programmed 6°C/min to 300 °C and held for 20 min. For the analysis of other unsubstituted PACs, GC oven temperature started from 60°C for 1.0 min, heated to 160°C at 15 °C/min, then 8°C/min to 300°C and held for 7.0 min. Data was acquired and analyzed with Agilent Enhanced MSD ChemStation.
Recoveries of o-terphenyl and d50-tetracosane, surrogates for GC-FID analysis of TPH, were determined to be 90 ± 9% and 94 ± 9% for all the oil samples. The recoveries of five deuterated PAC surrogates: d8-naphthalene, d10-acenaphthene, d10-phenanthrene, d12-benz(a)anthracene, and d12-perylene were 67 ± 13%, 77 ± 10%, 87 ± 8%, 96 ± 9%, and 96 ± 9%, respectively, for GC-MS analysis of PACs and APACs for all oil samples. All the recoveries were considered to be within acceptable limits for analysis. We performed a method blank analysis to monitor the laboratory background at every X samples. For quality control, ESTS reference oil Prudhoe Bay crude oil (13% weathered) was used as the reference oil standard.

2 Supplementary tables

SI Table 1: List of compounds analyzed and included in the different summary groups (i.e. ΣPAC46, ΣPACalk, and ΣPAH16). ΣPAC46, includes all listed compounds.

Compound	Parent or alkylated	EPA 16
Acenaphthene	parent	TRUE
Acenaphthylene	parent	TRUE
Anthracene	parent	TRUE
Benz[a]anthracene	parent	TRUE
Benzo[a]pyrene	parent	TRUE
Benzo[b]fluoranthene	parent	TRUE
Benzo[e]pyrene	Parent	FALSE
Benzo[ghi]perylene	parent	TRUE
Benzo[k]fluoranthene	parent	TRUE
Benzonaphthothiophene - C0	parent	FALSE
Benzonaphthothiophene - C1	alkylated	FALSE
Benzonaphthothiophene - C2	alkylated	FALSE
Benzonaphthothiophene - C3	alkylated	FALSE
Benzonaphthothiophene - C4	alkylated	FALSE
Biphenyl	parent	FALSE
Chrysene - C0	parent	TRUE
Chrysene - C1	alkylated	FALSE
Chrysene - C2	alkylated	FALSE
Chrysene - C3	alkylated	FALSE
Dibenzo[a,h]anthracene	parent	TRUE
Dibenzothiophene - C0	parent	FALSE
Dibenzothiophene - C1	alkylated	FALSE
Dibenzothiophene - C2	alkylated	FALSE
Dibenzothiophene - C3	alkylated	FALSE
Fluoranthene - C0	parent	TRUE
Fluoranthene - C1	alkylated	FALSE
Fluoranthene - C2	alkylated	FALSE
Fluoranthene - C3	alkylated	FALSE
Fluoranthene - C4	alkylated	FALSE

SI Table 1 contd.

Compound	Parent or alkylated	EPA 16
Fluorene - C0	parent	TRUE
Fluorene - C1	alkylated	FALSE
Fluorene - C2	alkylated	FALSE
Fluorene - C3	alkylated	FALSE
Indeno[1,2,3-cd]pyrene	parent	TRUE
Naphthalene - C0	parent	TRUE
Naphthalene - C1	alkylated	FALSE
Naphthalene - C2	alkylated	FALSE
Naphthalene - C3	alkylated	FALSE
Naphthalene - C4	alkylated	FALSE
Perylene	parent	FALSE
Phenanthrene - C0	parent	TRUE
Phenanthrene - C1	alkylated	FALSE
Phenanthrene - C2	alkylated	FALSE
Phenanthrene - C3	alkylated	FALSE
Phenanthrene - C4	alkylated	FALSE
Pyrene	parent	TRUE

SI Table 2: Reporting limits for those PACs for which standards were available as measured in water samples.

Compound	Reporting limit in water (ng/L)
1-Methylnaphthalene	0.5
1-Methylphenanthrene	0.7
2-Methylnaphthalene	0.5
2,3,5-Trimethylnaphthalene	0.7
2,6-Dimethylnaphthalene	0.6
Acenaphthene	0.6
Acenaphthylene	0.5
Anthracene	0.6
Benzo(a)anthracene	1
Benzo(a)pyrene	1.3
Benzo(b)fluoranthene	0.7
Benzo(e)pyrene	0.8
Benzo(ghi)perylene	2.5
Benzo(k)fluoranthene	0.8
Biphenyl	0.4
Chrysene	0.8
d10-Acenaphtnene	0.7
d10-Phenanhrene	0.5
d12-Benz(a)anthracene	1.2
d12-Perylene	0.8
d8-naphthalene	0.6
Dibenz(ah)anthrance	3.3
Dibenzothiophene	0.4
Fluoranthene	0.5
Fluorene	0.6
Indeno(1,2,3-cd)pyrene	2.9
Naphthalene	0.5
Perylene	1.2
Phenanthrene	0.4
Pyrene	0.5

SI Table 3: Summary of weather parameters monitored over the study. Temporal trends are provided in SI figures 2 and 3

Parameter	Value
Mean daily air temperature (°C)	20.3
Mean daily minimum air temperature (°C)	19.7
Mean daily maximum air temperature (°C)	20.9
Mean daily relative humidity (%)	69.5
Mean daily minimum relative humidity (%)	64.4
Mean daily maximum relative humidity (%)	76.1
Mean wind speed (m/s)	2
Mean wind direction (Degrees)	186.1
Total precipitation (mm)	149
Total evaporation (mm)	389.6
Mean water temperature at depth of 75 cm (°C)	22.3
Mean light intensity at depth of75 cm (Lux)	8766.9

SI Table 4: Summary of the rates of tritium loss due to accounted processes (K_{theo}, precipitation, evaporation and decay), the measured loss rate (k_{tot}) and the estimated loss due to exchange with the lake (k_{leak}), the standard deviation of these rates as well as the derived half-life for the speciffic processes are also presented.

Treatment	K_{theo}	K_{theo} SD	Theoretical loss half-life	K_{tot}	K_{tot} SD	Measured half-life	K_{leak}	Exchange half-life
NFC	-8.6E-04	4.0E-05	806	-5.4E-03	3.6E-04	129	-4.5E-03	154
FFC	-9.3E-04	5.0E-05	745	-9.9E-03	4.4E-04	70	-9.0E-03	77
1.5 L	-8.5E-04	4.0E-05	815	-5.4E-03	3.6E-04	128	-4.6E-03	152
2.9 L	-9.0E-04	4.0E-05	770	-6.4E-03	4.2E-04	109	-5.5E-03	126
5.5 L	-9.3E-04	5.0E-05	745	-5.1E-03	3.3E-04	136	-4.2E-03	166
18.1 L	-8.3E-04	4.0E-05	835	-3.6E-02	9.9E-04	19	-3.5E-02	20
42.3 L	-8.3E-04	4.0E-05	835	-4.6E-03	3.7E-04	152	-3.7E-03	185
81.8 L	-9.0E-04	4.0E-05	770	-1.7E-02	9.8E-04	41	-1.6E-02	44
179.8 L	-9.6E-04	5.0E-05	722	-4.4E-03	4.0E-04	158	-3.4E-03	202

SI Table 5: Summary of the results of individual t-tests performed to assess the differences in water column TPH concentrations measured from samples collected from the top or bottom sampling ports. Results for Shapiro-wilks test of normality for each dataset (top or bottom) as well as Levine test of homogeneity of variance are also presented. Individual t-tests were conducted for each sampling day in each intensive limnocorral.

Treatment	Study day	Shapiro top	Shapiro bottom	Levine test	t-test	sig
NFC	1	0.287	0.673	0.48	0.223	no
	2	0.436	0.935	0.206	0.341	no
	4	0.263	0.215	0.927	0.036	*
	8	0.199	0.607	0.569	0.799	no
	15	0.571	0.279	0.671	0.526	no
	22	0.024	0.26	0.424	0.42	no
	28	0.557	0.317	0.653	0.334	no
	42	0.11	0.048	0.559	0.087	no
	56	0.135	0.365	0.74	0.902	no
	70	0.07	0.588	0.634	0.866	no
1.5 L	1	0.131	0.396	0.77	0.094	no
	2	0.766	0.013	0.405	0.477	no
	4	0.947	0.523	0.41	0.435	no
	8	0.768	0.342	0.735	0.569	no
	15	0.117	0.164	0.505	0.326	no
	22	0.469	0.405	0.395	0.996	no
	28	0.592	0.616	0.414	0.878	no
	42	0.586	0.467	0.844	0.871	no
	56	0.224	0.073	0.805	0.754	no
	70	0.222	0.176	0.355	0.7	no

SI Table 5 contd.

Treatment	Study day	Shapiro top	Shapiro bottom	Levine test	t-test	sig
18.1 L	1	NA	NA	0.219	0.549	no
	2	0.46	0.033	0.725	0.919	no
	4	0.212	0.955	0.771	0.746	no
	8	0.851	0.421	0.874	0.887	no
	15	0.858	0.962	0.917	0	**
	22	0.271	0.442	0.383	0.519	no
	28	0.615	0.403	0.531	0.945	no
	42	0.677	0.482	0.734	0.354	no
	56	0.432	0.644	0.742	0.635	no
	70	0.521	0.646	0.754	0.443	no
179.8 L	1	0.053	0.839	0.832	0.354	no
	2	0.57	0.605	0.469	0.15	no
	4	0.234	0.785	0.906	0.503	no
	7	0.227	0.683	0.864	0.905	no
	8	0.835	0.604	0.231	0.549	no
	15	0.356	0.784	0.324	0.677	no
	22	0.141	0.675	0.49	0.095	no
	28	0.574	0.067	0.689	0.108	no
	42	0.709	0.996	0.388	0.78	no
	56	0.711	0.393	0.413	0.126	no
	70	0.319	0.862	0.26	0.34	no

SI Table 6: Summary of the linear regression of the water column concentration of total petroleum hydrocarbons (TPH) against the logarithm of the volume of oil added for each sampling day. Control treatments were not included in this regression.

Study day	Intercept	Slope	r^2	p- value	sig
-3	7.658	50.82	0.073	0.193	no
0	-17.74	232.006	0.097	0.121	no
1	16.319	102.868	0.17	0.033	*
2	28.584	110.992	0.072	0.194	no
4	121.906	185.958	0.7	0	**
8	416.07	120.489	0.85	0	**
15	531.471	8.676	0.702	0	**
22	455.6	-52.809	0.736	0	**
28	587.307	-159.522	0.733	0	**
42	654.221	-107.868	0.708	0	**
56	670.25	-198.262	0.691	0	**
70	834.753	-293.099	0.694	0	**

SI Table 7: Summary of the linear regression of the water column concentration of total petroleum hydrocarbons (TPH) against time and the volume of oil added (including interactive term). The 18.1 L and 81.8 L treatments were excluded when fitting this model

Term	df	Sum of squares	Mean square	Statistic	p - value	sig
Study day	1	861176.75	861176.75	26.6	1.97E-06	**
Volume of poured oil	1	8187752.15	8187752.15	252.92	9.75E-26	**
interaction	1	3417298.06	3417298.06	105.6	5.82E-16	**
Residuals	75	2427503.87	32366.7183	NA	NA	NA

SI Table 8: Summary of the linear regression of the water column concentration of each subgroup of polycyclic aromatic compounds against time and the volume of oil added (including interactive term).

Group	Term	df	Sum of squares	Mean square	Statistic	p-Value	Significant
ΣPAC_{46}	Treatment	1	71961891.16	71961891.16	379.16	0.000	**
	Study day	1	111054.28	111054.28	0.59	0.445	no
	Interaction	1	14833718.30	14833718.30	78.16	0.000	**
	Residuals	332	63011983.68	189795.13			
ΣPAC_{alk}	Treatment	1	65952121.61	65952121.61	371.89	0.000	**
	Study day	1	130935.92	130935.92	0.74	0.391	no
	Interaction	1	13777251.80	13777251.80	77.69	0.000	**
	Residuals	332	58878035.02	177343.48			
ΣPAH_{16}	Treatment	1	43991.86	43991.86	89.80	0.000	**
	Study day	1	41.75	41.75	0.09	0.771	no
	Interaction	1	11288.62	11288.62	23.04	0.000	**
	Residuals	332	162650.94	489.91			

SI Table 9: Summary of the linear regression of the water column concentration of of each subgroup of polycyclic aromatic compounds against the logarithm of the volume of oil added for each sampling day. Control treatments were not included in this regression.

Group	Study day	Intercept	Slope	r^2	p- value	sig
ΣPAC_{46}	1	209.2	169.0	0.51	0.000	**
	2	39.0	296.6	0.02	0.550	no
	4	-119.9	574.7	0.16	0.049	*
	7	-147.0	1098.9	0.30	0.101	no
	8	345.5	802.0	0.59	0.000	**
	15	678.7	512.0	0.69	0.000	**
	22	746.6	201.8	0.63	0.000	**
	28	816.2	36.4	0.68	0.000	**
	42	591.5	-26.8	0.64	0.000	**
	56	647.7	-245.8	0.76	0.000	**
	70	948.0	-402.6	0.62	0.000	**
ΣPAC_{alk}	1	162.5	150.5	0.48	0.000	**
	2	42.6	251.3	0.02	0.470	no
	4	-100.4	529.2	0.14	0.071	no
	7	-142.2	1056.4	0.31	0.095	no
	8	339.3	764.8	0.61	0.000	**
	15	649.6	494.7	0.68	0.000	**
	22	712.3	192.6	0.62	0.000	**
	28	775.8	34.0	0.67	0.000	**
	42	571.3	-45.5	0.61	0.000	**
	56	618.8	-245.5	0.75	0.000	**
	70	902.2	-390.8	0.63	0.000	**
ΣPAH_{16}	1	39.7	13.0	0.61	0.000	**
	2	-8.5	31.5	0.10	0.110	no
	4	-13.2	28.8	0.41	0.001	**
	7	-7.5	29.0	0.39	0.053	no
	8	-1.1	22.6	0.02	0.559	no
	15	11.0	15.1	0.66	0.000	**
	22	16.4	10.0	0.70	0.000	**
	28	24.8	3.3	0.71	0.000	**
	42	15.3	14.8	0.15	0.055	no
	56	21.2	0.8	0.76	0.000	**
	70	30.2	-5.5	0.55	0.000	**

SI Table 10: Summary of the linear regression of the maximum water column concentration of ΣPAC46, ΣPACalk and ΣPAH16 measured in the limno-corrals. Only data for the treated enclosures was considered in these regressions.

Group	Intercept	Slope	r^2	p- value	sig
ΣPAC_{46}	751.934	649.825	0.671	0.024	*
ΣPAC_{alk}	704.204	638.422	0.662	0.026	*
ΣPAH_{16}	51.839	34.778	0.869	0.002	**

SI Table 11: Summary of the linear regression of the sediment concentration of each subgroup of polycyclic aromatic compounds against time and the volume of oil added (including interactive term).

Group	Term	df	Sum of squares	Mean square	Statistic	p-Value	Significant
ΣPAC_{46}	Treatment	1	3912.527174	3912.527174	6.130154793	0.015862602	*
	Study day	1	34223.57731	34223.57731	53.62156405	4.31E-10	**
	Interaction	1	5210.753552	5210.753552	8.164218276	0.00570923	**
	Residuals	66	42124.02496	638.2428024	NA	NA	NA
ΣPAC_{alk}	Treatment	1	3668.598466	3668.598466	6.503799922	0.013092896	*
	Study day	1	29121.73139	29121.73139	51.62786719	7.58E-10	**
	Interaction	1	4646.931389	4646.931389	8.238217477	0.005506213	**
	Residuals	66	37228.62045	564.0700068	NA	NA	NA
ΣPAH_{16}	Treatment	1	2.001451742	2.001451742	0.384435147	0.537374052	no
	Study day	1	89.56136626	89.56136626	17.20278151	9.80E-05	**
	Interaction	1	4.37202429	4.37202429	0.839770336	0.362798832	no
	Residuals	66	343.6101405	5.20621425	NA	NA	NA

SI Table 12: Summary of the linear regression of the sediment concentration of of each subgroup of polycyclic aromatic compounds against the logarithm of the volume of oil added for each sampling day. Control treatments were not included in this regression.

Group	Study day	Intercept	Slope	r^2	p- value	sig
ΣPAC_{46}	1	2.187	30.757	0.072	0.561	no
	2	-4.289	23.583	0.082	0.534	no
	7	0.305	14.594	0.003	0.907	no
	15	-2.506	37.696	0.18	0.343	no
	22	22.552	30.241	0.301	0.26	no
	28	11.378	37.828	0.166	0.365	no
	42	19.817	51.938	0.129	0.429	no
	70	44.456	48.166	0.427	0.112	no
ΣPAC_{alk}	1	1.776	19.395	0.104	0.481	no
	2	-2.708	13.585	0.074	0.556	no
	7	0.039	7.726	0	0.982	no
	15	-2.14	27.027	0.168	0.362	no
	22	22.198	21.08	0.351	0.215	no
	28	11.143	27.778	0.185	0.335	no
	42	19.581	41.7	0.137	0.413	no
	70	42.253	34.745	0.42	0.115	no
ΣPAH_{16}	1	0.489	8.937	0.048	0.637	no
	2	-1.164	7.745	0.072	0.561	no
	7	0.288	5.181	0.019	0.766	no
	15	-0.05	7.836	0.001	0.943	no
	22	0.141	6.849	0.002	0.935	no
	28	0.268	7.202	0.039	0.671	no
	42	0.132	7.162	0.003	0.9	no
	70	1.38	10.362	0.378	0.142	no

SI Table 13: Summary of analysis of variance tests (ANOVA) conducted for each metal and metal fraction to determine the effect of oil treatment on their water column concentrations.

Parameter	Fraction	Term	df	Sum of squares	Mean square	Statistic	P - value	sig
Aluminum	Total	Treatment	3	579.735	193.245	2.396	0.100	no
		Residuals	19	1532.700	80.668			
	Dissolved	Treatment	3	249.539	83.180	2.387	0.101	no
		Residuals	19	662.200	34.853			
Arsenic	Total	Treatment	3	0.018	0.006	1.292	0.306	no
		Residuals	19	0.087	0.005			
	Dissolved	Treatment	3	0.072	0.024	0.947	0.438	no
		Residuals	19	0.480	0.025			
Barium	Total	Treatment	3	0.489	0.163	0.149	0.929	no
		Residuals	19	20.775	1.093			
	Dissolved	Treatment	3	2.551	0.850	0.568	0.643	no
		Residuals	19	28.442	1.497			
Boron	Total	Treatment	3	1.512	0.504	2.413	0.098	no
		Residuals	19	3.967	0.209			
	Dissolved	Treatment	3	0.286	0.095	0.337	0.799	no
		Residuals	19	5.367	0.282			
Bismuth	Total	Treatment	3	0.000	0.000	1.412	0.270	no
		Residuals	19	0.001	0.000			
	Dissolved	Treatment	3	0.000	0.000	0.626	0.607	no
		Residuals	19	0.000	0.000			
Cadmium	Total	Treatment	3	0.000	0.000	0.094	0.962	no
		Residuals	19	0.004	0.000			
	Dissolved	Treatment	3	0.000	0.000	1.042	0.397	no
		Residuals	19	0.000	0.000			

SI Table 13 contd.

Parameter	Fraction	Term	df	Sum of squares	Mean square	Statistic	P - value	sig
Cobalt	Total	Treatment	3	0.000	0.000	3.061	0.053	no
		Residuals	19	0.001	0.000			
	Dissolved	Treatment	3	0.000	0.000	2.899	0.062	no
		Residuals	19	0.001	0.000			
Chromium	Total	Treatment	3	0.011	0.004	0.571	0.641	no
		Residuals	19	0.125	0.007			
	Dissolved	Treatment	3	0.213	0.071	1.173	0.346	no
		Residuals	19	1.152	0.061			
Copper	Total	Treatment	3	13.369	4.456	0.660	0.587	no
		Residuals	19	128.355	6.756			
	Dissolved	Treatment	3	0.170	0.057	0.961	0.431	no
		Residuals	19	1.120	0.059			
Iron	Total	Treatment	3	1619.068	539.689	1.605	0.221	no
		Residuals	19	6387.367	336.177			
	Dissolved	Treatment	3	6.090	2.030	0.006	0.999	no
		Residuals	19	6428.867	338.361			
Lithium	Total	Treatment	3	0.011	0.004	0.811	0.503	no
		Residuals	19	0.086	0.005			
	Dissolved	Treatment	3	0.010	0.003	0.756	0.532	no
		Residuals	19	0.087	0.005			
Manganese	Total	Treatment	3	1841.197	613.732	7.024	0.002	**
		Residuals	19	1660.121	87.375			
	Dissolved	Treatment	3	293.588	97.863	0.806	0.506	no
		Residuals	19	2306.404	121.390			

SI Table 13 contd.

Parameter	Fraction	Term	df	Sum of squares	Mean square	Statistic	P - value	sig
Molybdenum	Total	Treatment	3	0.001	0.000	4.258	0.018	*
		Residuals	19	0.002	0.000			
	Dissolved	Treatment	3	0.003	0.001	1.130	0.362	no
		Residuals	19	0.018	0.001			
Nickel	Total	Treatment	3	4.523	1.508	0.260	0.854	no
		Residuals	19	110.367	5.809			
	Dissolved	Treatment	3	0.347	0.116	2.718	0.073	no
		Residuals	19	0.808	0.043			
Lead	Total	Treatment	3	0.058	0.019	0.191	0.901	no
		Residuals	19	1.915	0.101			
	Dissolved	Treatment	3	0.902	0.301	0.375	0.772	no
		Residuals	19	15.217	0.801			
Selenium	Total	Treatment	3	0.000	0.000	2.312	0.109	no
		Residuals	19	0.001	0.000			
	Dissolved	Treatment	3	0.000	0.000	0.308	0.819	no
		Residuals	19	0.002	0.000			
Tin	Total	Treatment	3	0.001	0.000	0.410	0.748	no
		Residuals	19	0.020	0.001			
	Dissolved	Treatment	3	0.015	0.005	1.602	0.222	no
		Residuals	19	0.061	0.003			
Strontium	Total	Treatment	3	9.991	3.330	1.632	0.215	no
		Residuals	19	38.782	2.041			
	Dissolved	Treatment	3	7.745	2.582	1.259	0.317	no
		Residuals	19	38.961	2.051			

SI Table 13 contd.

Parameter	Fraction	Term	df	Sum of squares	Mean square	Statistic	P - value	sig
Titanium	Total	Treatment	3	0.480	0.160	0.773	0.523	no
		Residuals	19	3.933	0.207			
	Dissolved	Treatment	3	0.457	0.152	2.925	0.060	no
		Residuals	19	0.990	0.052			
Thallium	Total	Treatment	3	0.000	0.000	2.152	0.127	no
		Residuals	19	0.000	0.000			
	Dissolved	Treatment	3	0.000	0.000	0.176	0.911	no
		Residuals	19	0.000	0.000			
Uranium	Total	Treatment	3	0.000	0.000	1.080	0.381	no
		Residuals	19	0.001	0.000			
	Dissolved	Treatment	3	0.000	0.000	1.369	0.282	no
		Residuals	19	0.001	0.000			
Vanadium	Total	Treatment	3	0.023	0.008	4.995	0.010	*
		Residuals	19	0.029	0.002			
	Dissolved	Treatment	3	0.006	0.002	3.850	0.026	*
		Residuals	19	0.010	0.001			
Tungsten	Total	Treatment	3	0.000	0.000	0.789	0.515	no
		Residuals	19	0.002	0.000			
	Dissolved	Treatment	3	0.000	0.000	NaN	NaN	no
		Residuals	19	0.000	0.000			

SI Table 13 contd.

Parameter	Fraction	Term	df	Sum of squares	Mean square	Statistic	P - value	sig
Yttrium	Total	Treatment	3	0.000	0.000	0.283	0.837	no
		Residuals	19	0.002	0.000			
	Dissolved	Treatment	3	0.000	0.000	0.361	0.782	no
		Residuals	19	0.001	0.000			
Zinc	Total	Treatment	3	3797.570	1265.857	0.845	0.486	no
		Residuals	19	28457.300	1497.753			
	Dissolved	Treatment	3	3636.713	1212.238	0.938	0.442	no
		Residuals	19	24549.200	1292.063			

SI Table 14: Sumary of linera regression fit for the the basic water quality parameters measured via hand-held probe.

Parameter	Term	df	Sum of squares	Mean square	Statistic	p-Value	Significant
pH							
	Oil volume	1	0.18	0.18	2.36	0.126	no
	Time	1	2.01	2.01	27.09	0	**
	Oil volume:Time	1	0.01	0.01	0.09	0.768	no
	Residuals	140	10.4	0.07	NA	NA	no
Conductivity (µS/cm)							
	Oil volume	1	2.97	2.97	0.47	0.493	no
	Time	1	155.89	155.89	24.76	0	**
	Oil volume:Time	1	7.58	7.58	1.2	0.274	no
	Residuals	140	881.53	6.3	NA	NA	no
Dissolved oxygen (mg/L)							
	Oil volume	1	3.16	3.16	35.97	0	**
	Time	1	2.01	2.01	22.9	0	**
	Oil volume:Time	1	0.13	0.13	1.52	0.22	no
	Residuals	140	12.31	0.09	NA	NA	no
Dissolved oxygen (%)							
	Oil volume	1	386.96	386.96	22.96	0	**
	Time	1	1287.37	1287.37	76.37	0	**
	Oil volume:Time	1	5.42	5.42	0.32	0.572	no
	Residuals	140	2359.99	16.86	NA	NA	no

*: p-value < 0.05
**: p_value < 0.01

SI Table 15: Sumary of linera regression fit of the pH to the volume of oil applied for each sampling day.

Parameter	Study day	intercept	slope	r^2	p- value	sig
pH	-14	0.285	6.389	0.403	0.125	no
	-13	-0.005	6.216	0.001	0.951	no
	-8	0.012	6.415	0.059	0.6	no
	-4	-0.08	7.393	0.21	0.3	no
	-3	-0.014	7.488	0.013	0.857	no
	-2	0.046	7.312	1	NaN	no
	2	-0.062	8.073	0.112	0.464	no
	4	-0.103	7.858	0.726	0.015	*
	5	-0.019	7.692	0.089	0.515	no
	8	-0.084	7.955	0.615	0.037	*
	13	0.019	7.836	0.051	0.625	no
	15	-0.04	7.985	0.575	0.048	*
	19	0.019	8.207	0.042	0.661	no
	20	-0.008	8.203	0.013	0.81	no
	22	-0.007	8.266	0.002	0.928	no
	27	-0.052	7.47	0.448	0.1	no
	29	-0.101	7.635	0.89	0.001	**
	34	-0.013	7.678	0.039	0.672	no
	41	-0.168	8.228	0.953	0	**
	42	-0.079	7.774	0.688	0.021	*
	57	-0.136	7.507	0.958	0	**
	63	-0.217	7.943	0.944	0	**

SI Table 16: Sumary of linera regression fit of the conductivity to the volume of oil applied for each sampling day.

Parameter	Study day	intercept	slope	r^2	p- value	sig
Conductivity (µS/cm)	-14	1.033	17.472	0.524	0.066	no
	-13	0.396	18.239	0.166	0.364	no
	-8	-0.169	19.917	0.014	0.801	no
	-4	-1.706	24.193	0.562	0.052	no
	-3	0.783	21.578	0.578	0.136	no
	-2	1.528	18.078	1	NaN	no
	2	1.202	20.269	0.461	0.094	no
	4	-0.211	19.967	0.113	0.461	no
	5	-1.069	25.714	0.54	0.06	no
	8	0.256	19.978	0.044	0.651	no
	13	1.722	20.501	0.61	0.038	*
	15	0.367	20.558	0.082	0.534	no
	19	0.563	21.467	0.237	0.268	no
	20	-0.511	21.329	0.175	0.35	no
	22	-0.328	21.966	0.069	0.571	no
	27	0.027	22.539	0	0.972	no
	29	-0.148	22.606	0.007	0.861	no
	34	-0.264	23.603	0.022	0.75	no
	41	0.53	21.649	0.089	0.515	no
	42	-0.27	23.182	0.014	0.8	no
	57	-0.173	25.779	0.005	0.88	no
	63	-0.117	26.569	0.002	0.922	no

SI Table 17: Sumary of linera regression fit of the dissolved oxigen (as percentage from saturation) to the volume of oil applied for each sampling day.

Parameter	Study day	intercept	slope	r^2	p- value	sig
Dissolved oxygen (%)	-14	-1.224	102.357	0.545	0.058	no
	-13	-0.625	102.051	0.368	0.148	no
	-8	-0.843	98.499	0.52	0.067	no
	-4	-0.164	101.283	0.008	0.845	no
	-3	-0.421	105.641	0.523	0.167	no
	-2	1.069	101.754	1	NaN	no
	2	-2.36	116.394	0.585	0.045	*
	4	-2.211	109.901	0.419	0.116	no
	5	-1.883	100.992	0.412	0.12	no
	8	-2.635	105.967	0.646	0.029	*
	13	-1.796	102.116	0.315	0.19	no
	15	-1.613	99.853	0.397	0.129	no
	19	-0.845	104.901	0.138	0.411	no
	20	-0.871	101.018	0.103	0.482	no
	22	-1.045	103.285	0.123	0.44	no
	27	-1.808	95.302	0.627	0.034	*
	29	-2.338	99.239	0.739	0.013	*
	34	-3.294	99.731	0.768	0.01	**
	41	-4.33	104.377	0.89	0.001	**
	42	-3.346	100.694	0.741	0.013	*
	57	-1.386	99.509	0.732	0.014	*
	63	-1.673	95.582	0.566	0.051	no

SI Table 18: Sumary of linera regression fit of the dissolved oxigen (mg/L) to the volume of oil applied for each sampling day.

Parameter	Study day	intercept	slope	r^2	p- value	sig
Dissolved oxygen (mg/L)	-14	-0.187	9.288	0.395	0.13	no
	-13	-0.061	9.389	0.155	0.383	no
	-8	-0.071	8.619	0.375	0.144	no
	-4	0.031	8.24	0.022	0.752	no
	-3	-0.037	8.915	0.669	0.09	no
	-2	0.107	8.665	1	NaN	no
	2	-0.136	9.053	0.49	0.08	no
	4	-0.193	8.865	0.419	0.116	no
	5	-0.195	8.33	0.524	0.066	no
	8	-0.236	8.591	0.756	0.011	*
	13	-0.178	8.37	0.409	0.122	no
	15	-0.16	8.299	0.518	0.068	no
	19	-0.057	8.27	0.112	0.463	no
	20	-0.148	8.124	0.309	0.195	no
	22	-0.132	8.101	0.409	0.122	no
	27	-0.236	7.928	0.855	0.003	**
	29	-0.225	7.954	0.799	0.007	**
	34	-0.293	8.155	0.759	0.011	*
	41	-0.329	8.471	0.813	0.006	**
	42	-0.322	8.6	0.746	0.012	*
	57	-0.14	8.2	0.752	0.011	*
	63	-0.186	8.205	0.612	0.038	*

SI Table 19: Sumary of linera regression fit between the diferent water quality parameters and the volume of oil applied for each sampling day.

Parameter	Study day	intercept	slope	r^2	p- value	sig
Alkalinity	-14	5.589	133.052	0.35	0.162	no
	-8	1.704	142.865	0.142	0.405	no
	-2	0.974	150.543	0.022	0.752	no
	6	0.304	165.82	0.002	0.924	no
	13	-1.718	172.922	0.029	0.714	no
	20	23.819	173.607	0.069	0.569	no
	27	-3.807	184.862	0.072	0.561	no
	41	-2.703	185.249	0.036	0.684	no
	55	-1.536	183.117	0.007	0.857	no
	69	-7.263	199.589	0.164	0.367	no
Ca	-14	0.014	2.049	0.076	0.55	no
	-8	0.012	2.201	0.074	0.555	no
	-2	0.025	2.24	0.263	0.239	no
	6	-0.006	2.527	0.002	0.92	no
	13	0.046	2.537	0.071	0.564	no
	20	0.014	2.663	0.005	0.883	no
	27	0.005	2.784	0.001	0.962	no
	41	0.023	2.851	0.008	0.852	no
	55	0.023	2.748	0.006	0.865	no
	69	0.017	2.738	0.004	0.899	no
Cl	-14	0.013	0.15	0.606	0.039	*
	-8	0.009	0.173	0.533	0.063	no
	-2	0.031	0.165	0.359	0.155	no
	6	-0.003	0.196	0.034	0.691	no
	13	0.006	0.188	0.058	0.603	no
	20	-0.007	0.2	0.366	0.15	no
	27	-0.014	0.215	0.235	0.27	no
	41	-0.002	0.161	0.026	0.728	no
	55	0	0.153	0.001	0.947	no
	69	-0.004	0.168	0.074	0.556	no

SI Table 19 contd.

Parameter	Study day	intercept	slope	r^2	p- value	sig
DIC	-14	3.374	139.943	0.482	0.083	no
	-8	5.381	150.577	0.579	0.047	*
	-2	2.18	150.576	0.122	0.443	no
	6	6.181	165.322	0.282	0.22	no
	13	10.037	166.751	0.258	0.244	no
	20	2.524	182.437	0.041	0.662	no
	27	-0.328	194.308	0	0.967	no
	41	2.087	191.308	0.014	0.803	no
	55	-5.241	189.995	0.087	0.52	no
	69	-8.939	210.041	0.154	0.384	no
DOC	-14	0.285	397.514	0.001	0.955	no
	-8	-16.722	438.818	0.466	0.091	no
	-2	-33.692	462.506	0.353	0.159	no
	6	15.15	420.072	0.333	0.175	no
	13	60.724	400.567	0.405	0.124	no
	20	60.66	399.929	0.619	0.036	*
	27	84.985	386.97	0.639	0.031	*
	41	88.043	390.008	0.567	0.051	no
	55	68.129	431.378	0.347	0.164	no
	69	97.173	423.461	0.467	0.09	no
Fe	-14	0	0.07	0.508	0.072	no
	-8	-0.005	0.073	0.235	0.27	no
	-2	-0.003	0.061	0.236	0.269	no
	6	-0.008	0.064	0.445	0.102	no
	13	-0.008	0.035	0.161	0.372	no
	20	-0.002	0.029	0.012	0.819	no
	27	-0.006	0.026	0.114	0.459	no
	41	-0.01	0.03	0.275	0.227	no
	55	-0.006	0.024	0.137	0.414	no
	69	-0.009	0.025	0.228	0.279	no

SI Table 19 contd.

Parameter	Study day	intercept	slope	r^2	p- value	sig
K	-14	-0.001	0.368	0.003	0.905	no
	-8	-0.001	0.406	0.007	0.861	no
	-2	0.004	0.404	0.204	0.309	no
	6	-0.015	0.464	0.312	0.193	no
	13	-0.006	0.445	0.041	0.665	no
	20	-0.005	0.432	0.014	0.799	no
	27	-0.026	0.464	0.389	0.135	no
	41	-0.013	0.445	0.13	0.426	no
	55	-0.01	0.442	0.13	0.428	no
	69	-0.014	0.452	0.094	0.503	no
Mg	-14	0.003	0.528	0.097	0.497	no
	-8	0	0.571	0.002	0.922	no
	-2	0.002	0.566	0.042	0.658	no
	6	-0.006	0.618	0.056	0.609	no
	13	0.005	0.606	0.021	0.759	no
	20	-0.006	0.622	0.017	0.779	no
	27	-0.003	0.587	0.004	0.888	no
	41	-0.003	0.579	0.003	0.9	no
	55	-0.002	0.653	0.003	0.911	no
	69	-0.002	0.648	0.001	0.934	no
Mn	-14	0	0	NaN	NaN	no
	-8	0.004	0.003	0.095	0.502	no
	-2	0.007	0.003	0.244	0.259	no
	6	0.008	-0.001	0.144	0.401	no
	13	0	0	NaN	NaN	no
	20	-0.001	0.01	0.002	0.932	no
	27	-0.002	0.007	0.046	0.644	no
	41	-0.001	0.001	0.578	0.047	*
	55	0	0.002	0.01	0.831	no
	69	-0.001	0.001	0.871	0.002	**

SI Table 19 contd.

Parameter	Study day	intercept	slope	r^2	p- value	sig
Na	-14	0.002	0.796	0.026	0.73	no
	-8	0.006	0.805	0.237	0.268	no
	-2	0.039	0.783	0.376	0.143	no
	6	-0.014	0.868	0.473	0.088	no
	13	0	0.845	0	0.967	no
	20	-0.006	0.849	0.058	0.604	no
	27	-0.021	0.852	0.451	0.099	no
	41	-0.014	0.857	0.521	0.067	no
	55	-0.018	0.902	0.454	0.097	no
	69	-0.021	0.923	0.322	0.184	no
NH3-N	-14	-0.476	3.858	0.111	0.465	no
	-8	0.372	13.839	0.004	0.891	no
	-2	-0.647	12.635	0.025	0.735	no
	6	-0.192	9.373	0.047	0.641	no
	13	-0.305	4.796	0.035	0.688	no
	20	0.279	0.093	0.165	0.365	no
	27	-0.127	5.01	0.012	0.814	no
	41	-1.667	24.432	0.466	0.091	no
	55	0.191	34.77	0.01	0.835	no
	69	0.105	0.303	0.011	0.825	no
NO2-N	-14	0	1	NaN	NaN	no
	-8	0.304	-0.08	0.236	0.269	no
	-2	0	0	NaN	NaN	no
	6	0	0	NaN	NaN	no
	13	-0.289	1.205	0.355	0.158	no
	20	0	0	NaN	NaN	no
	27	0	0	NaN	NaN	no
	41	0	1	NaN	NaN	no
	55	0	2	NaN	NaN	no
	69	0	0	NaN	NaN	no

SI Table 19 contd.

Parameter	Study day	intercept	slope	r^2	p- value	sig
NO3-N	-14	0.436	8.19	0.015	0.796	no
	-8	0.583	0.013	0.362	0.153	no
	-2	0.763	2.797	0.619	0.036	*
	6	0.934	2.877	0.159	0.376	no
	13	0.867	-0.614	0.355	0.158	no
	20	0.139	3.69	0.015	0.797	no
	27	0.14	2.261	0.003	0.903	no
	41	0.816	0.019	0.058	0.604	no
	55	0.327	1.035	0.227	0.279	no
	69	-0.049	6.202	0.002	0.928	no
SO4	-14	0.009	1.116	0.165	0.367	no
	-8	0.016	1.095	0.201	0.313	no
	-2	0.039	1.01	0.636	0.032	*
	6	0.023	0.963	0.156	0.381	no
	13	0.045	0.934	0.445	0.102	no
	20	0.059	0.919	0.555	0.055	no
	27	0.076	0.896	0.681	0.022	*
	41	0.137	0.821	0.74	0.013	*
	55	0.174	0.725	0.761	0.01	**
	69	0.227	0.658	0.742	0.013	*
SRSi	-14	0.001	1.194	0.002	0.931	no
	-8	0	1.132	0	0.994	no
	-2	-0.001	0.998	0	0.981	no
	6	-0.053	0.818	0.356	0.157	no
	13	-0.007	0.642	0.005	0.882	no
	20	0.033	0.551	0.04	0.665	no
	27	0.096	0.495	0.178	0.345	no
	41	0.217	0.445	0.387	0.136	no
	55	0.28	0.491	0.44	0.104	no
	69	0.422	0.547	0.512	0.071	no

SI Table 19 contd.

Parameter	Study day	intercept	slope	r^2	p- value	sig
Susp C	-14	-3.826	448.814	0.006	0.865	no
	-8	-59.007	589.083	0.193	0.323	no
	-2	-26.67	556.821	0.076	0.549	no
	6	-44.167	562.127	0.56	0.053	no
	13	45.26	617.716	0.114	0.46	no
	20	59.954	595.178	0.089	0.516	no
	27	-48.46	603.489	0.265	0.237	no
	41	31.157	383.056	0.059	0.599	no
	55	9.772	391.251	0.005	0.884	no
	69	39.97	362.961	0.08	0.538	no
Susp N	-14	4.46	49.766	0.122	0.443	no
	-8	-2.302	59.882	0.061	0.592	no
	-2	-2.379	60.532	0.031	0.704	no
	6	-3.692	61.582	0.134	0.42	no
	13	-3.314	86.141	0.077	0.547	no
	20	2.458	75.273	0.024	0.738	no
	27	-5.614	58.907	0.36	0.154	no
	41	3.553	51.015	0.066	0.578	no
	55	6.576	31.251	0.132	0.422	no
	69	7.901	44.33	0.201	0.313	no
Particulate P	-14	0.578	8.733	0.031	0.707	no
	-8	-0.123	7.862	0.007	0.855	no
	-2	-0.539	10.363	0.055	0.614	no
	6	-0.208	6.393	0.055	0.613	no
	13	0.228	6.868	0.039	0.671	no
	20	0.568	5.889	0.316	0.189	no
	27	-0.28	5.908	0.166	0.363	no
	41	0.539	3.78	0.109	0.47	no
	55	-0.406	5.059	0.161	0.372	no
	69	-0.415	7.213	0.067	0.576	no

SI Table 19 contd.

Parameter	Study day	intercept	slope	r^2	p- value	sig
TDN	-14	9.852	223.298	0.717	0.016	*
	-8	2.413	252.099	0.084	0.53	no
	-2	2.432	237.791	0.142	0.404	no
	6	6.327	241.108	0.11	0.468	no
	13	-3.502	211.781	0.049	0.633	no
	20	-2.837	273.696	0.031	0.706	no
	27	1.61	244.636	0.007	0.862	no
	41	2.199	253.643	0.021	0.759	no
	55	-4.596	268.097	0.101	0.487	no
	69	3.736	249.509	0.05	0.63	no
TDP	-14	0.691	1.968	0.062	0.589	no
	-8	0.206	3.271	0.108	0.472	no
	-2	-0.004	4.696	0	0.99	no
	6	-0.009	5.077	0.001	0.941	no
	13	0.063	3.477	0.034	0.692	no
	20	0.178	3.41	0.648	0.029	*
	27	-0.022	2.744	0.004	0.896	no
	41	0.181	2.341	0.096	0.499	no
	55	0.089	2.198	0.046	0.643	no
	69	0.347	2.578	0.543	0.059	no
TDS	-14	0.978	21.967	0.235	0.271	no
	-8	-2.719	28.554	0.453	0.098	no
	-2	-0.163	23.624	0.013	0.811	no
	6	2.171	23.104	0.271	0.231	no
	13	-0.153	26.898	0.009	0.84	no
	20	51.382	-11.552	0.35	0.216	no
	27	-5.044	34.118	0.25	0.312	no
	41	0.258	25.003	0.001	0.948	no
	55	-5.729	31.994	0.128	0.487	no
	69	-1.99	36.379	0.02	0.789	no

SI Table 19 contd.

Parameter	Study day	intercept	slope	r^2	p- value	sig
TSS	-14	0.293	-0.067	0.57	0.05	*
	-8	0.271	0.245	0.451	0.098	no
	-2	0.284	0.23	0.093	0.505	no
	6	0.196	0.05	0.256	0.247	no
	13	-0.038	1.188	0.011	0.821	no
	20	-0.152	0.354	0.068	0.572	no
	27	-0.471	1.423	0.299	0.204	no
	41	-0.104	1.153	0.066	0.579	no
	55	-0.172	0.893	0.072	0.561	no
	69	-0.175	0.311	0.623	0.035	*
Turbidity	-14	0.103	0.561	0.302	0.201	no
	-8	0.126	0.458	0.422	0.114	no
	-2	-0.052	0.784	0.03	0.712	no
	6	-0.049	0.801	0.107	0.474	no
	13	0.116	0.519	0.382	0.139	no
	20	0.166	0.593	0.531	0.063	no
	27	-0.061	0.461	0.232	0.274	no
	41	0.069	0.327	0.463	0.093	no
	55	0.059	0.313	0.184	0.337	no

3 Supplementary figures

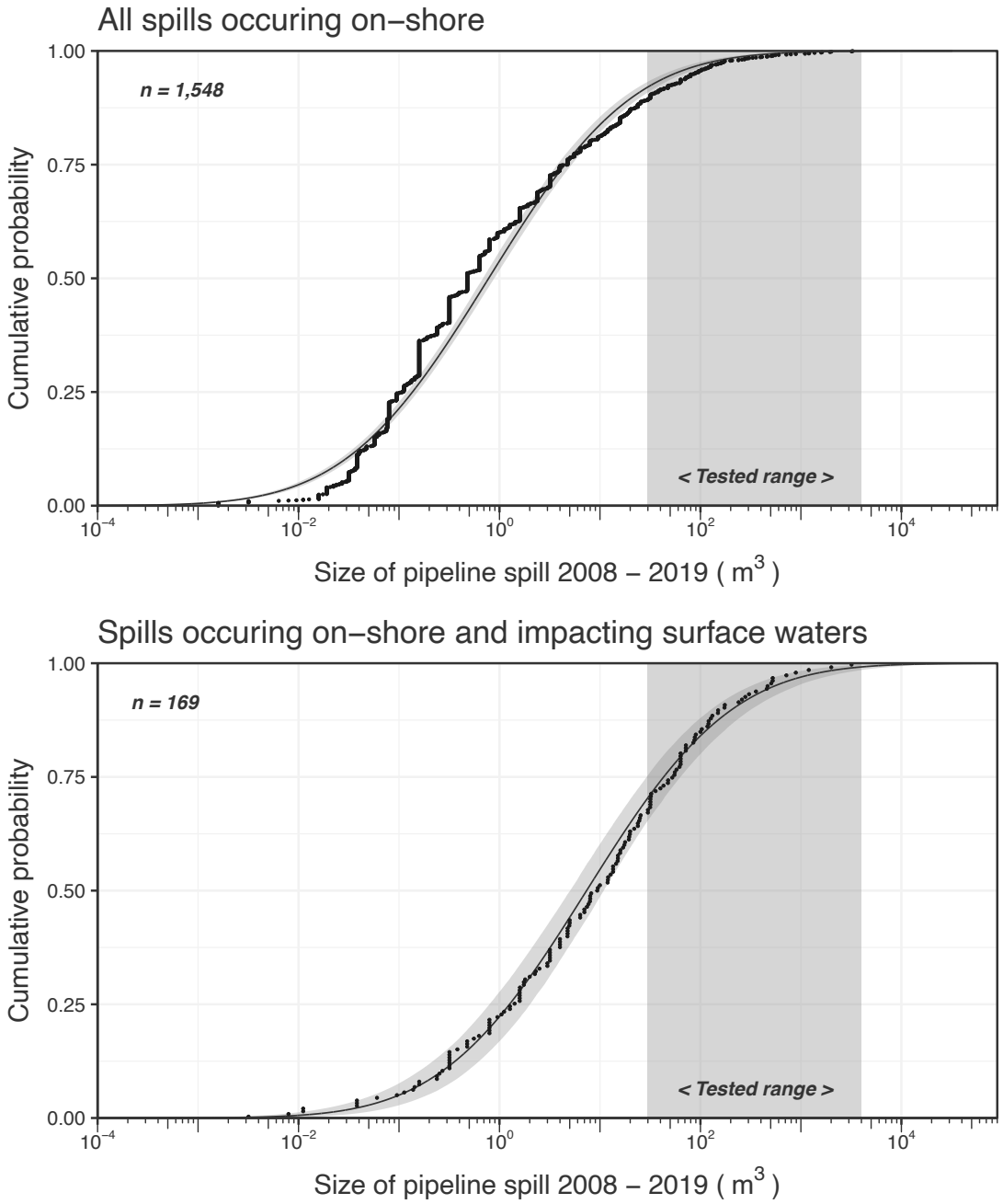

SI Figure 1: Cumulative probability distribution of observed on-shore pipeline crude oil spills in North America (US and Canada) during the period 2008 – 2019. Two subsets are considered; all on-shore spills (upper panel) and on-shore spills which resulted in an impact to surface waters (lower panel). The range of equivalent spill sizes applied in this study is presented as a shaded area.

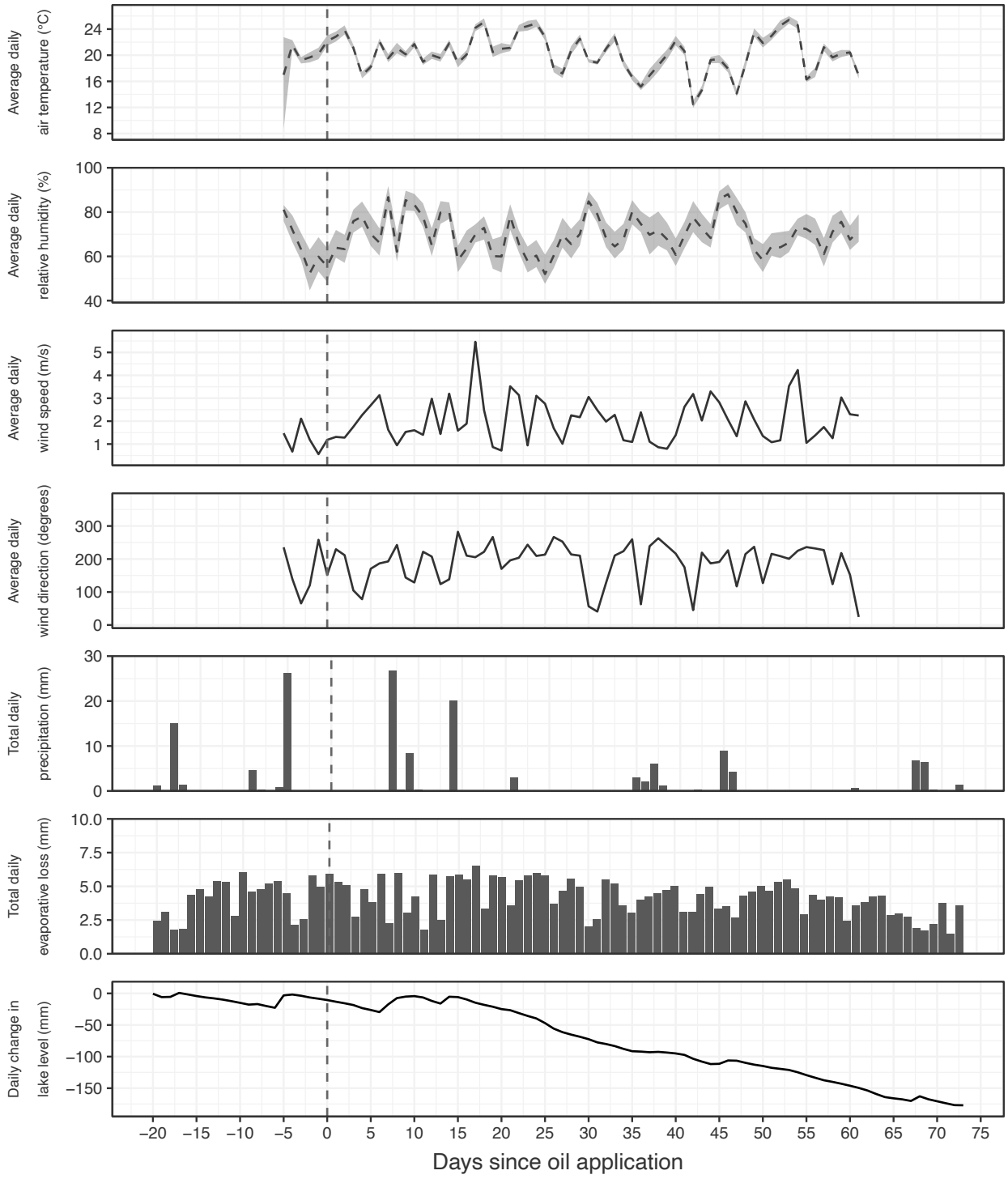

SI Figure 2: Main weather parameters measured over the study period. Dashed vertical line indicates the day of oil addition (day 0)

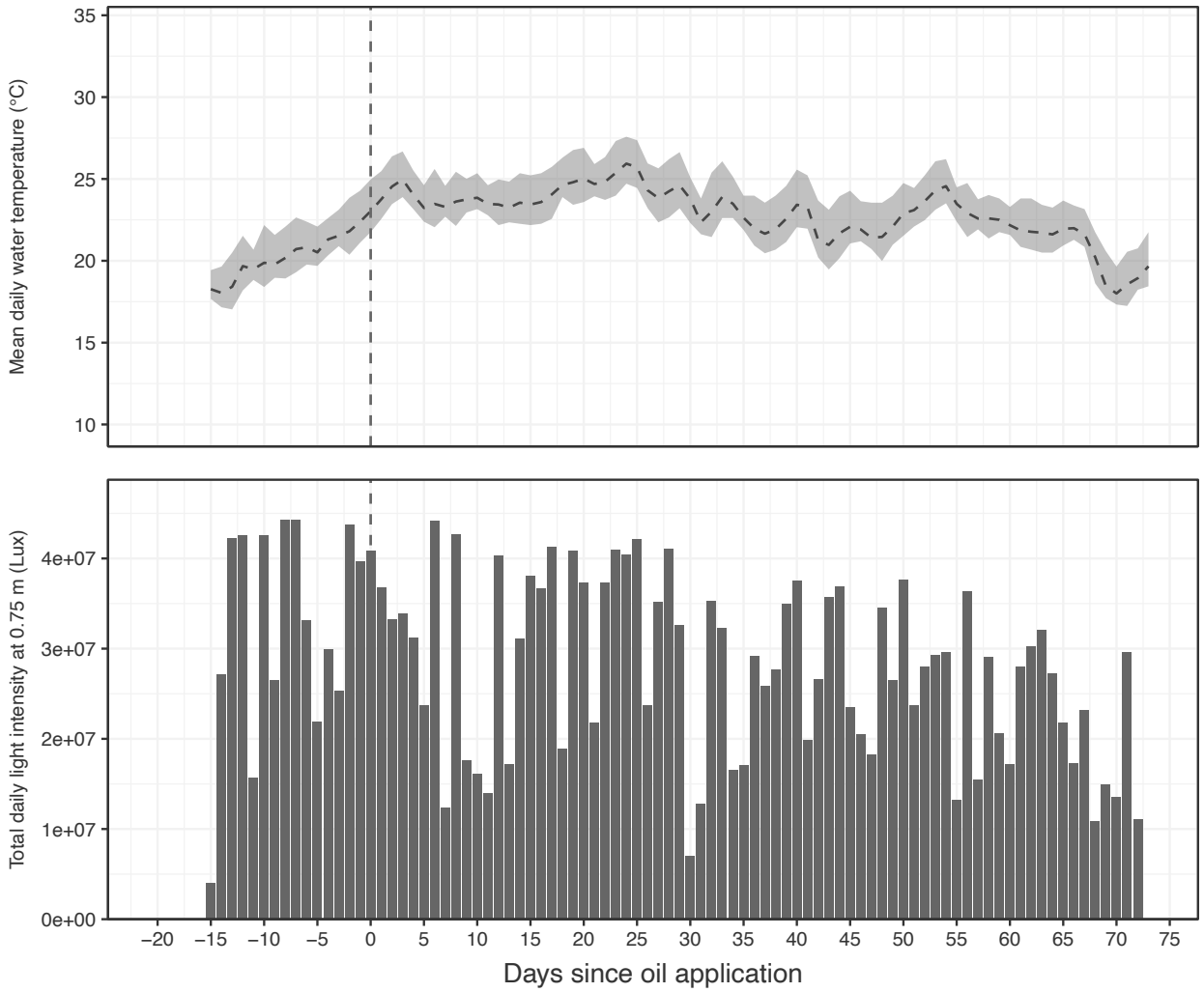

SI Figure 3: Mean water temperature and light intensity measured in the enclosures (depth ~0.75 m). Dashed vertical line indicates the day of oil addition (day 0)

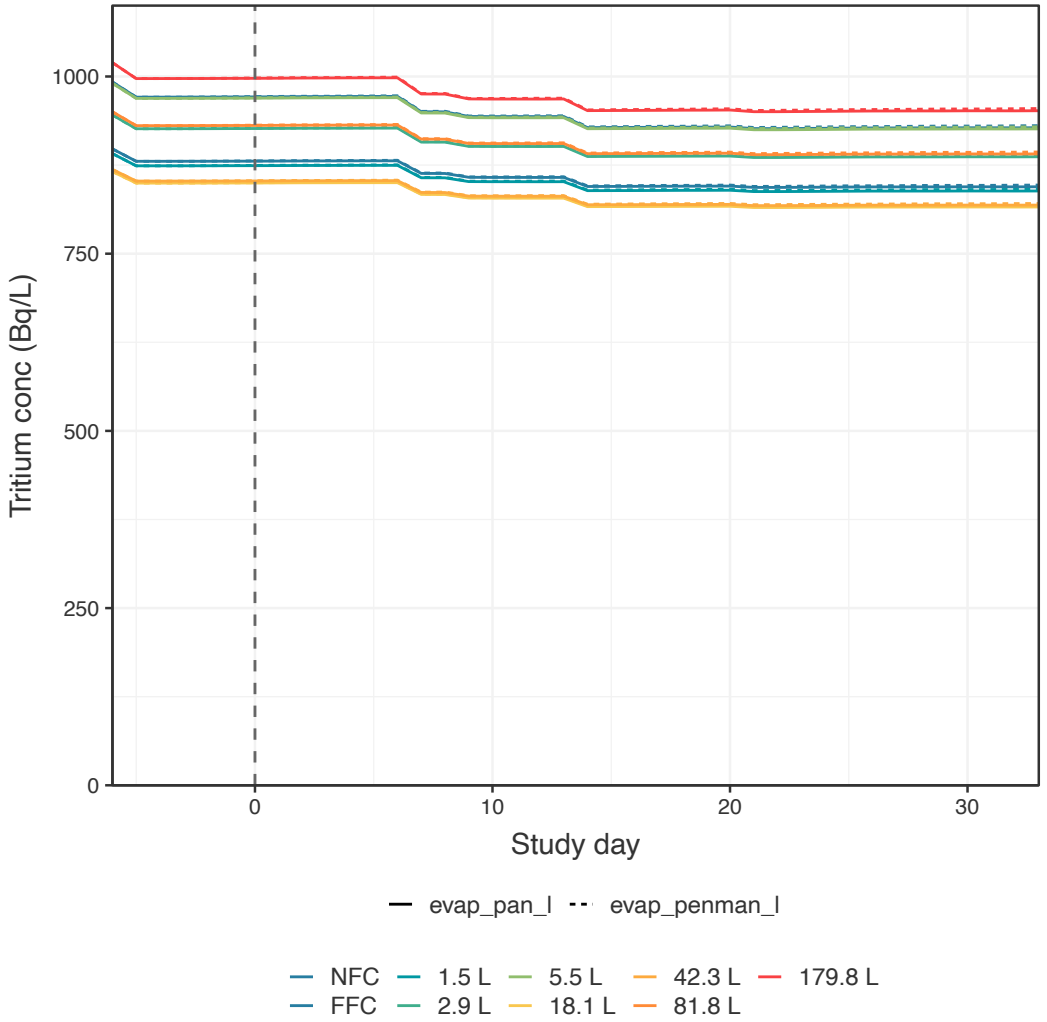

SI Figure 4: Estimated tritium activity concentration in each limnocorral under no exchange conditions with the surrounding lake. Results are presented for estimates made using evaporation data from a Class A evaporation pan or modeled using the Penman-Monteith (Allen et al., 1998) method. Dashed vertical line indicates the day of oil addition (day 0)

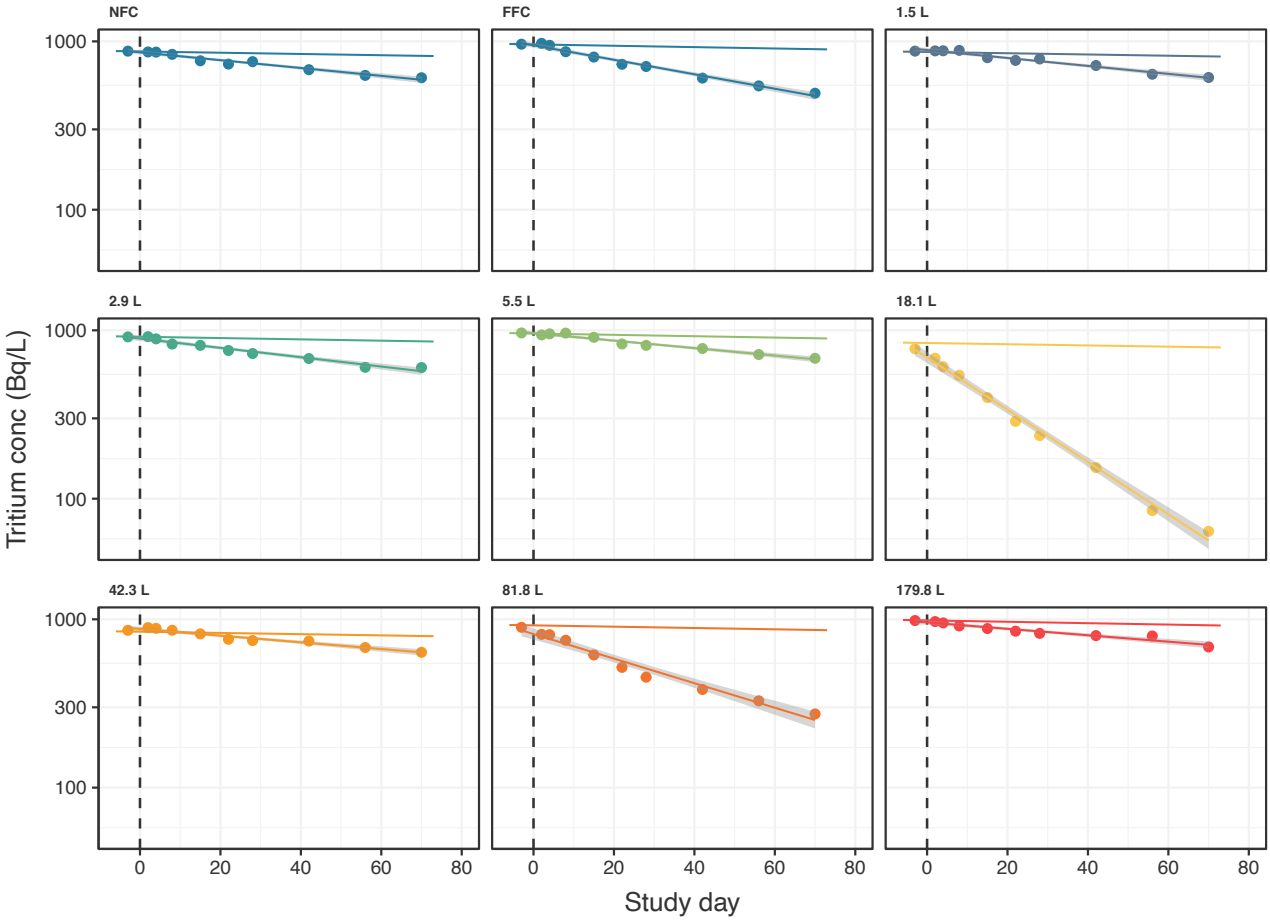

SI Figure 5: Measured vs Estimated tritium activity concentration for each limnocorral over the study period. Dashed vertical line indicates the day of oil addition (day 0)

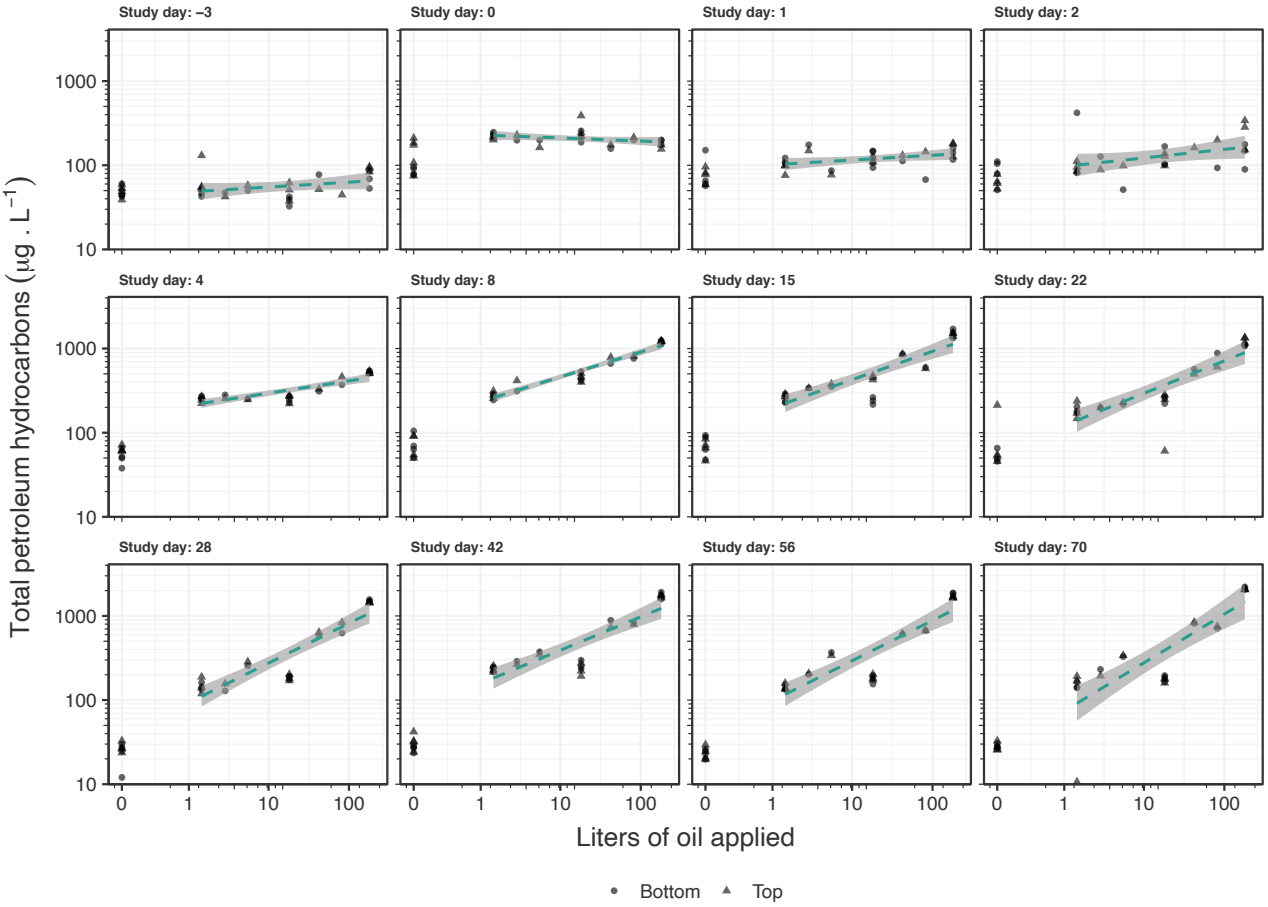

SI Figure 6: Relationship between the volume of oil applied and the water-column concentration of total petroleum hydrocarbons (TPH) in the water column. The control treatments were excluded from the regression.

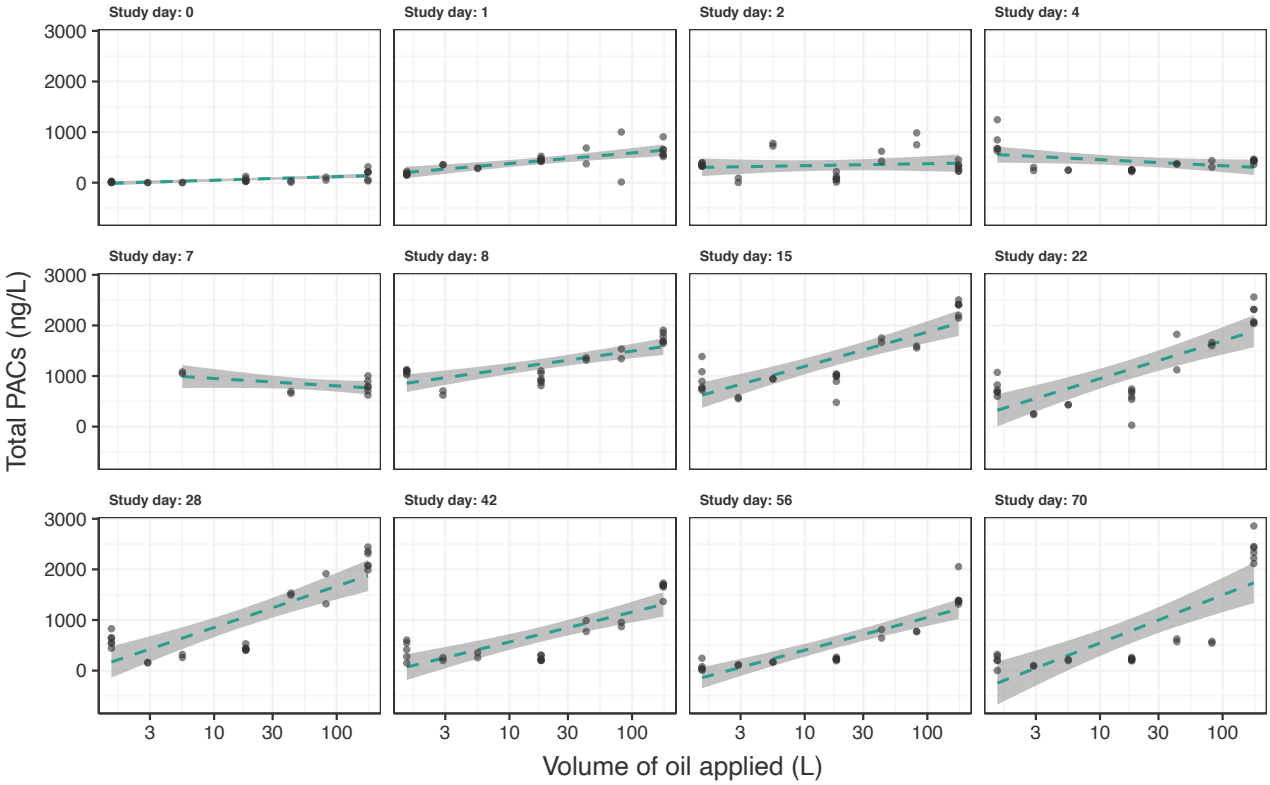

SI Figure 7: Relationship between the volume of oil applied and the water-column concentration of total polycyclic aromatic compounds (ΣPAC_{46}) in the water column. The control treatments were excluded from the regression.

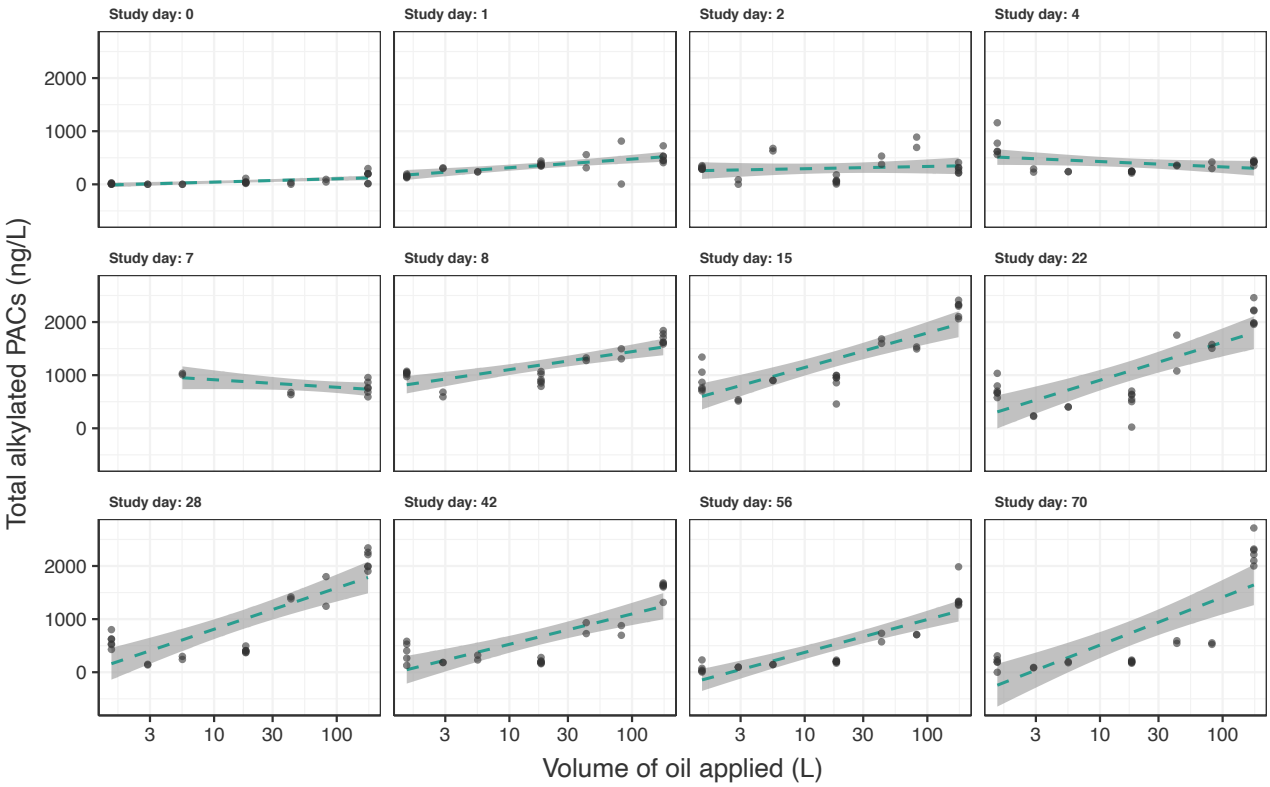

SI Figure 8: Relationship between the volume of oil applied and the water-column concentration of total alkylated aromatic polycyclic compounds (ΣPAC_{alk}) in the water column. The control treatments were excluded from the regression.

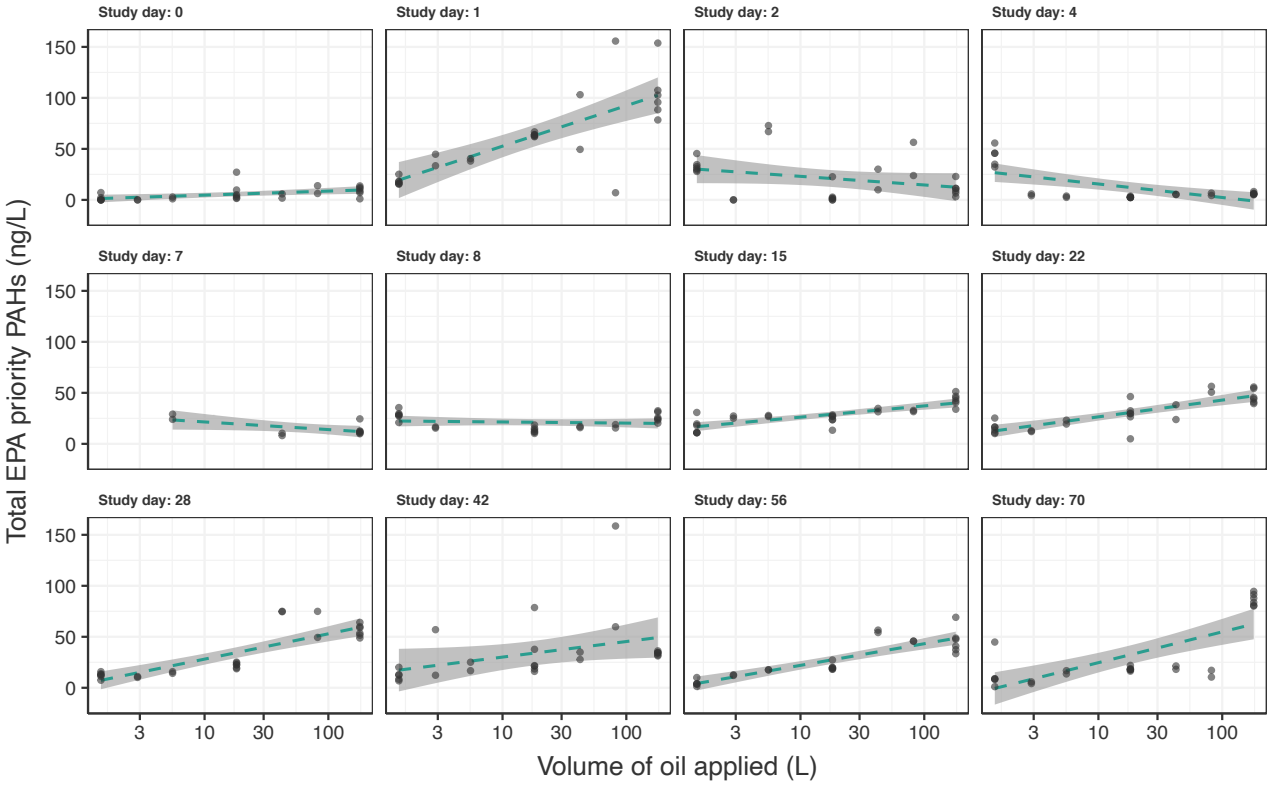

SI Figure 9: Relationship between the volume of oil applied and the water-column concentration of the sum of the 16 US EPA priority aromatic polycyclic hydrocarbons (ΣPAH_{16}) in the water column. The control treatments were excluded from the regression.

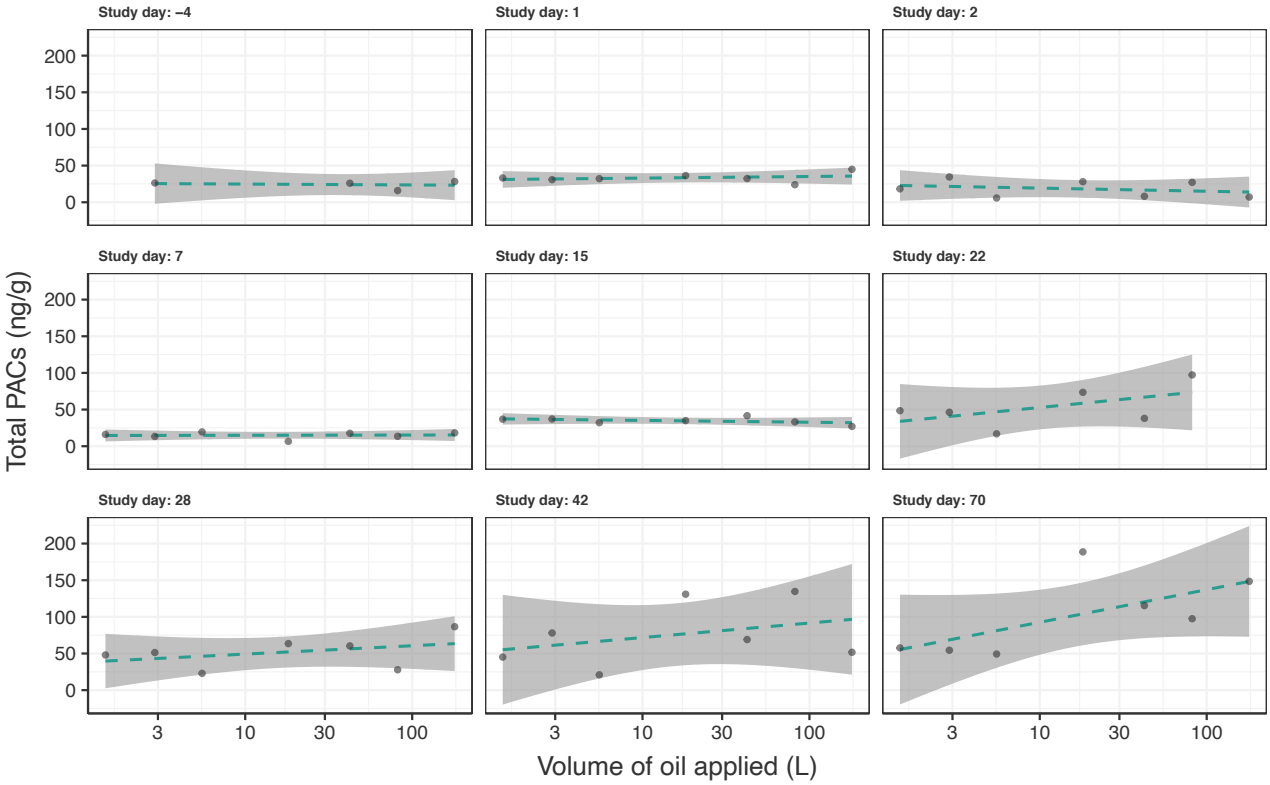

SI Figure 10: Relationship between the volume of oil applied and the sediment concentration of total polycyclic aromatic compounds (ΣPAC_{46}) in the water column. The control treatments were excluded from the regression

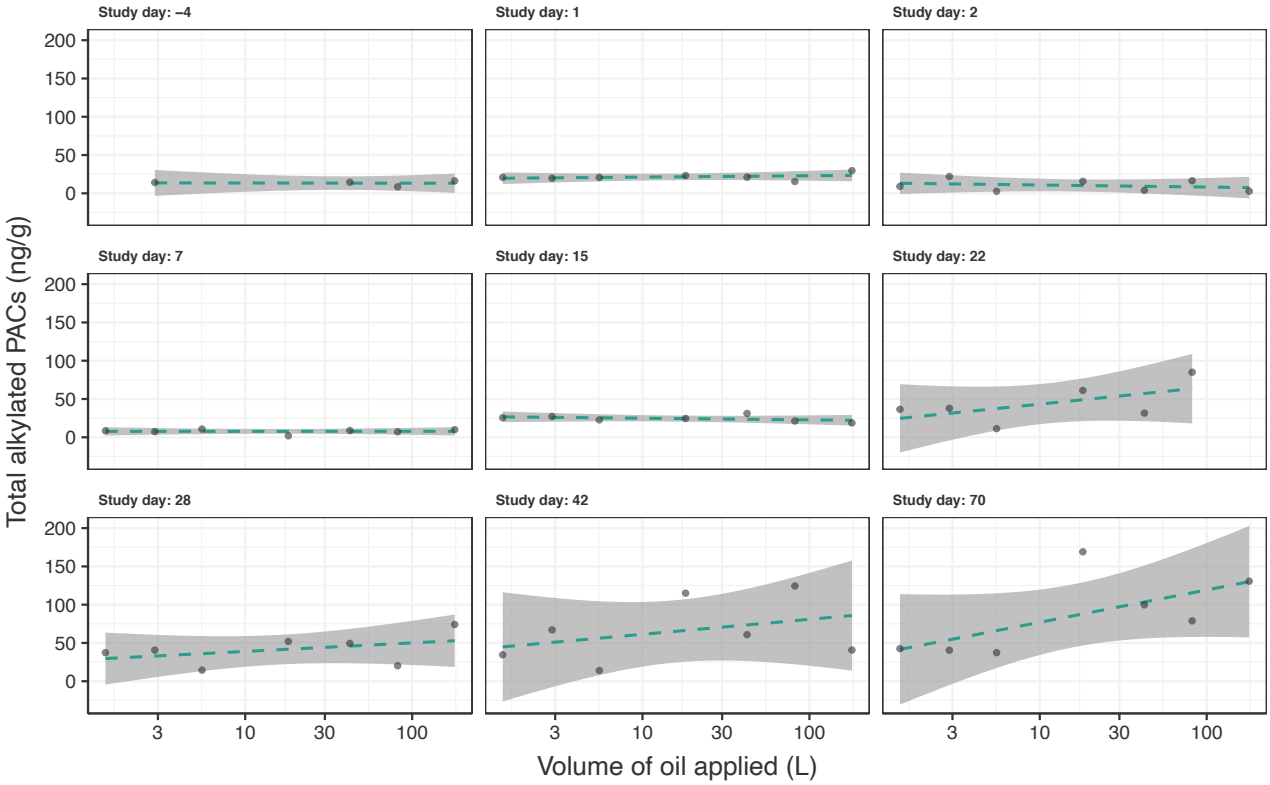

SI Figure 11: Relationship between the volume of oil applied and the sediment concentration of total alkylated aromatic polycyclic compounds (ΣPAC_{alk}) in the water column. The control treatments were excluded from the regression

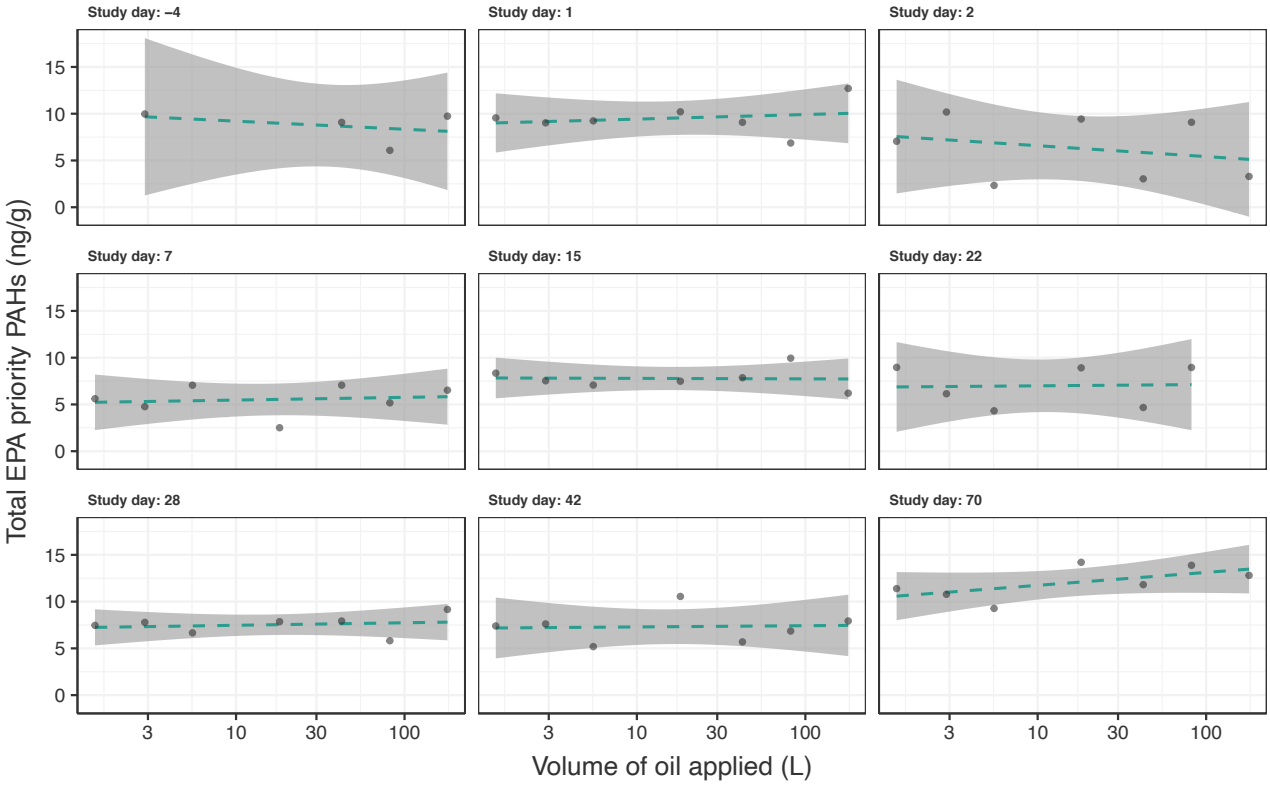

SI Figure 12: Relationship between the volume of oil applied and the sediment concentration of the sum of the 16 US EPA priority aromatic polycyclic hydrocarbons (ΣPAH_{16}) in the water column. The control treatments were excluded from the regression

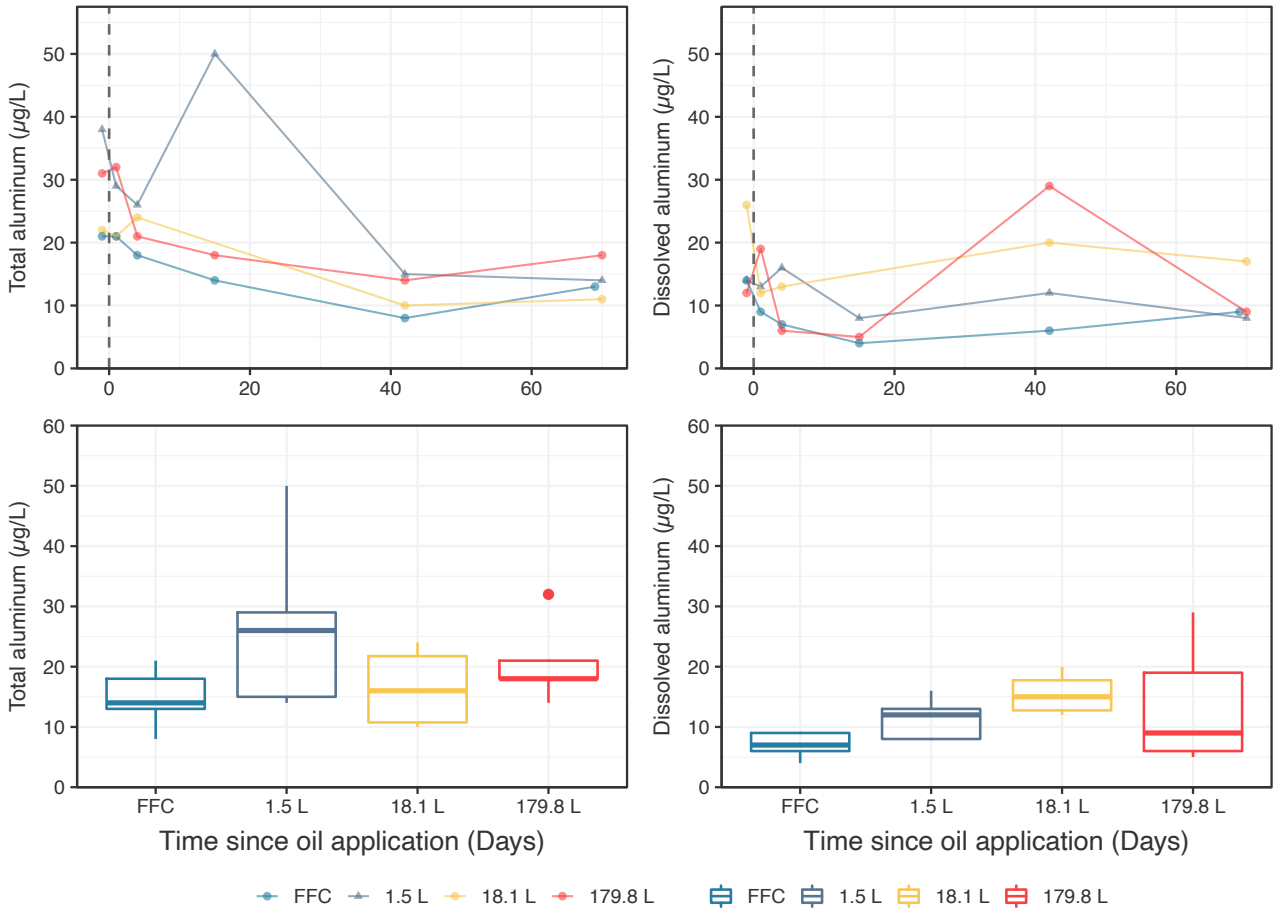

SI Figure 13: Upper panels: temporal progression of the concentrations of aluminum in the total (upper left) and dissolved (upper right) fractions of the water column. Lower panels: average values of the concentrations of aluminum in the total (lower left) and dissolved (lower right) fractions of the water column for the different treatments. Dashed vertical line in the upper panels indicates the day of oil addition (day 0)

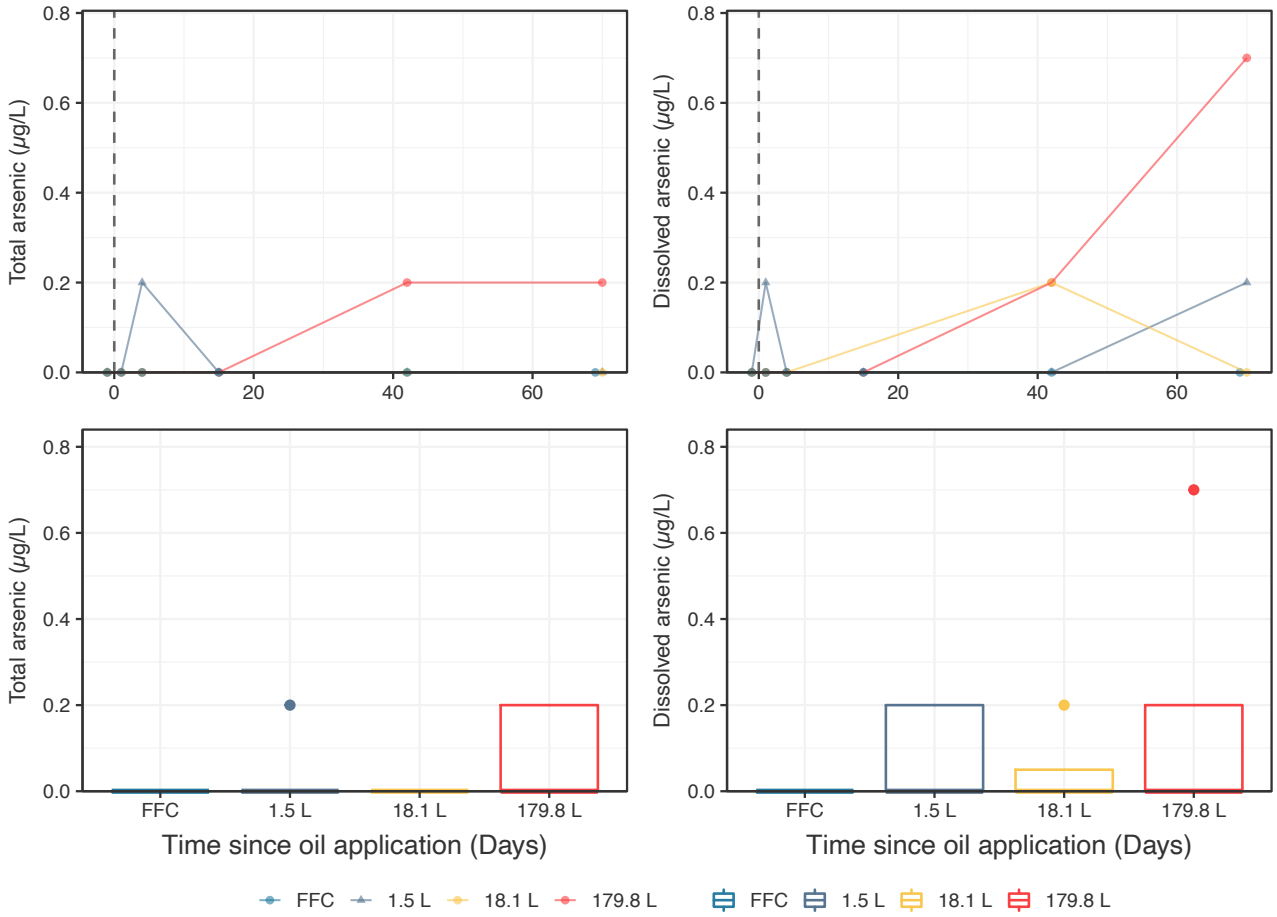

SI Figure 14: Upper panels: temporal progression of the concentrations of arsenic in the total (upper left) and dissolved (upper right) fractions of the water column. Lower panels: average values of the concentrations of arsenic in the total (lower left) and dissolved (lower right) fractions of the water column for the different treatments. Dashed vertical line in the upper panels indicates the day of oil addition (day 0)

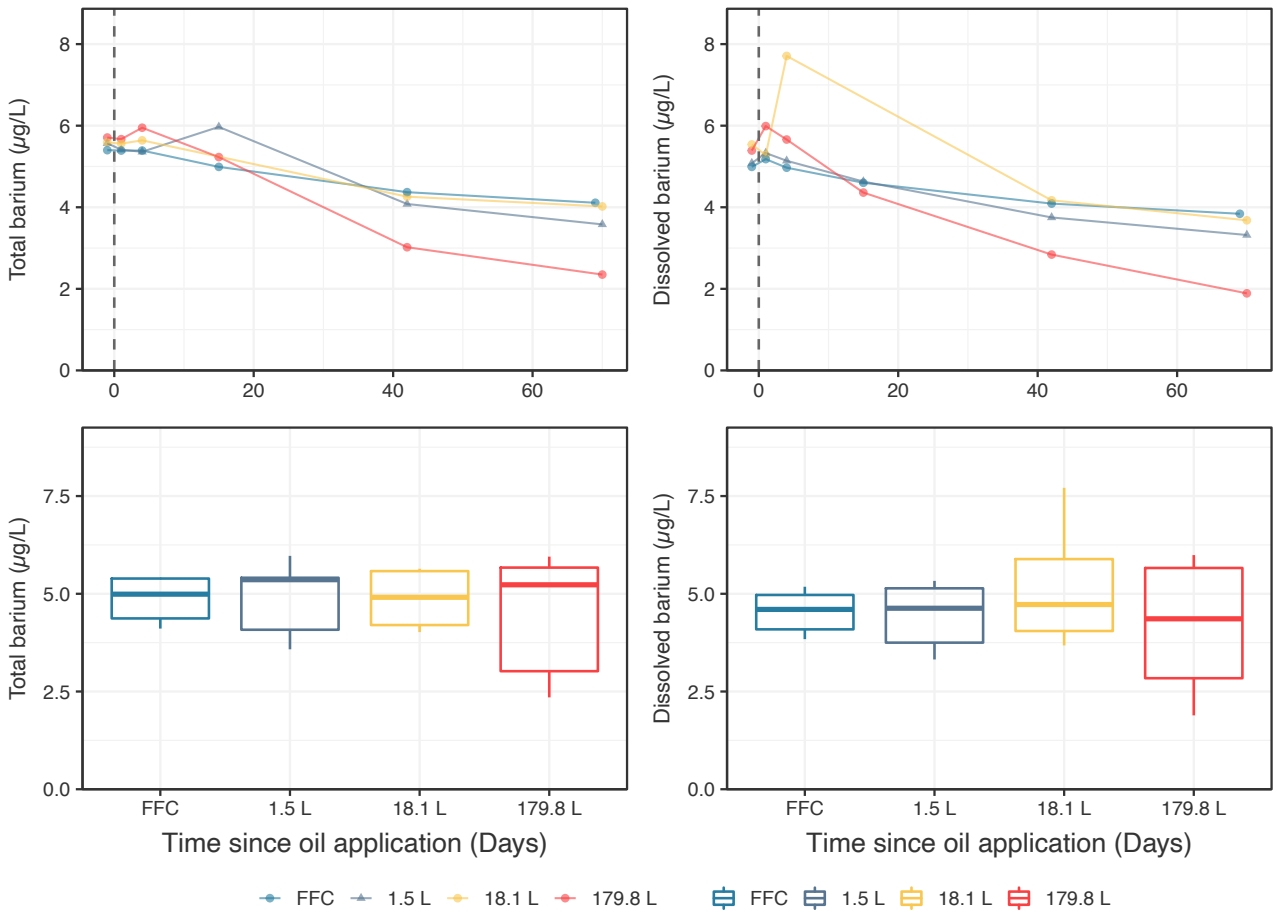

SI Figure 15: Upper panels: temporal progression of the concentrations of barium in the total (upper left) and dissolved (upper right) fractions of the water column. Lower panels: average values of the concentrations of barium in the total (lower left) and dissolved (lower right) fractions of the water column for the different treatments. Dashed vertical line in the upper panels indicates the day of oil addition (day 0)

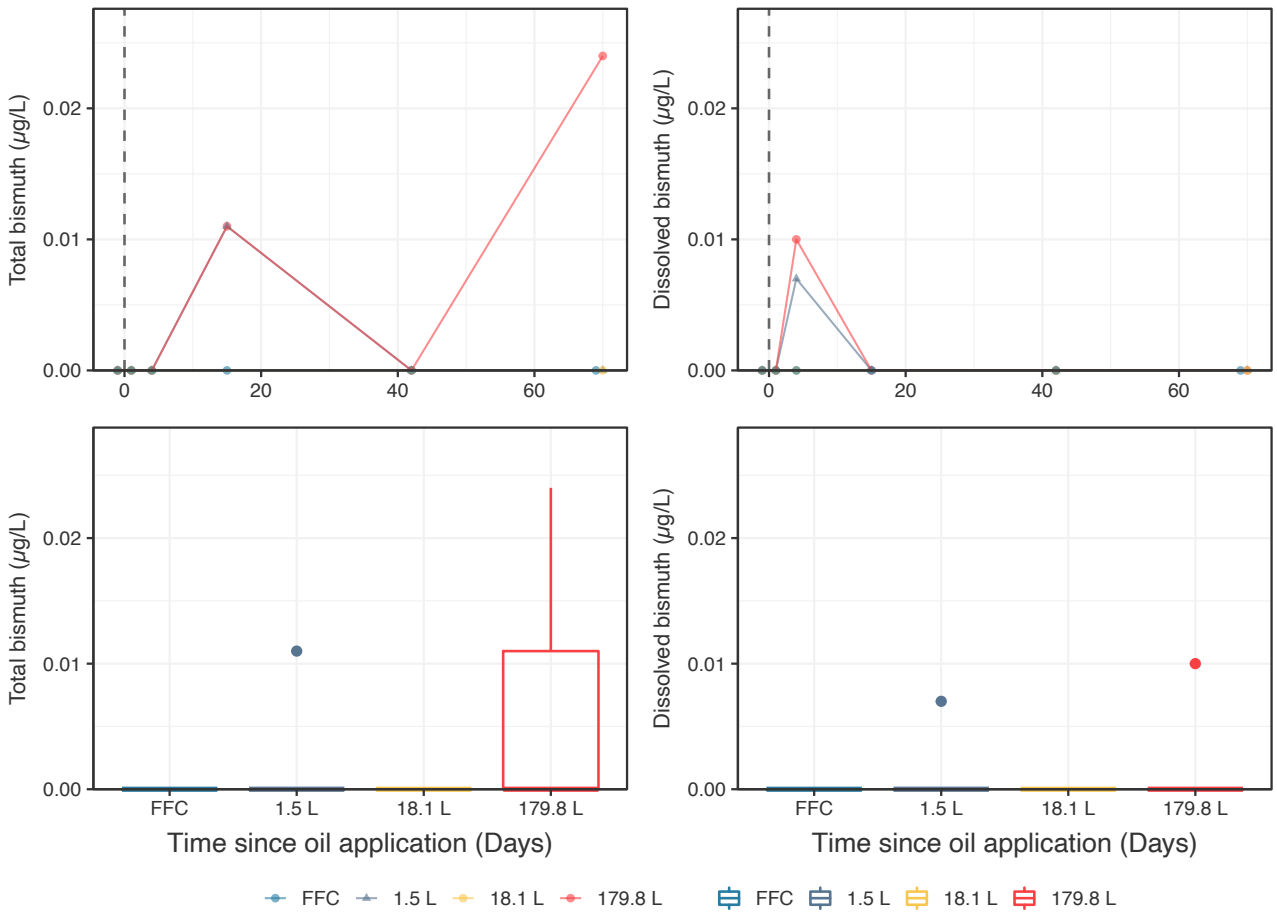

SI Figure 16: Upper panels: temporal progression of the concentrations of bismuth in the total (upper left) and dissolved (upper right) fractions of the water column. Lower panels: average values of the concentrations of bismuth in the total (lower left) and dissolved (lower right) fractions of the water column for the different treatments. Dashed vertical line in the upper panels indicates the day of oil addition (day 0)

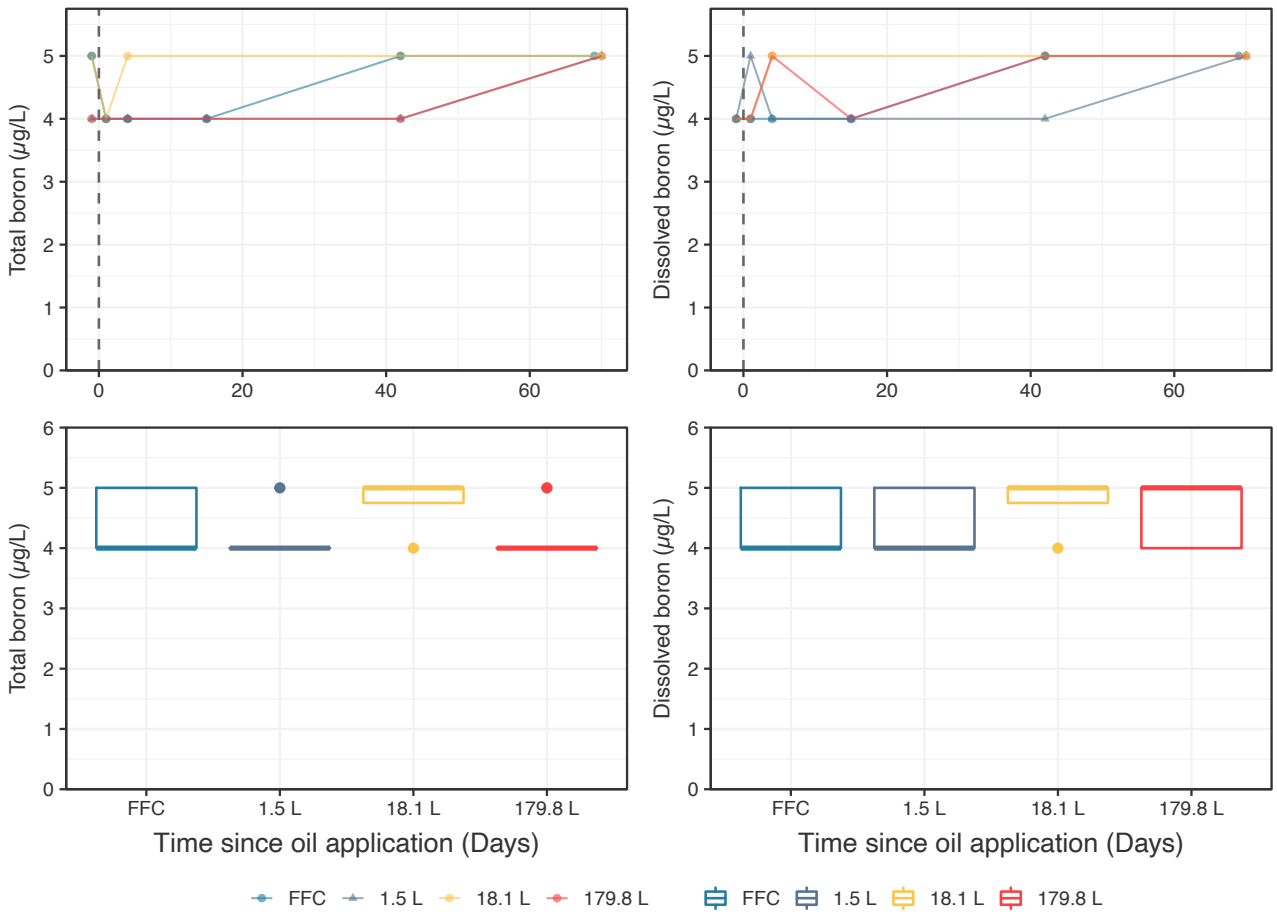

SI Figure 17: Upper panels: temporal progression of the concentrations of boron in the total (upper left) and dissolved (upper right) fractions of the water column. Lower panels: average values of the concentrations of boron in the total (lower left) and dissolved (lower right) fractions of the water column for the different treatments. Dashed vertical line in the upper panels indicates the day of oil addition (day 0)

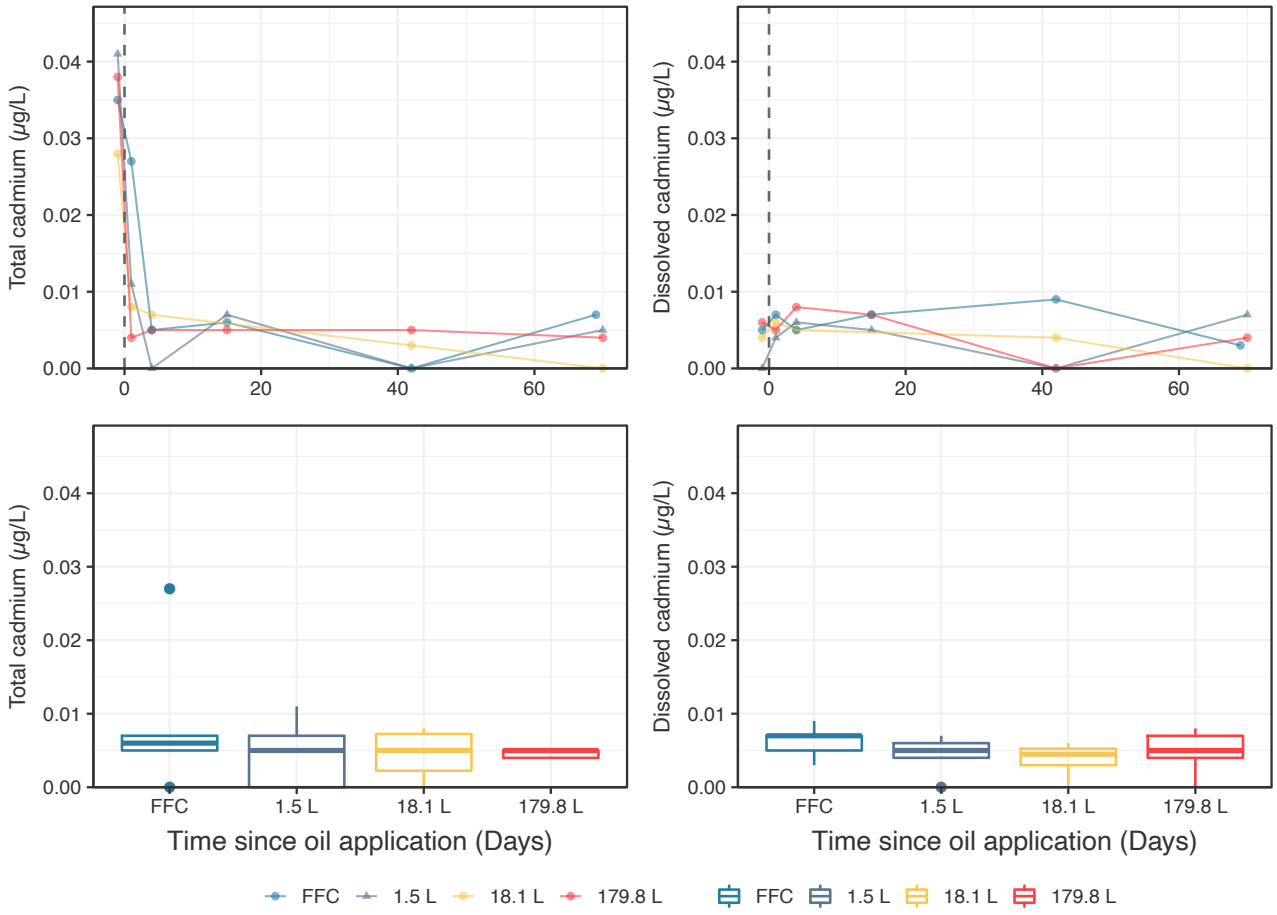

SI Figure 18: Upper panels: temporal progression of the concentrations of cadmium in the total (upper left) and dissolved (upper right) fractions of the water column. Lower panels: average values of the concentrations of cadmium in the total (lower left) and dissolved (lower right) fractions of the water column for the different treatments. Dashed vertical line in the upper panels indicates the day of oil addition (day 0)

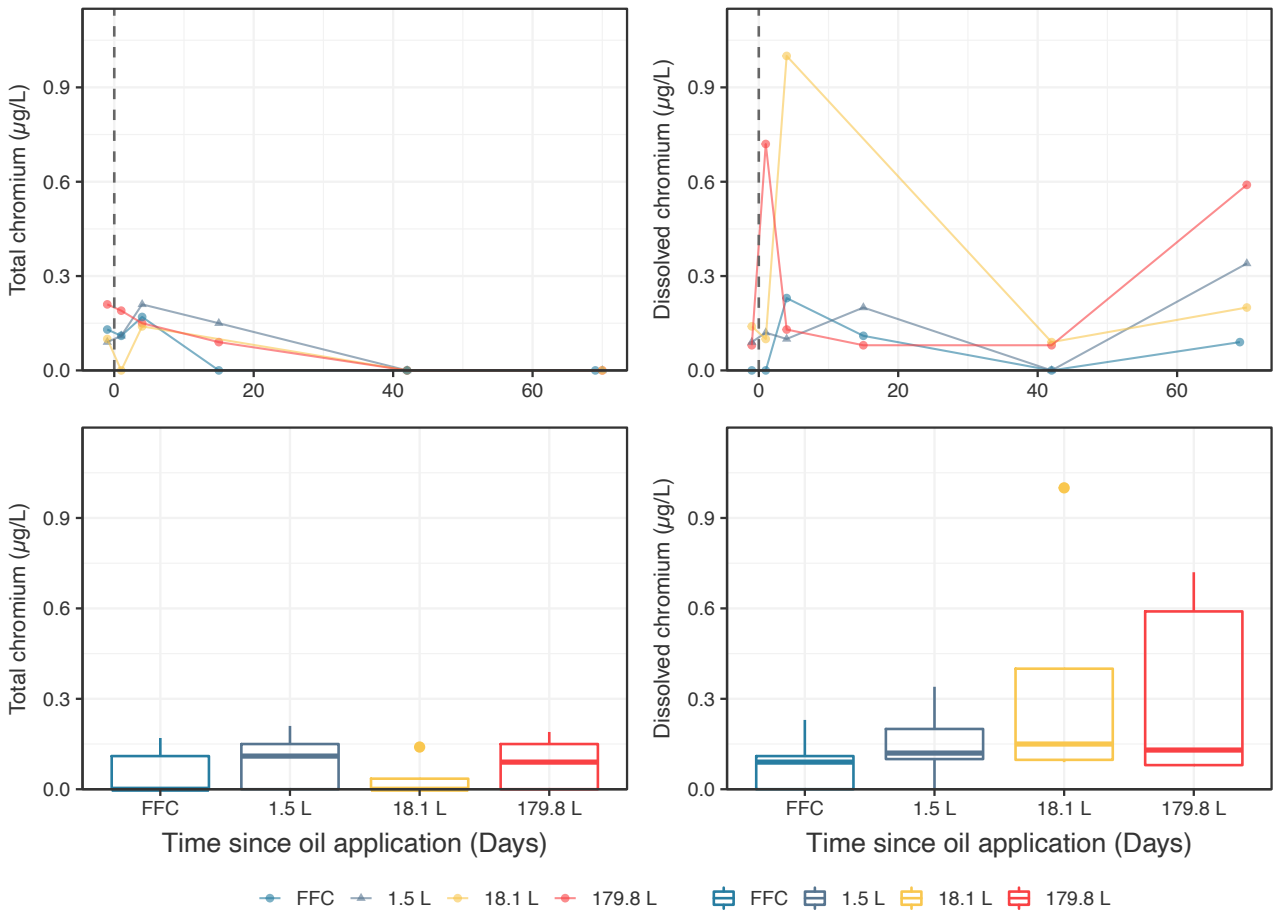

SI Figure 19: Upper panels: temporal progression of the concentrations of chromium in the total (upper left) and dissolved (upper right) fractions of the water column. Lower panels: average values of the concentrations of chromium in the total (lower left) and dissolved (lower right) fractions of the water column for the different treatments. Dashed vertical line in the upper panels indicates the day of oil addition (day 0)

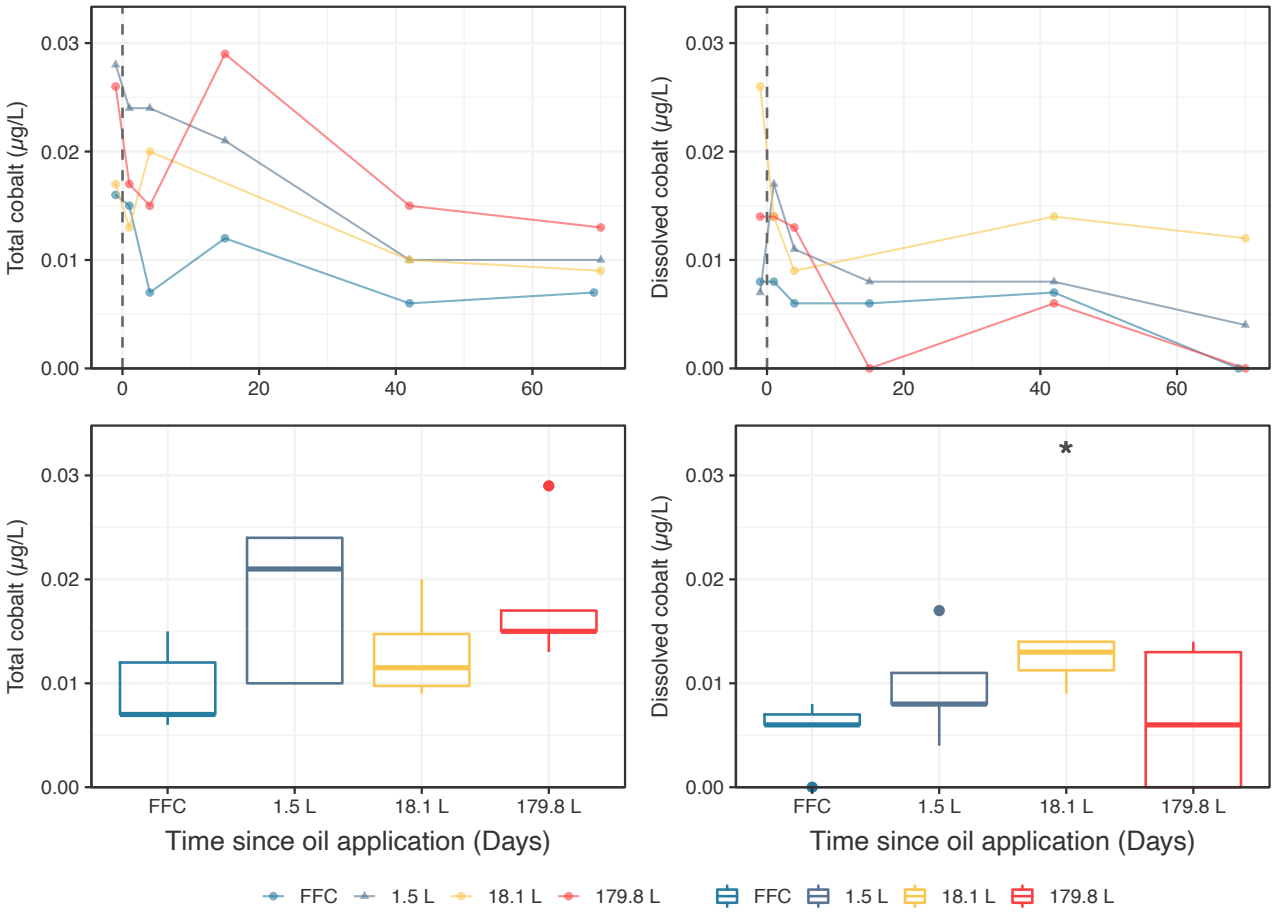

SI Figure 20: Upper panels: temporal progression of the concentrations of cobalt in the total (upper left) and dissolved (upper right) fractions of the water column. Lower panels: average values of the concentrations of cobalt in the total (lower left) and dissolved (lower right) fractions of the water column for the different treatments. Dashed vertical line in the upper panels indicates the day of oil addition (day 0)

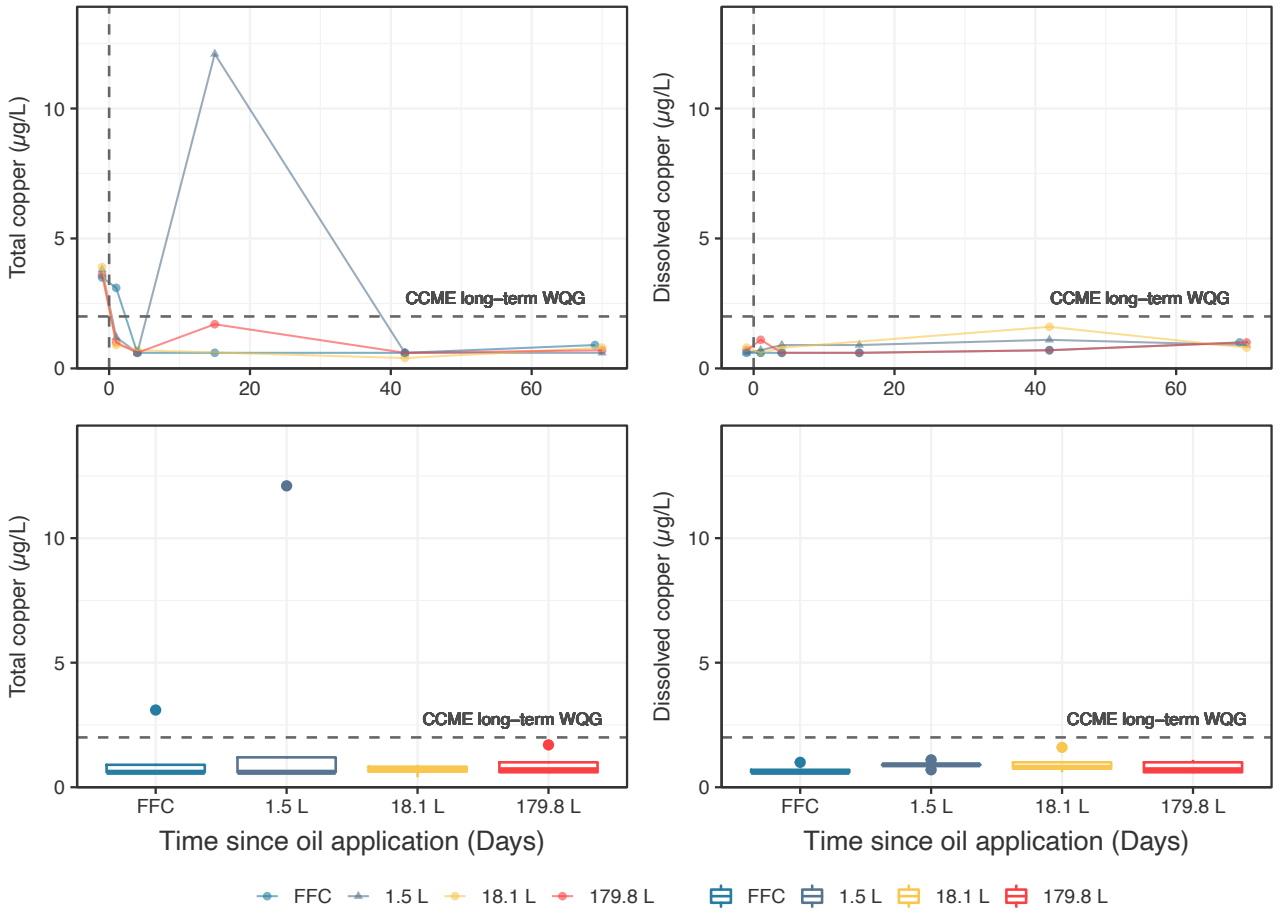

SI Figure 21: Upper panels: temporal progression of the concentrations of copper in the total (upper left) and dissolved (upper right) fractions of the water column. Lower panels: average values of the concentrations of copper in the total (lower left) and dissolved (lower right) fractions of the water column for the different treatments. Dashed vertical line in the upper panels indicates the day of oil addition (day 0). Dashed horizontal lines indicates the CCME long term water quality guideline value.

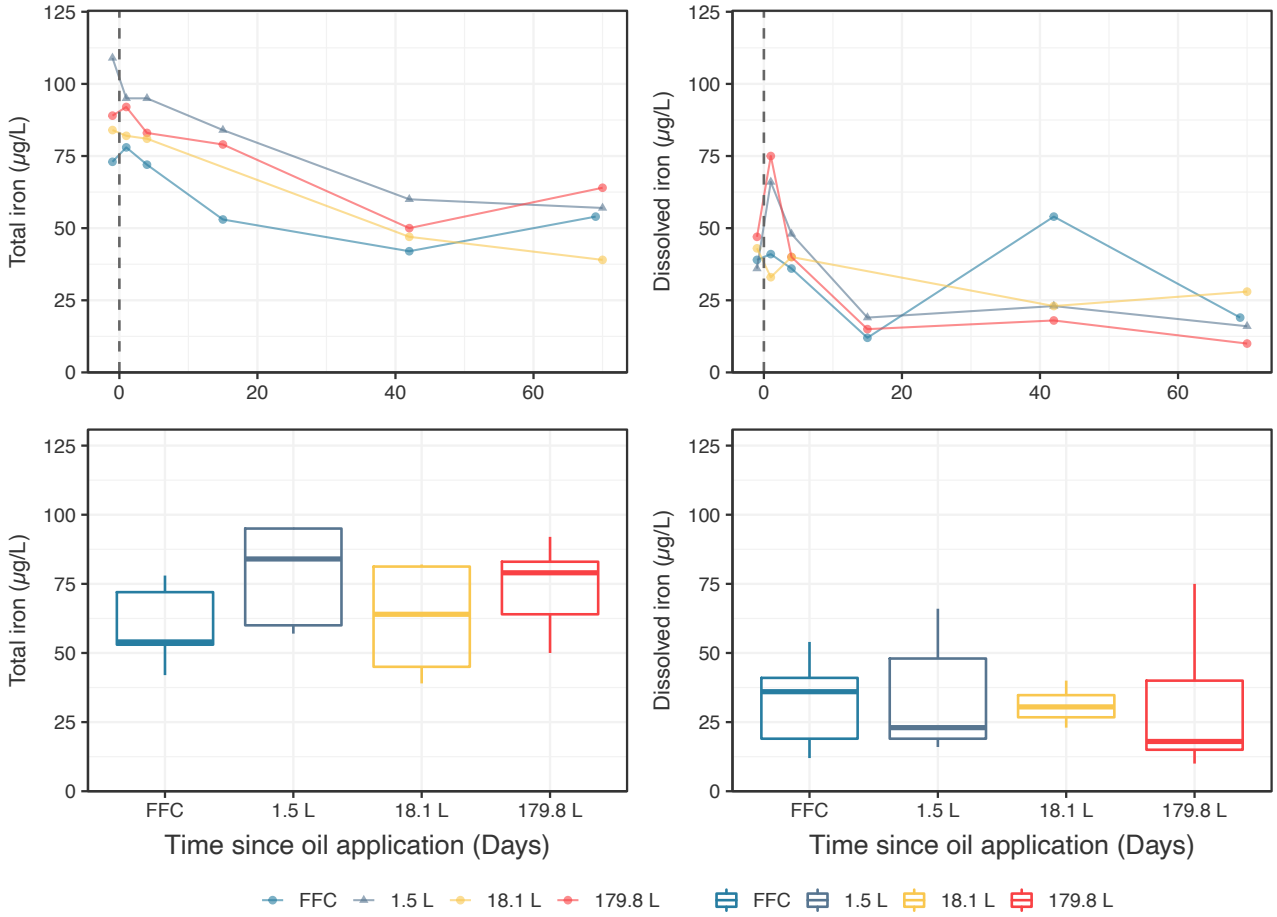

SI Figure 22: Upper panels: temporal progression of the concentrations of iron in the total (upper left) and dissolved (upper right) fractions of the water column. Lower panels: average values of the concentrations of iron in the total (lower left) and dissolved (lower right) fractions of the water column for the different treatments. Dashed vertical line in the upper panels indicates the day of oil addition (day 0)

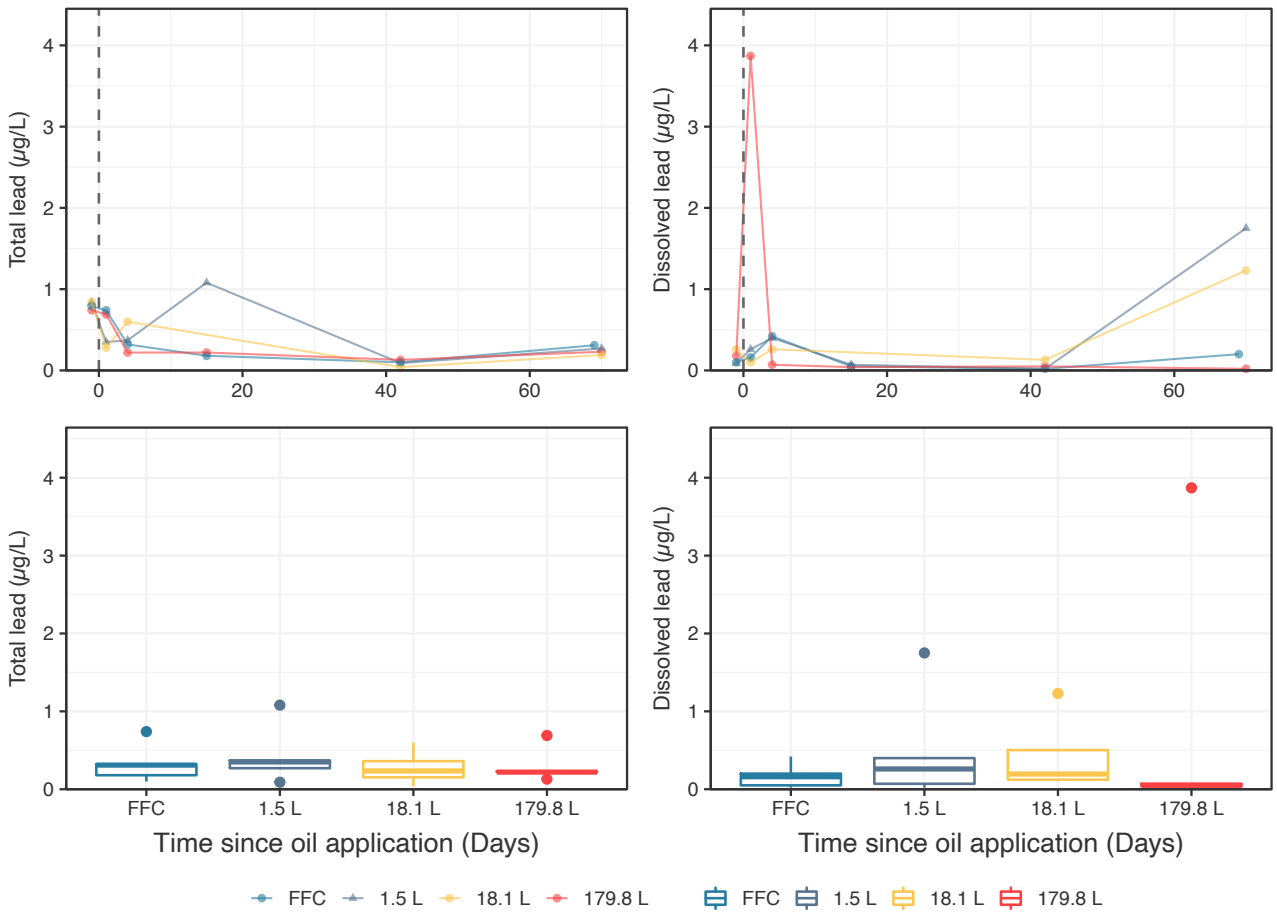

SI Figure 23: Upper panels: temporal progression of the concentrations of led in the total (upper left) and dissolved (upper right) fractions of the water column. Lower panels: average values of the concentrations of led in the total (lower left) and dissolved (lower right) fractions of the water column for the different treatments. Dashed vertical line in the upper panels indicates the day of oil addition (day 0)

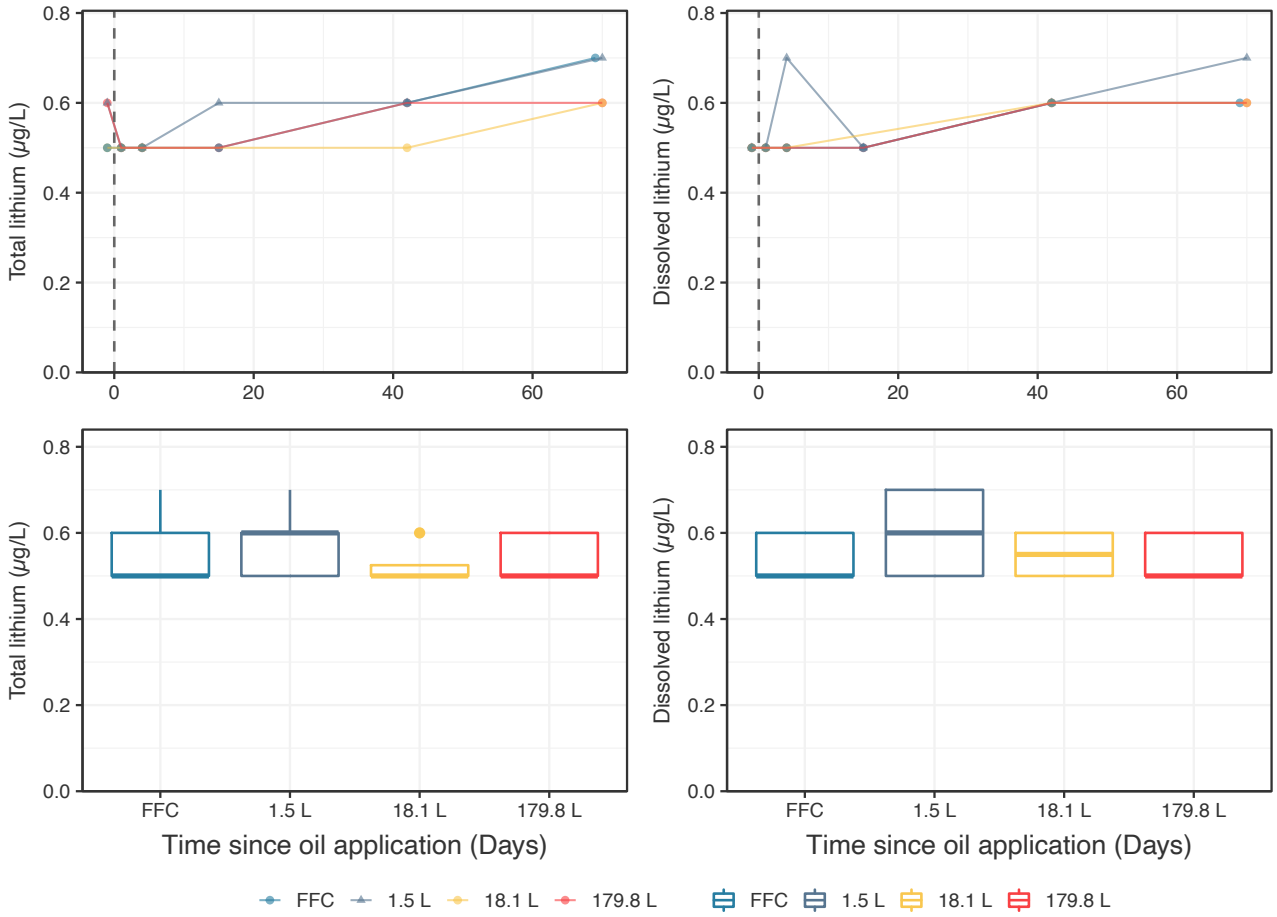

SI Figure 24: Upper panels: temporal progression of the concentrations of lithium in the total (upper left) and dissolved (upper right) fractions of the water column. Lower panels: average values of the concentrations of lithium in the total (lower left) and dissolved (lower right) fractions of the water column for the different treatments. Dashed vertical line in the upper panels indicates the day of oil addition (day 0)

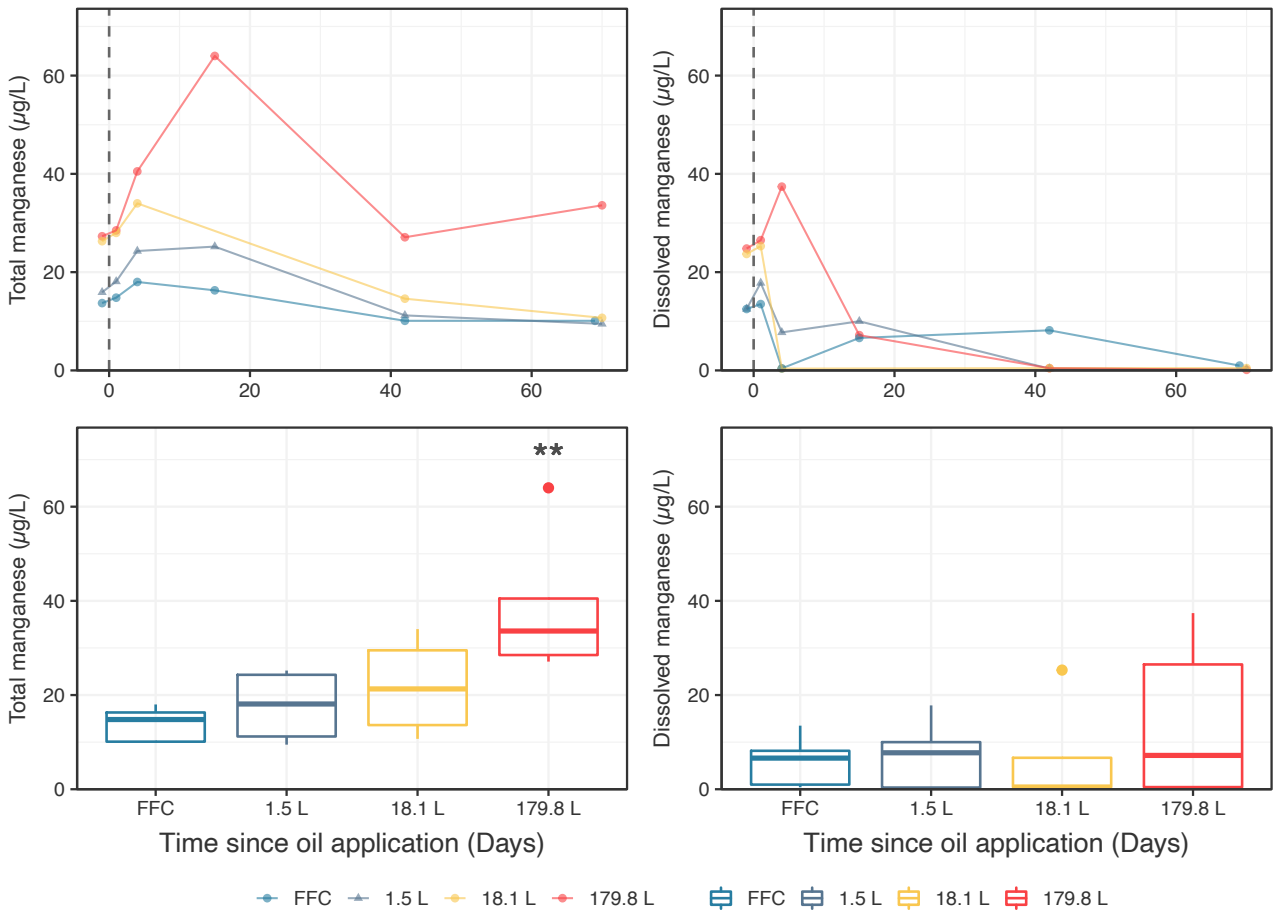

SI Figure 25: Upper panels: temporal progression of the concentrations of manganese in the total (upper left) and dissolved (upper right) fractions of the water column. Lower panels: average values of the concentrations of manganese in the total (lower left) and dissolved (lower right) fractions of the water column for the different treatments. Dashed vertical line in the upper panels indicates the day of oil addition (day 0)

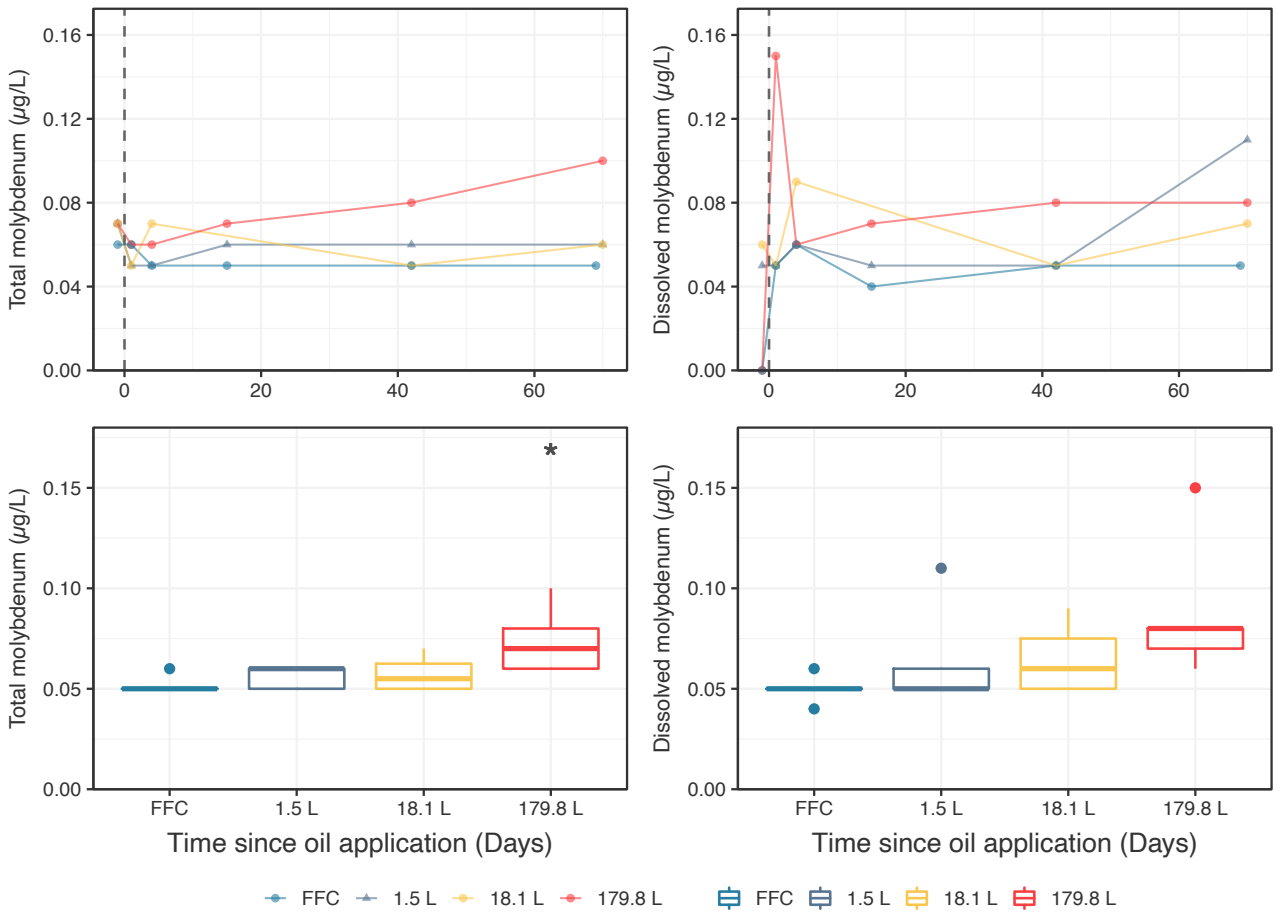

SI Figure 26: Upper panels: temporal progression of the concentrations of molybdenum in the total (upper left) and dissolved (upper right) fractions of the water column. Lower panels: average values of the concentrations of molybdenum in the total (lower left) and dissolved (lower right) fractions of the water column for the different treatments. Dashed vertical line in the upper panels indicates the day of oil addition (day 0)

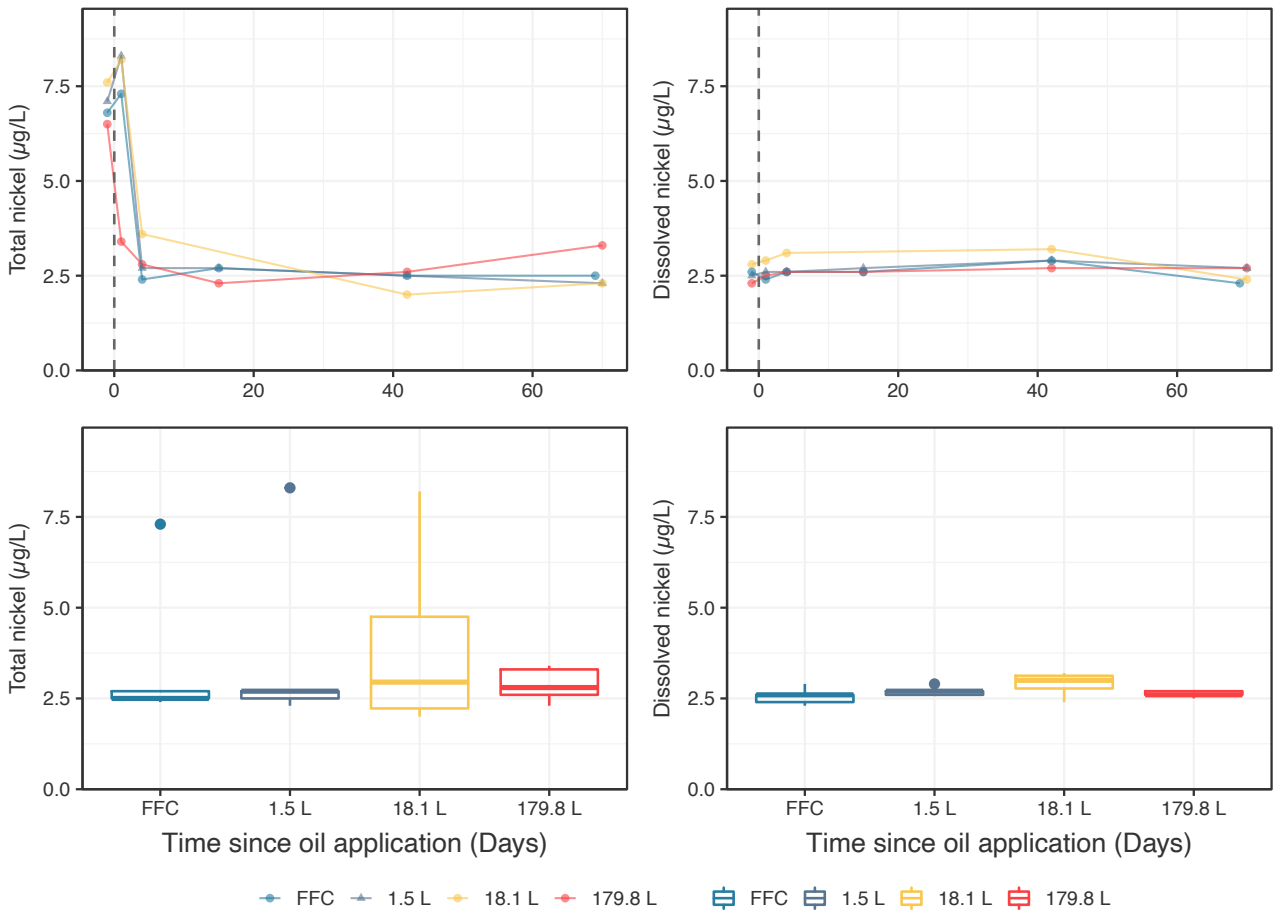

SI Figure 27: Upper panels: temporal progression of the concentrations of nickel in the total (upper left) and dissolved (upper right) fractions of the water column. Lower panels: average values of the concentrations of nickel in the total (lower left) and dissolved (lower right) fractions of the water column for the different treatments. Dashed vertical line in the upper panels indicates the day of oil addition (day 0)

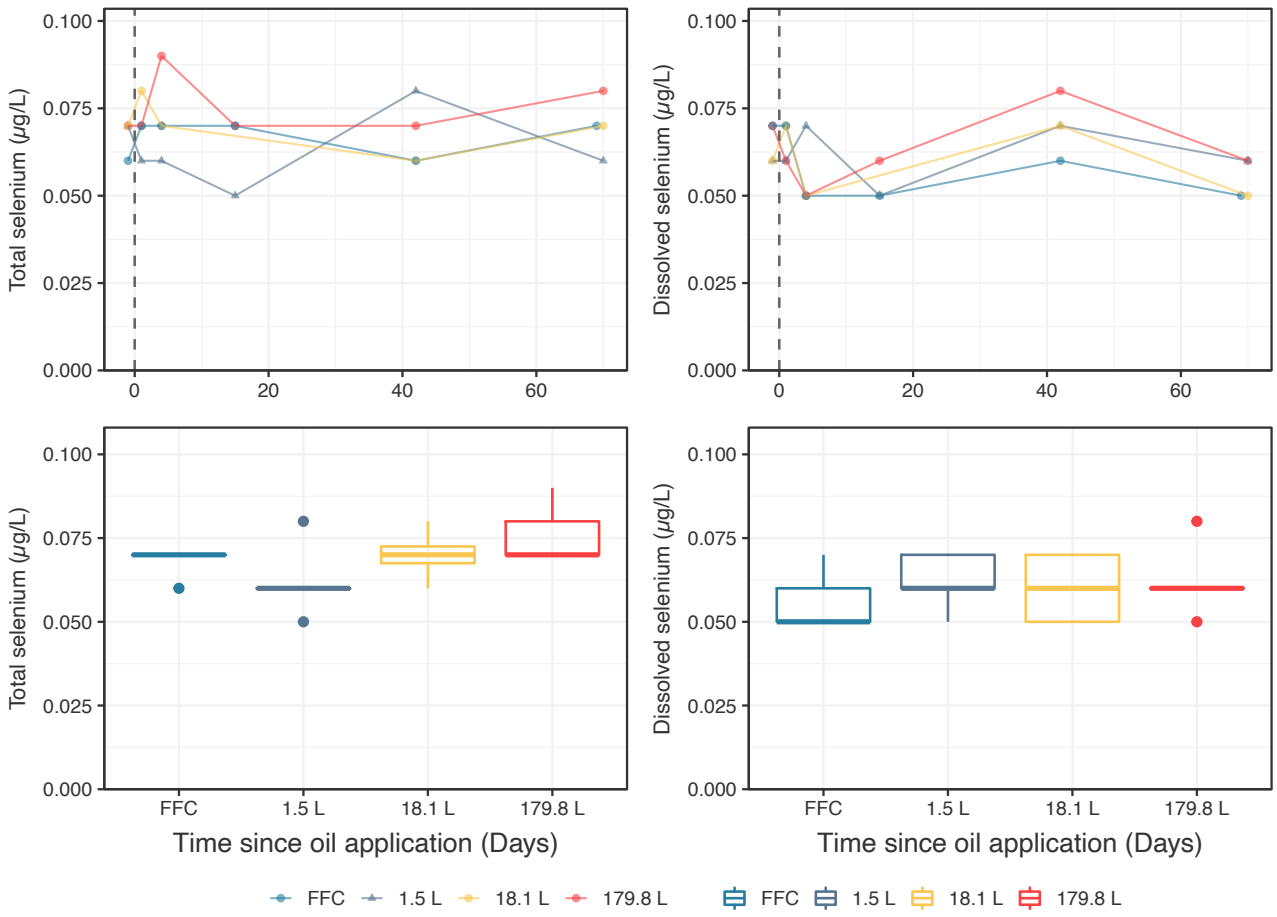

SI Figure 28: Upper panels: temporal progression of the concentrations of selenium in the total (upper left) and dissolved (upper right) fractions of the water column. Lower panels: average values of the concentrations of selenium in the total (lower left) and dissolved (lower right) fractions of the water column for the different treatments. Dashed vertical line in the upper panels indicates the day of oil addition (day 0)

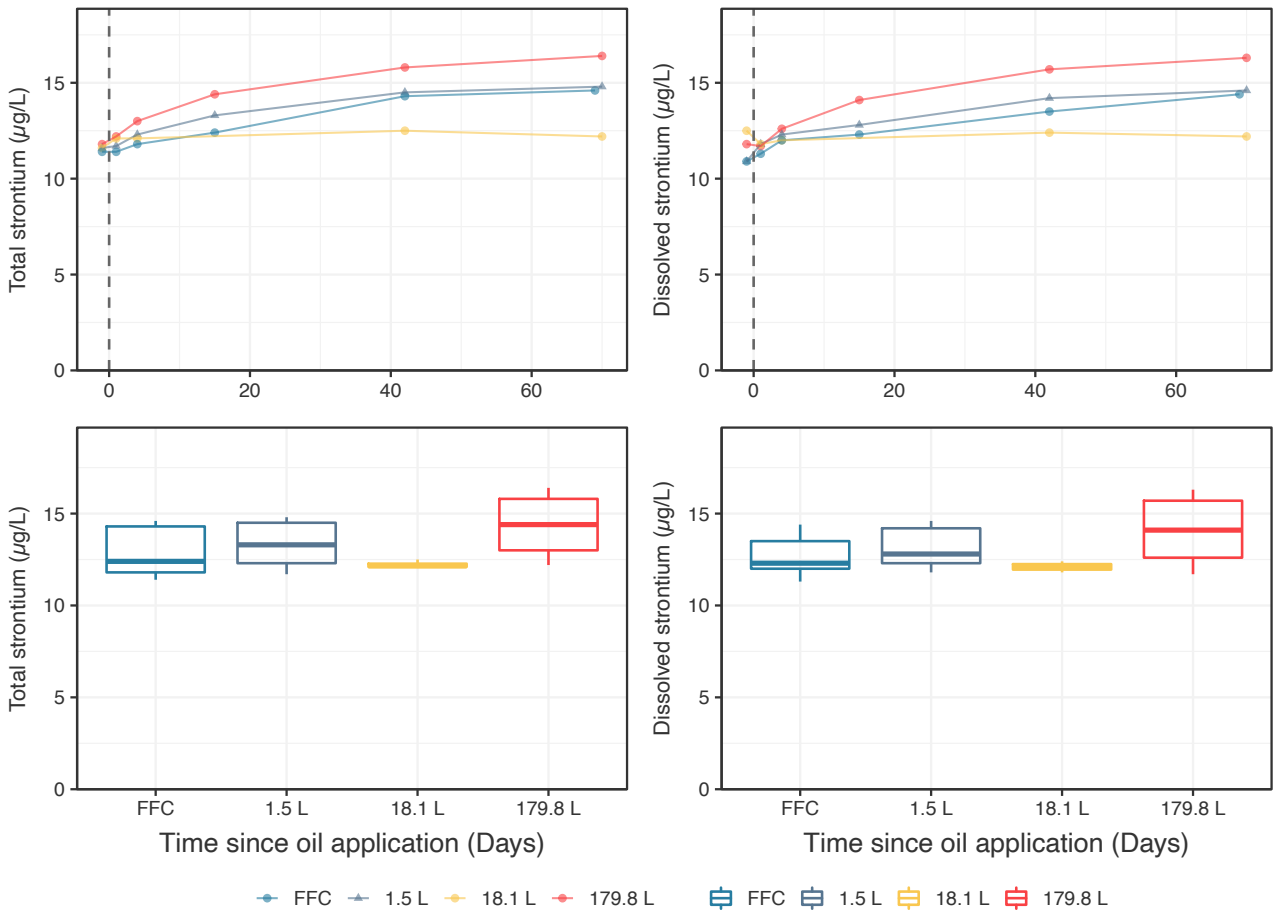

SI Figure 29: Upper panels: temporal progression of the concentrations of strontium in the total (upper left) and dissolved (upper right) fractions of the water column. Lower panels: average values of the concentrations of strontium in the total (lower left) and dissolved (lower right) fractions of the water column for the different treatments. Dashed vertical line in the upper panels indicates the day of oil addition (day 0)

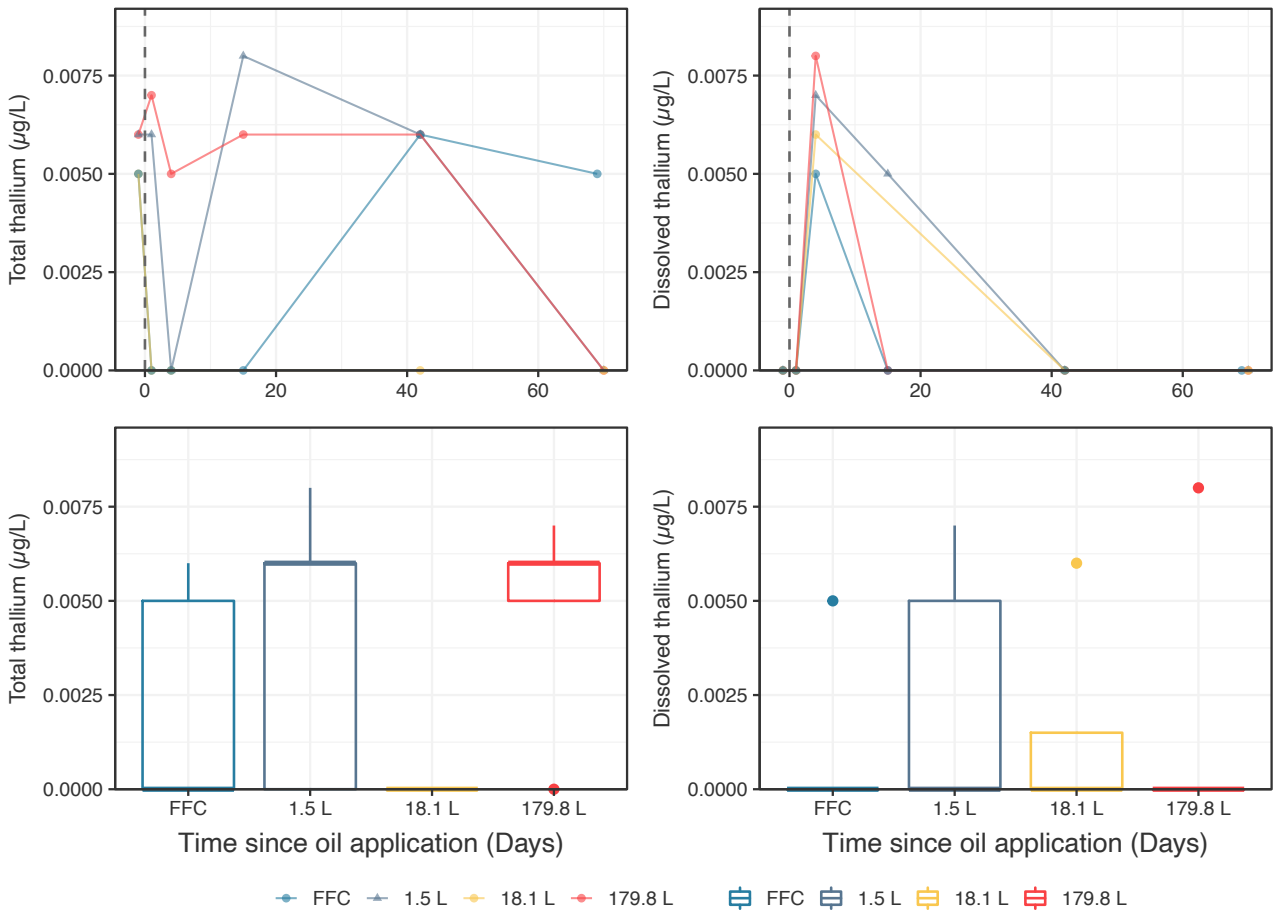

SI Figure 30: Upper panels: temporal progression of the concentrations of thalium in the total (upper left) and dissolved (upper right) fractions of the water column. Lower panels: average values of the concentrations of thalium in the total (lower left) and dissolved (lower right) fractions of the water column for the different treatments. Dashed vertical line in the upper panels indicates the day of oil addition (day 0)

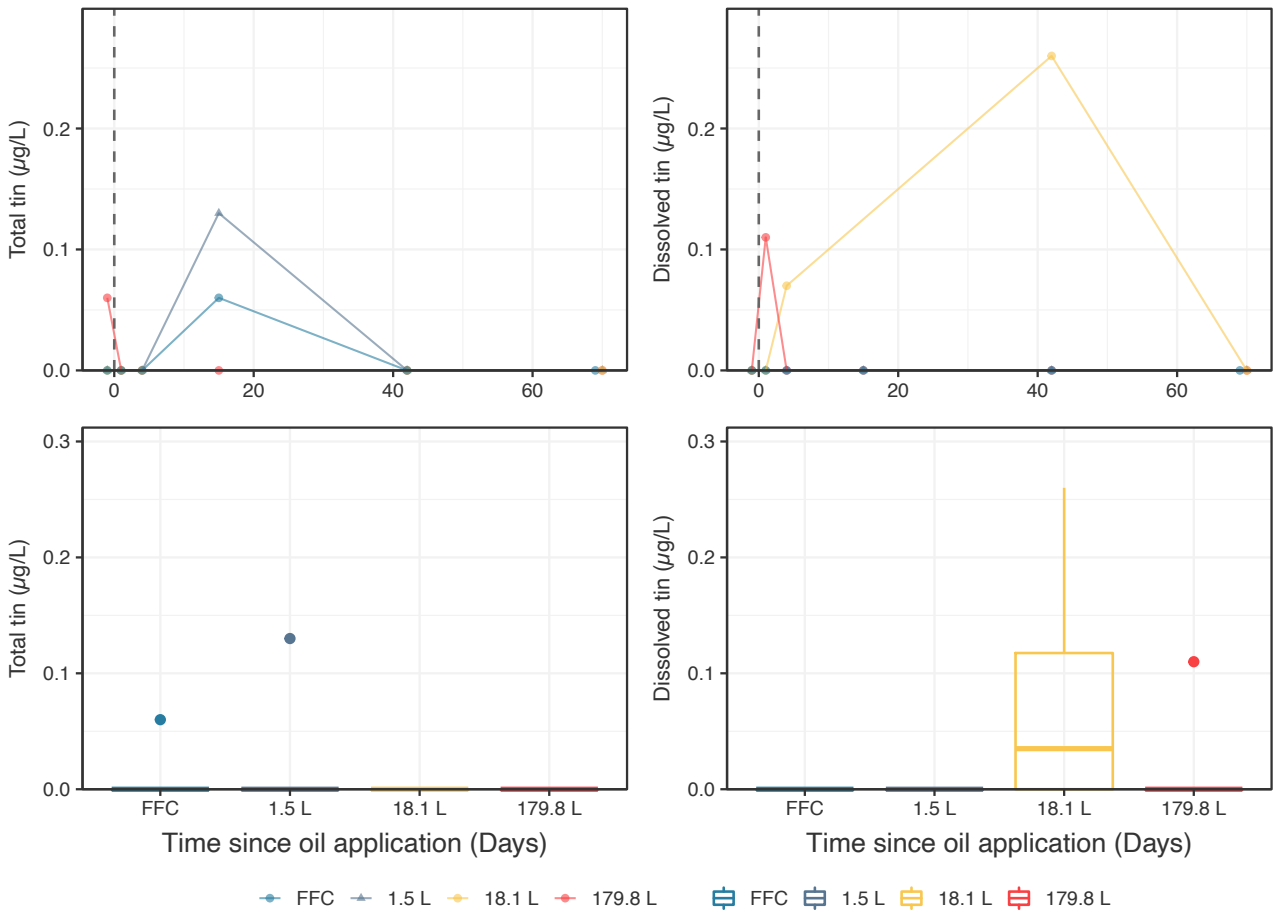

SI Figure 31: Upper panels: temporal progression of the concentrations of tin in the total (upper left) and dissolved (upper right) fractions of the water column. Lower panels: average values of the concentrations of tin in the total (lower left) and dissolved (lower right) fractions of the water column for the different treatments. Dashed vertical line in the upper panels indicates the day of oil addition (day 0)

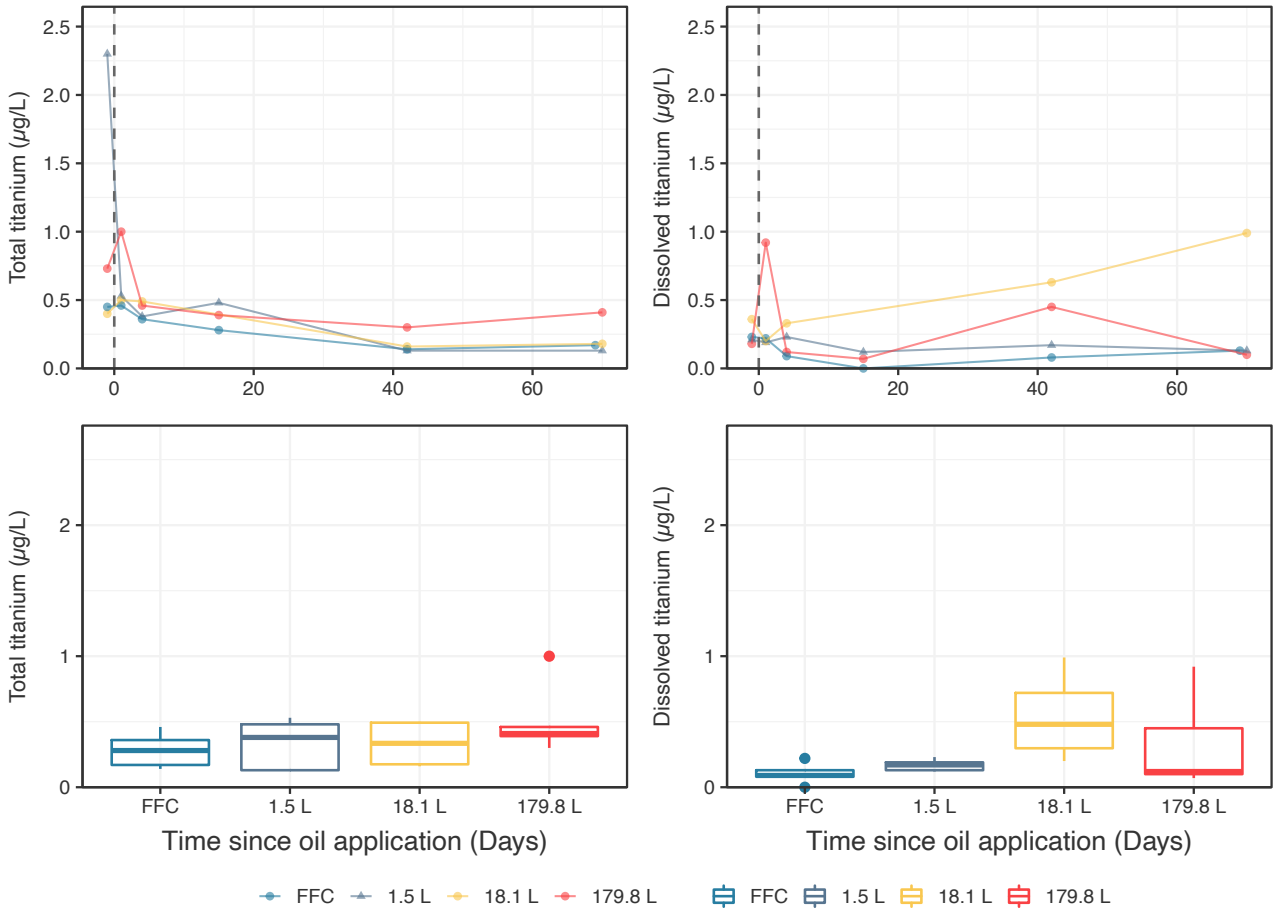

SI Figure 32: Upper panels: temporal progression of the concentrations of titanium in the total (upper left) and dissolved (upper right) fractions of the water column. Lower panels: average values of the concentrations of titanium in the total (lower left) and dissolved (lower right) fractions of the water column for the different treatments. Dashed vertical line in the upper panels indicates the day of oil addition (day 0)

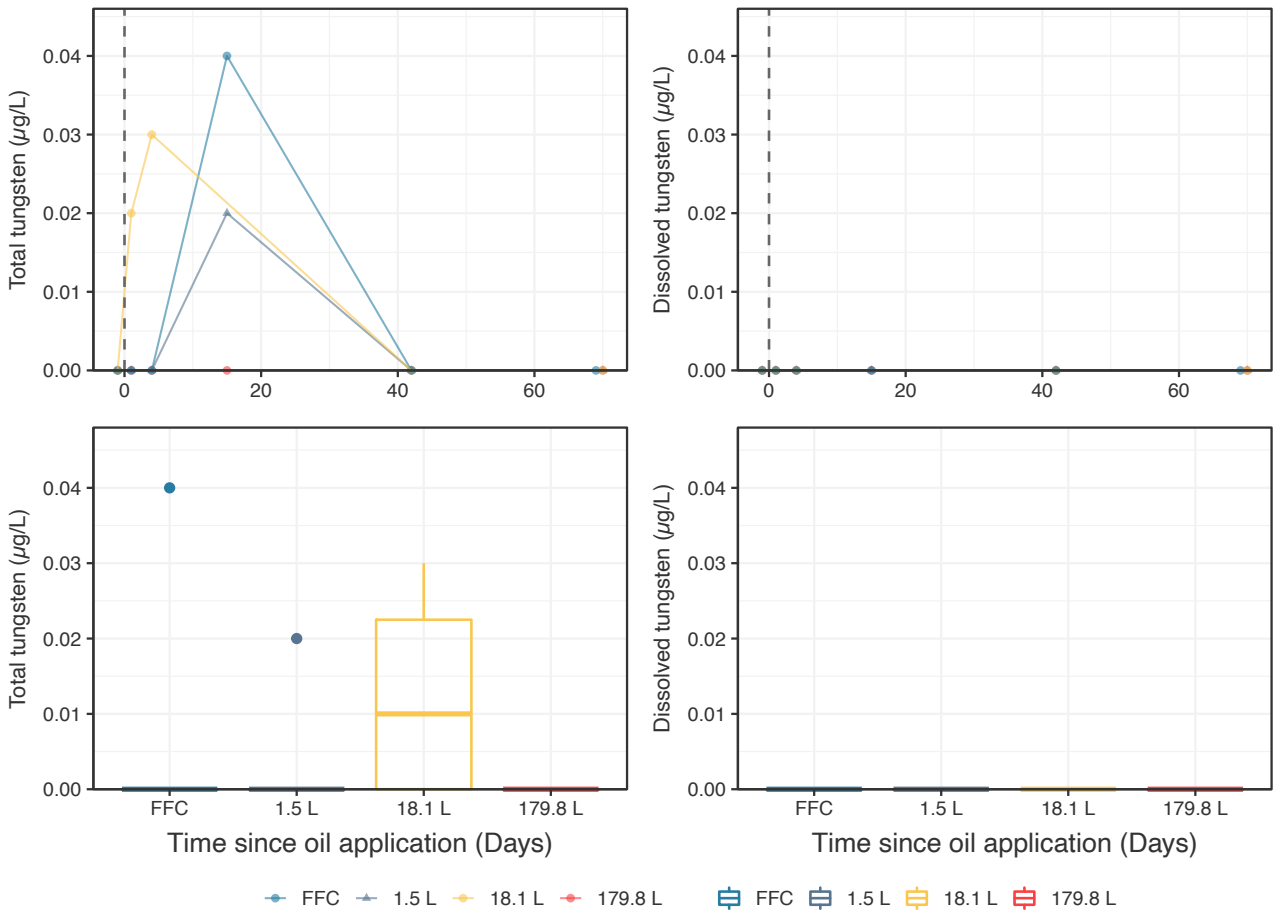

SI Figure 33: Upper panels: temporal progression of the concentrations of tungsten in the total (upper left) and dissolved (upper right) fractions of the water column. Lower panels: average values of the concentrations of tungsten in the total (lower left) and dissolved (lower right) fractions of the water column for the different treatments. Dashed vertical line in the upper panels indicates the day of oil addition (day 0)

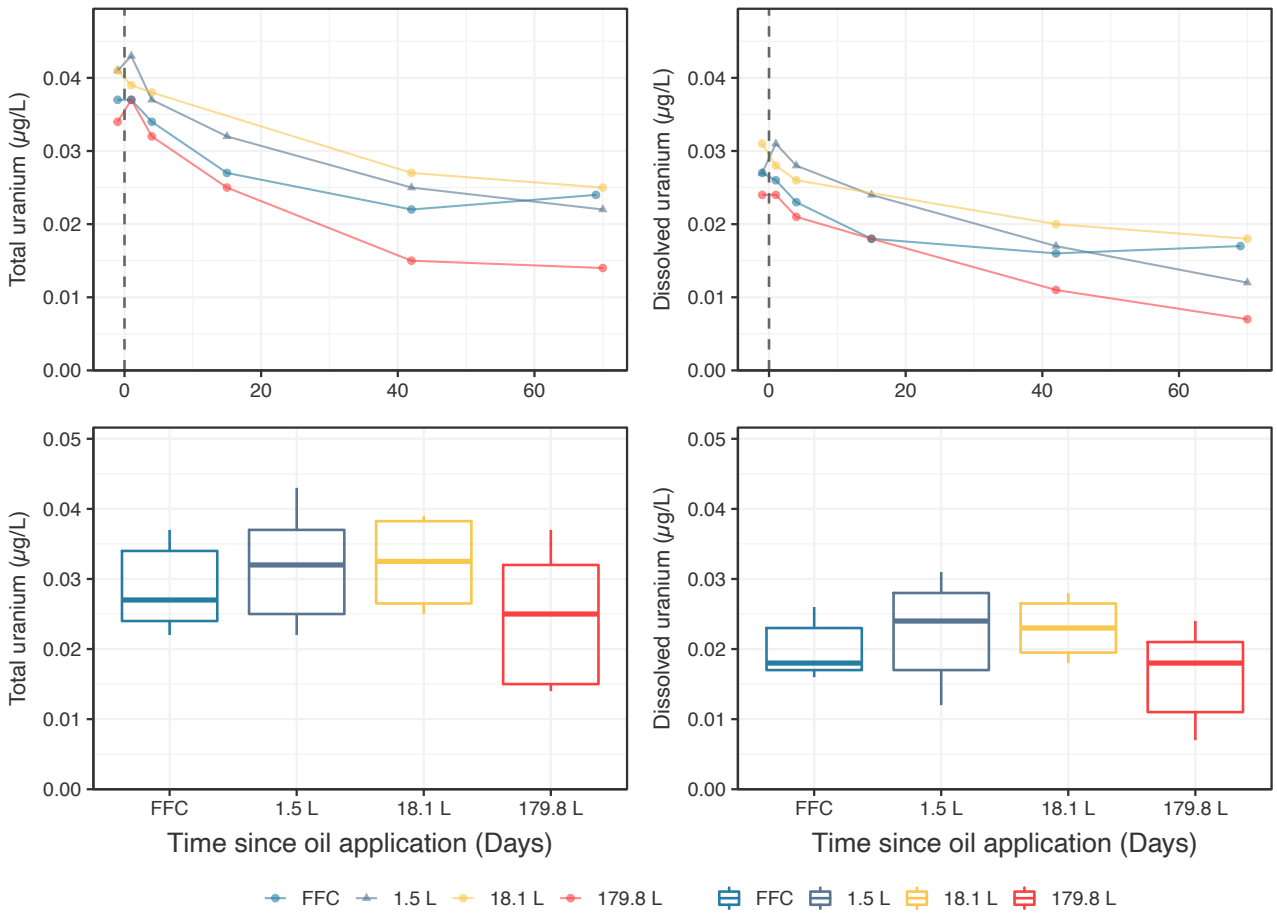

SI Figure 34: Upper panels: temporal progression of the concentrations of uranium in the total (upper left) and dissolved (upper right) fractions of the water column. Lower panels: average values of the concentrations of uranium in the total (lower left) and dissolved (lower right) fractions of the water column for the different treatments. Dashed vertical line in the upper panels indicates the day of oil addition (day 0)

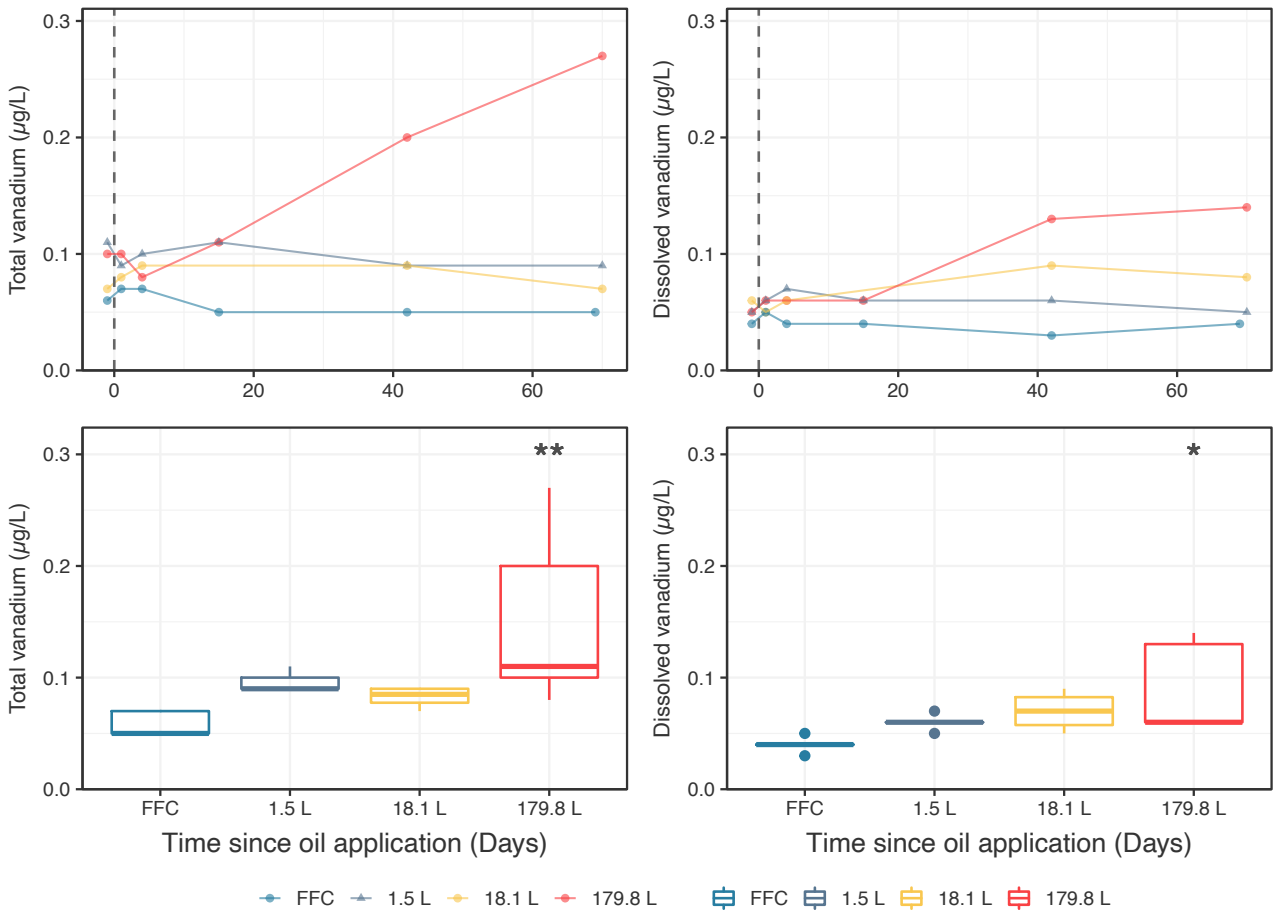

SI Figure 35: Upper panels: temporal progression of the concentrations of vanadium in the total (upper left) and dissolved (upper right) fractions of the water column. Lower panels: average values of the concentrations of vanadium in the total (lower left) and dissolved (lower right) fractions of the water column for the different treatments. Dashed vertical line in the upper panels indicates the day of oil addition (day 0)

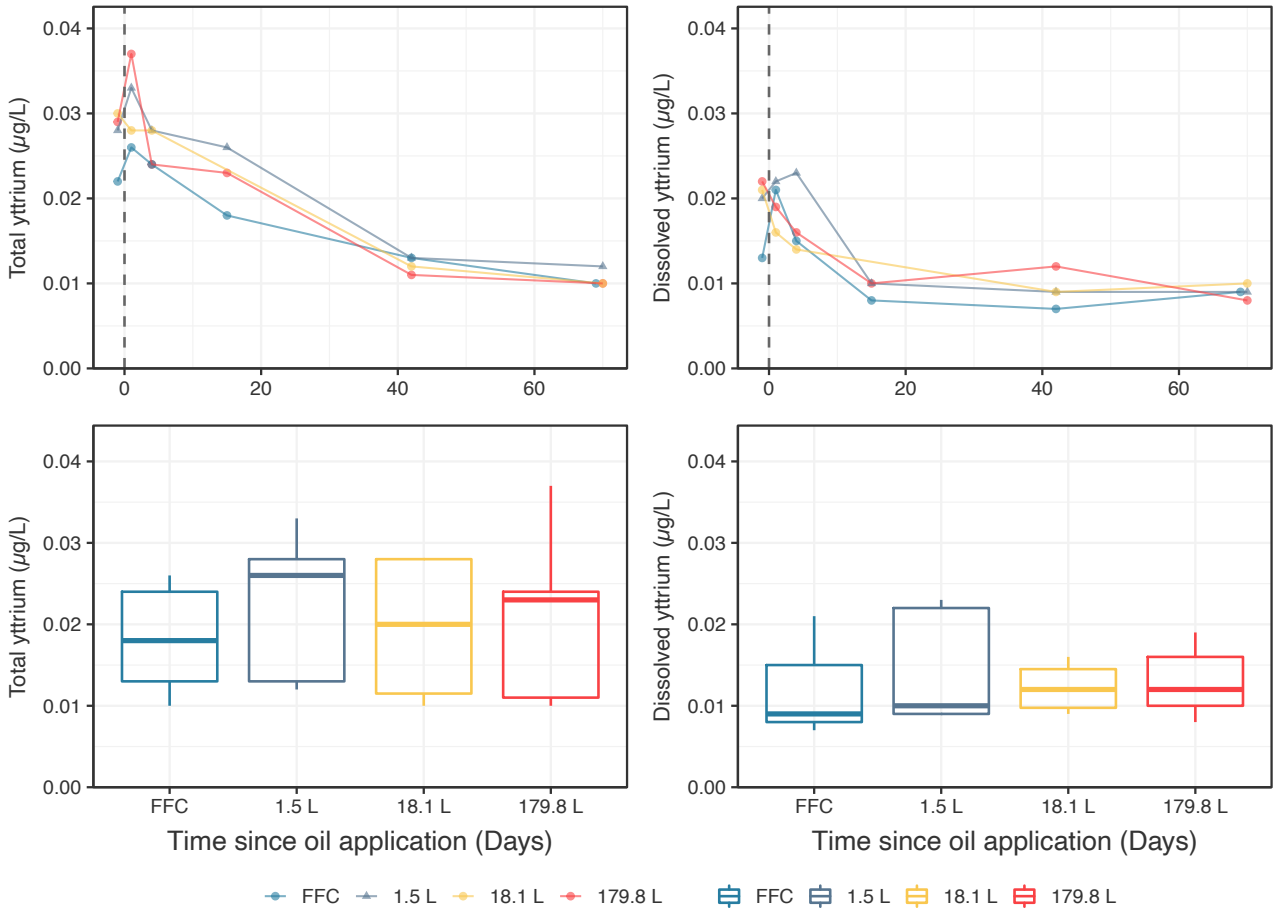

SI Figure 36: Upper panels: temporal progression of the concentrations of ytrium in the total (upper left) and dissolved (upper right) fractions of the water column. Lower panels: average values of the concentrations of ytrium in the total (lower left) and dissolved (lower right) fractions of the water column for the different treatments. Dashed vertical line in the upper panels indicates the day of oil addition (day 0)

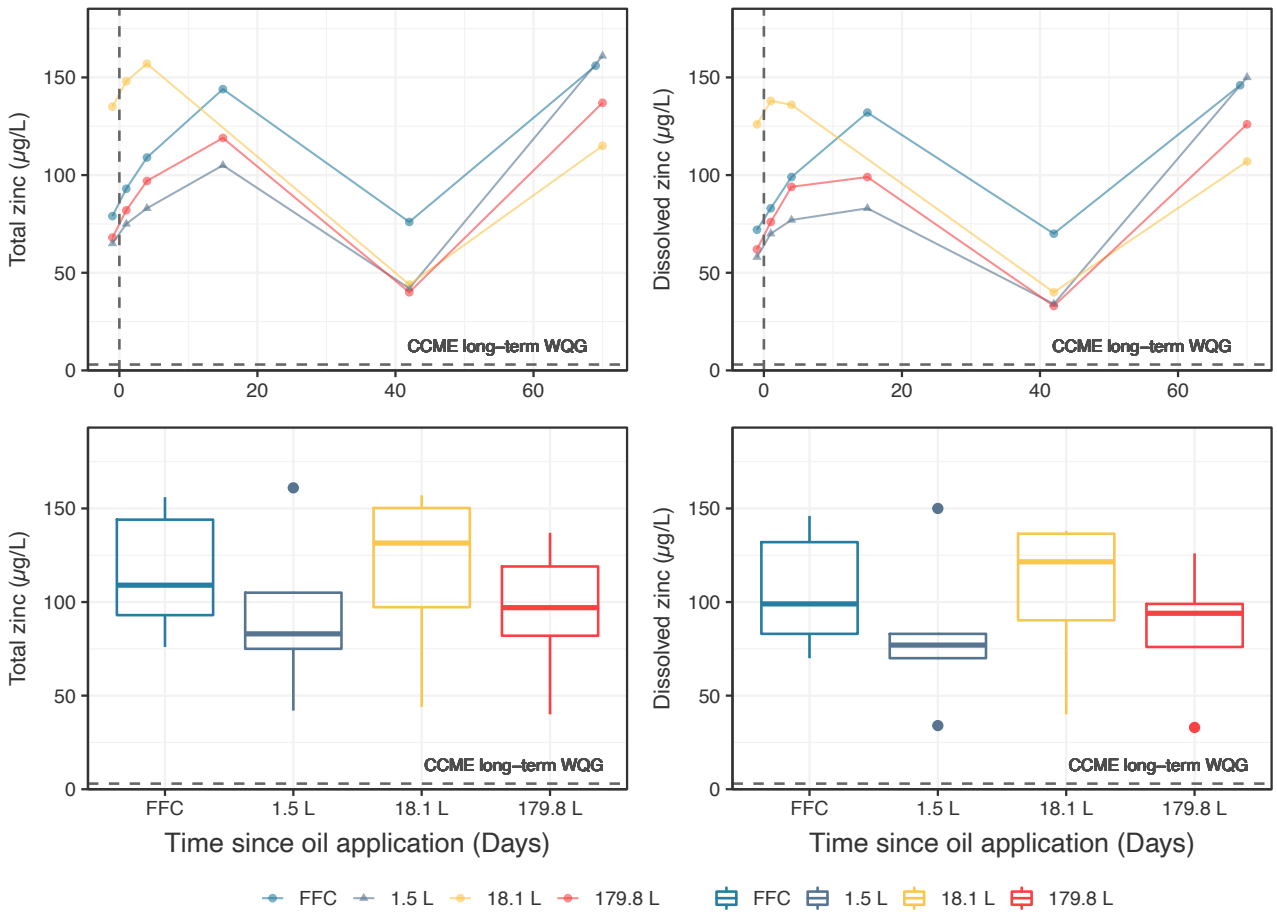

SI Figure 37: Upper panels: temporal progression of the concentrations of zinc in the total (upper left) and dissolved (upper right) fractions of the water column. Lower panels: average values of the concentrations of zinc in the total (lower left) and dissolved (lower right) fractions of the water column for the different treatments. Dashed vertical line in the upper panels indicates the day of oil addition (day 0). Dashed horizontal lines indicates the CCME long term water quality guideline value.

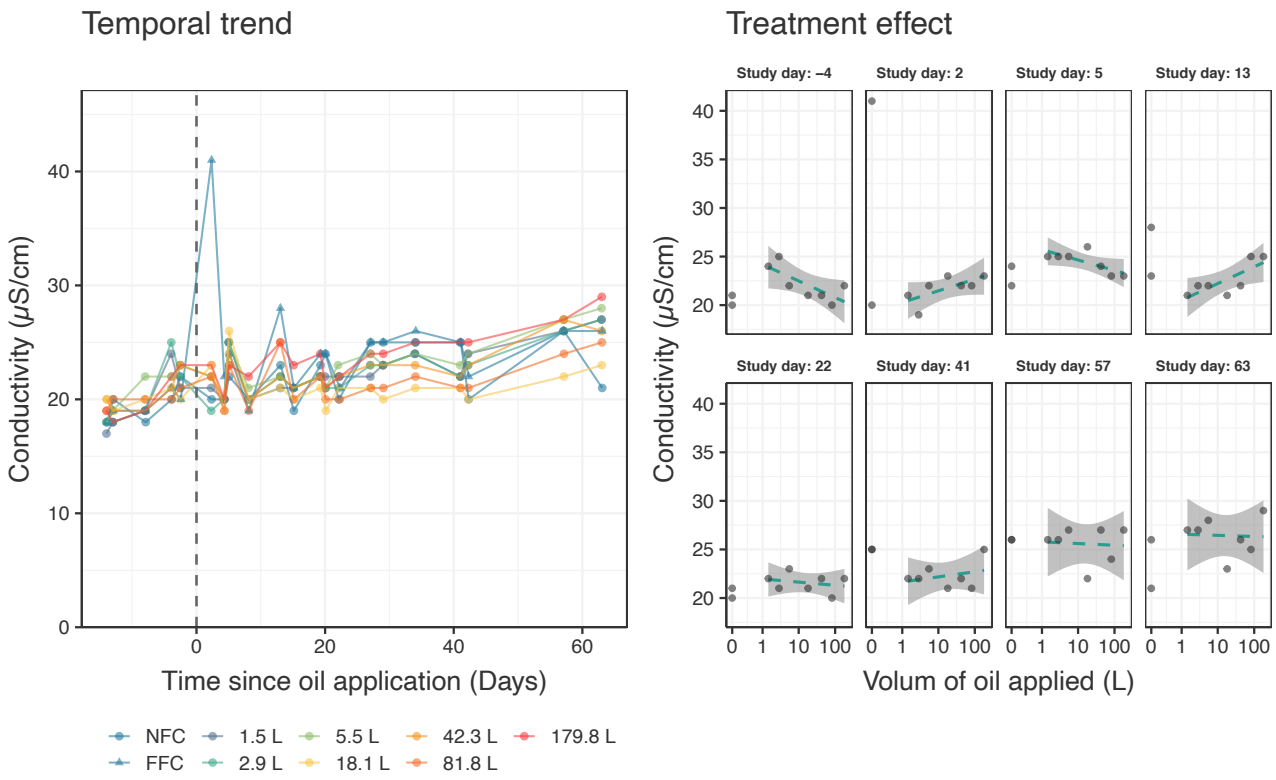

SI Figure 38: Temporal trend of conductivity throughout the study (left panel), and sampling-day-specific relation between conductivity and applied oil volume for a subset of sampling days (right panel). Dashed vertical line indicates the day of oil addition (day 0)

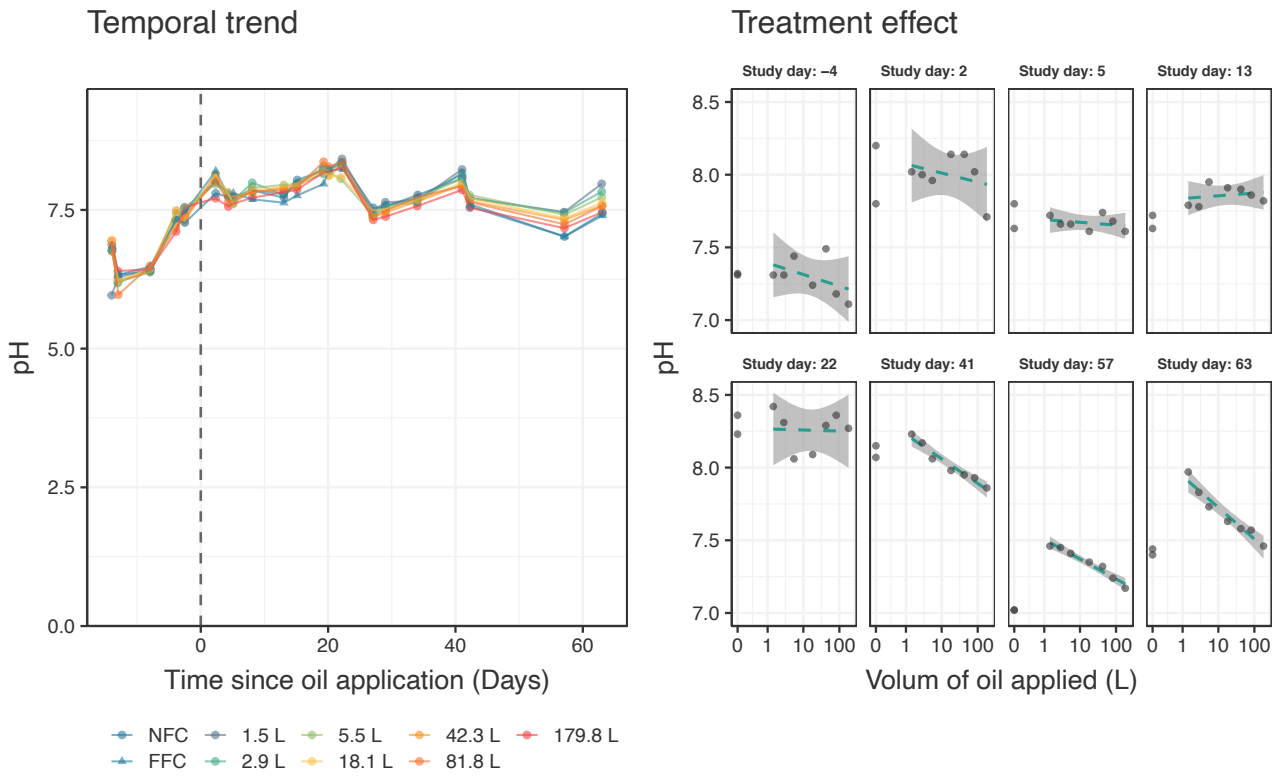

SI Figure 39: Temporal trend of pH throughout the study (left panel), and sampling-day-specific relation between pH and applied oil volume for a subset of sampling days (right panel). Dashed vertical line indicates the day of oil addition (day 0)

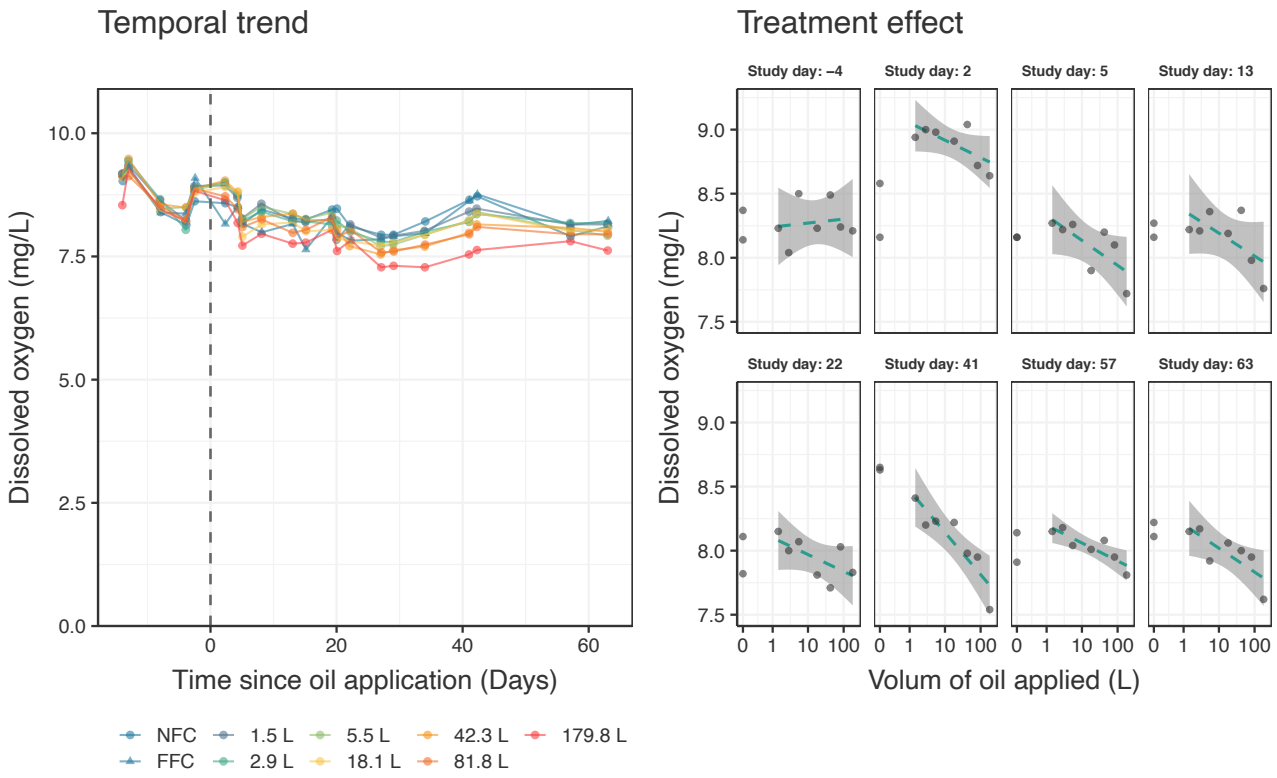

SI Figure 40: Temporal trend of dissolved oxygen (as mg/L) throughout the study (left panel), and sampling-day-specific relation between dissolved oxygen (as mg/L) and applied oil volume for a subset of sampling days (right panel). Dashed vertical line indicates the day of oil addition (day 0)

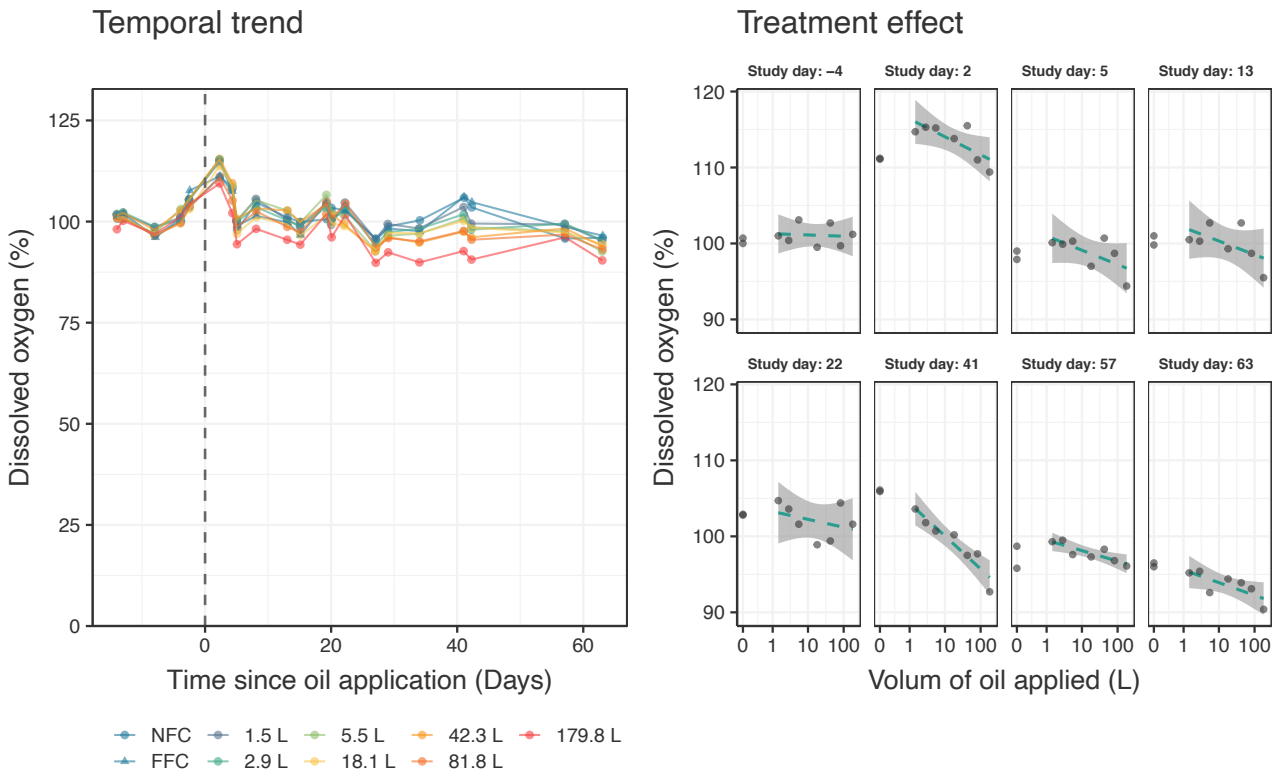

SI Figure 41: Temporal trend of dissolved oxygen (as % saturation) throughout the study (left panel), and sampling-day-specific relation between dissolved oxygen (as % saturation) and applied oil volume for a subset of sampling days (right panel). Dashed vertical line indicates the day of oil addition (day 0)

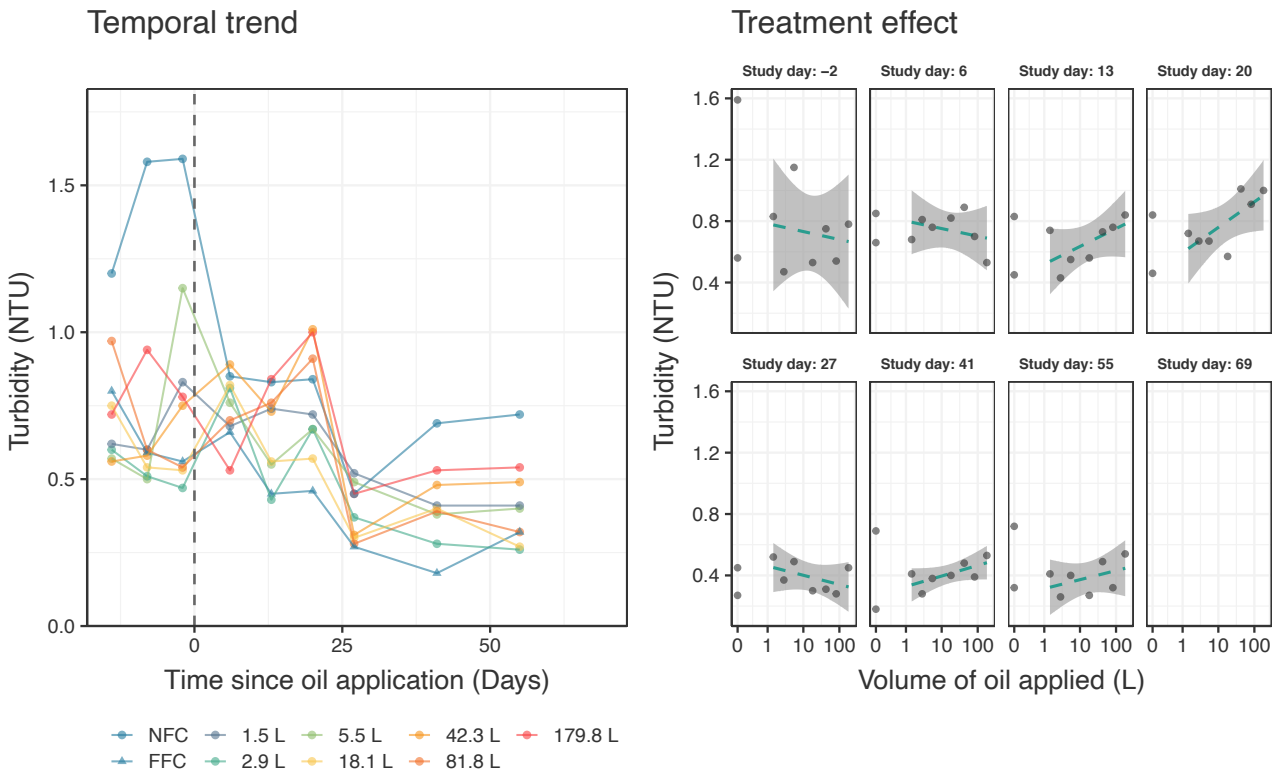

SI Figure 42: Temporal trend of turbidity throughout the study (left panel), and sampling-day-specific relation between turbidity and applied oil volume for a subset of sampling days (right panel). Dashed vertical line indicates the day of oil addition (day 0)

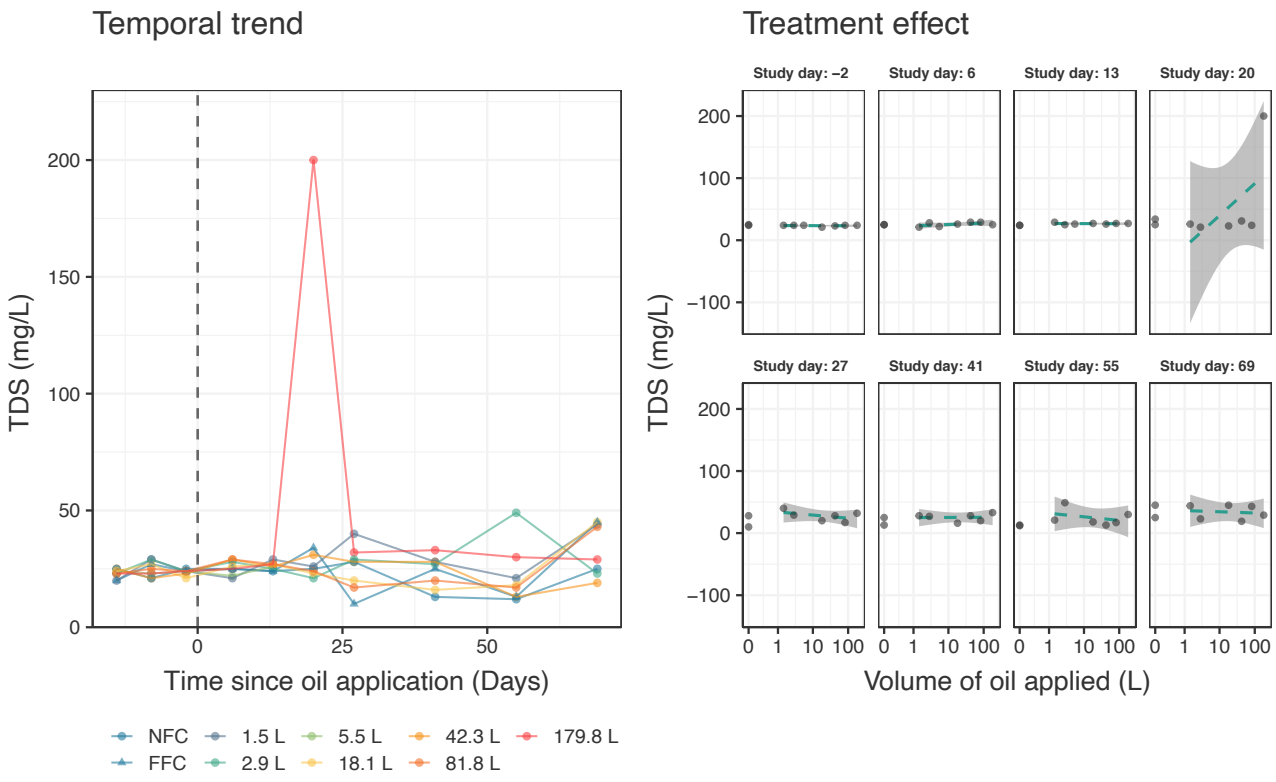

SI Figure 43: Temporal trend of total dissolved solids throughout the study (left panel), and sampling-day-specific relation between total dissolved solids and applied oil volume for a subset of sampling days (right panel). Dashed vertical line indicates the day of oil addition (day 0)

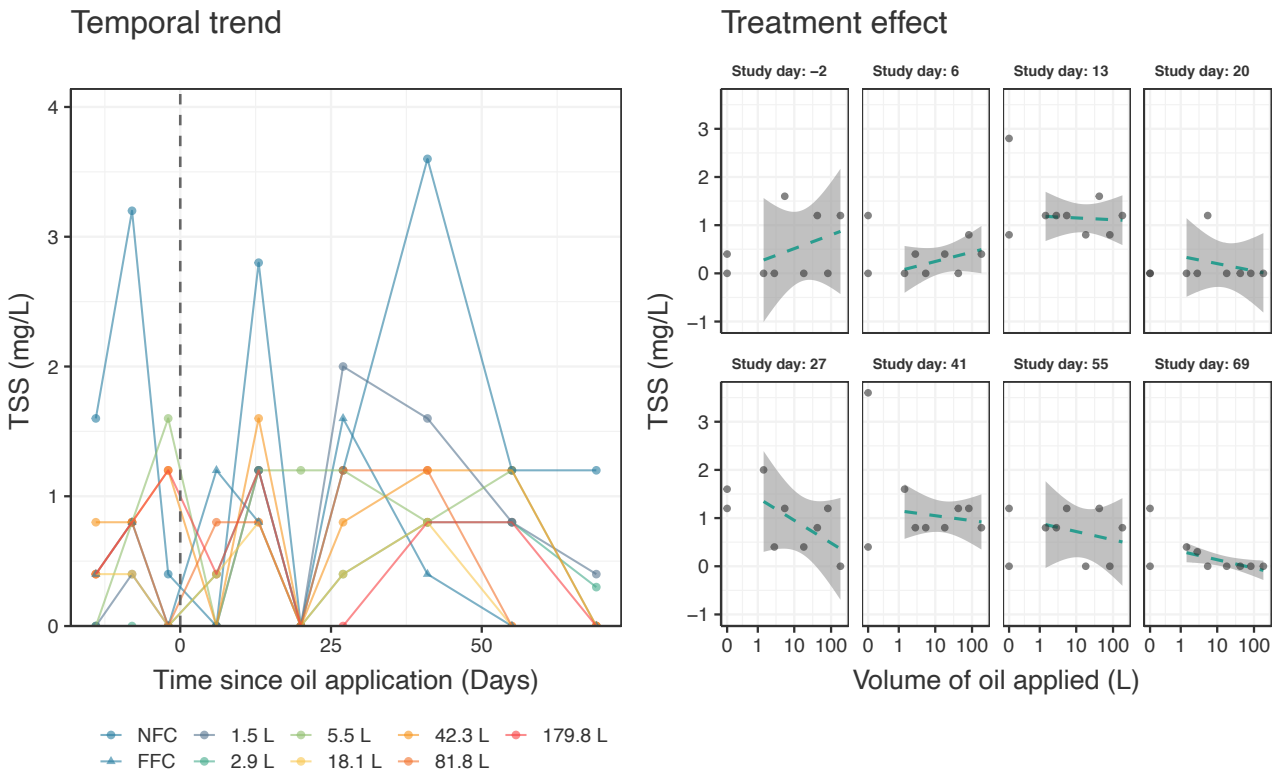

SI Figure 44: Temporal trend of total suspended solids throughout the study (left panel), and sampling-day-specific relation between total suspended solids and applied oil volume for a subset of sampling days (right panel). Dashed vertical line indicates the day of oil addition (day 0)

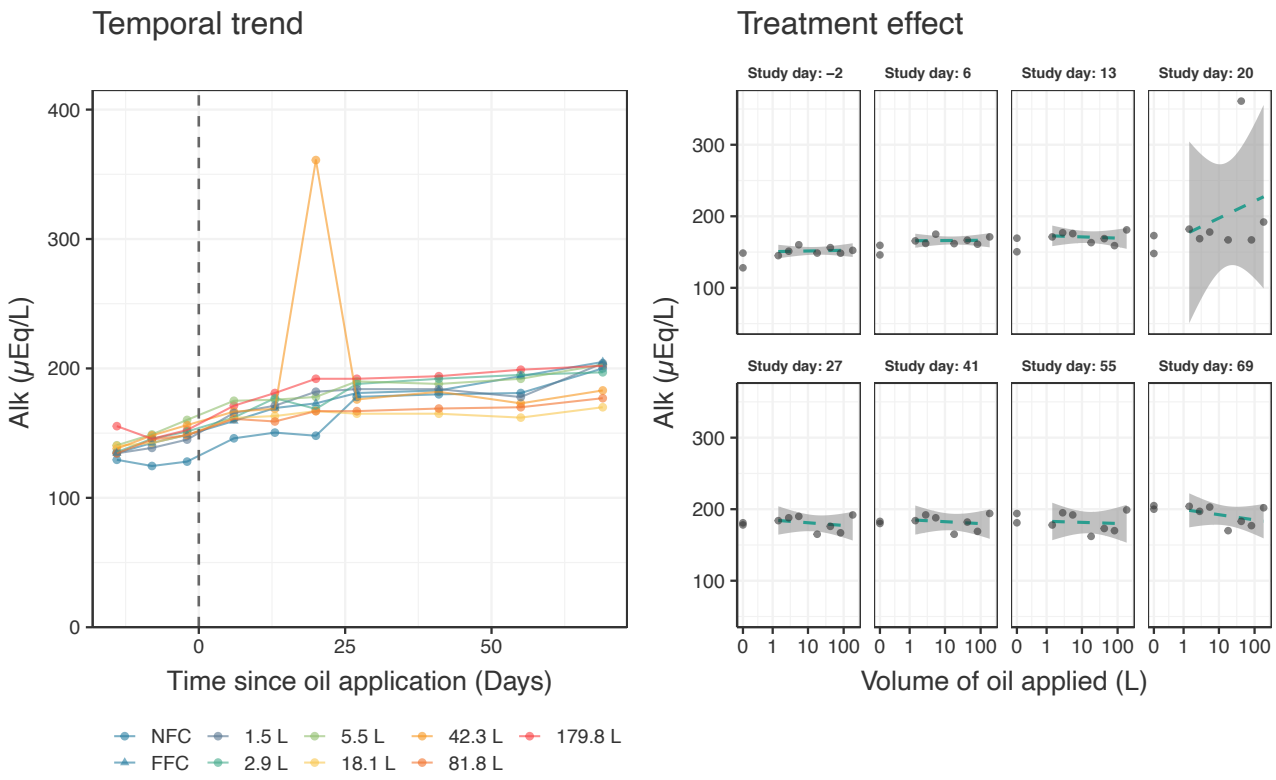

SI Figure 45: Temporal trend of alkalinity throughout the study (left panel), and sampling-day-specific relation between alkalinity and applied oil volume for a subset of sampling days (right panel). Dashed vertical line indicates the day of oil addition (day 0)

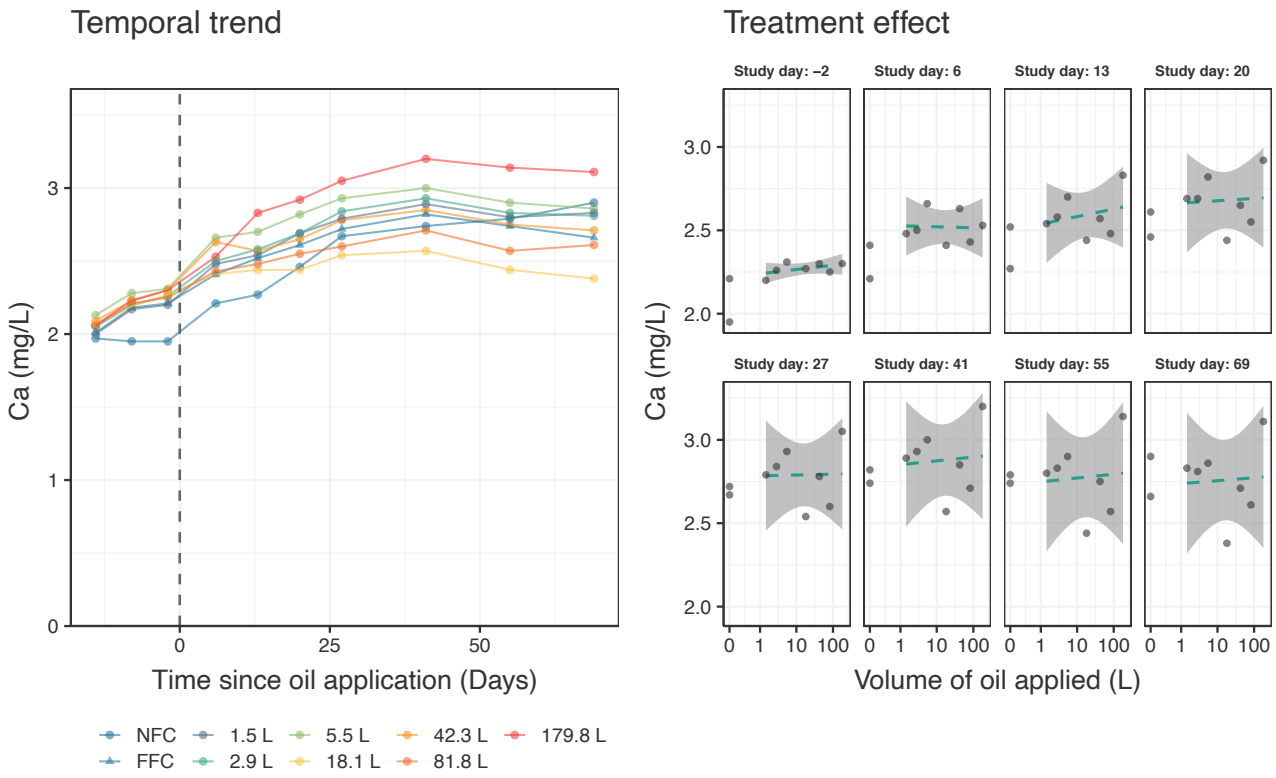

SI Figure 46: Temporal trend of calcium throughout the study (left panel), and sampling-day-specific relation between calcium and applied oil volume for a subset of sampling days (right panel). Dashed vertical line indicates the day of oil addition (day 0)

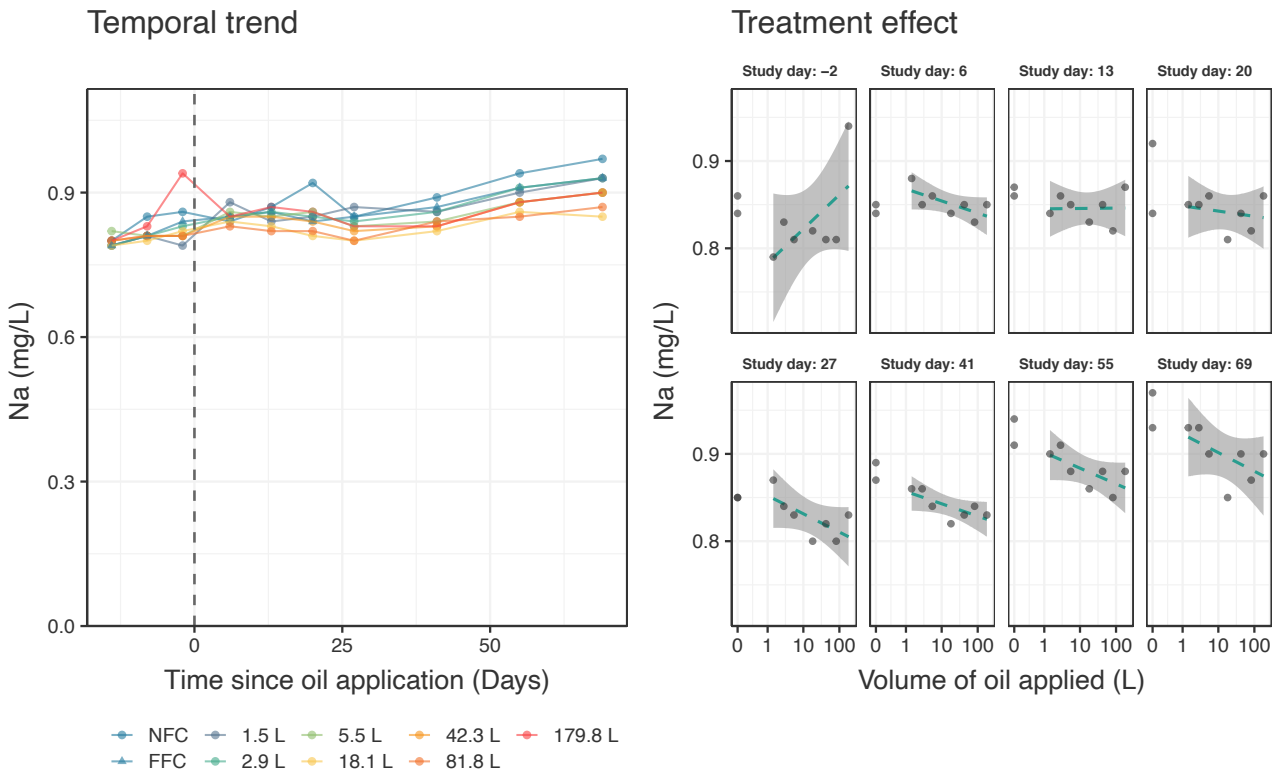

SI Figure 47: Temporal trend of sodium throughout the study (left panel), and sampling-day-specific relation between sodium and applied oil volume for a subset of sampling days (right panel). Dashed vertical line indicates the day of oil addition (day 0)

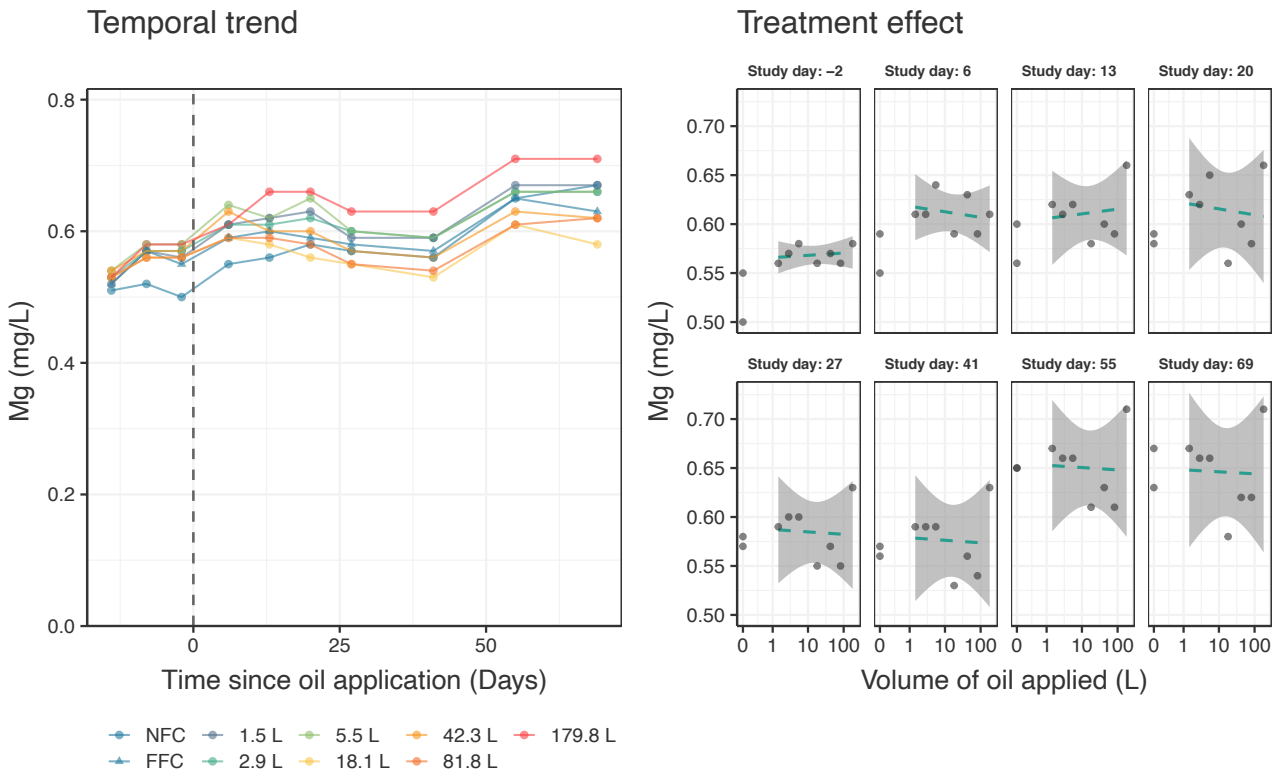

SI Figure 48: Temporal trend of magnesium throughout the study (left panel), and sampling-day-specific relation between magnesium and applied oil volume for a subset of sampling days (right panel). Dashed vertical line indicates the day of oil addition (day 0)

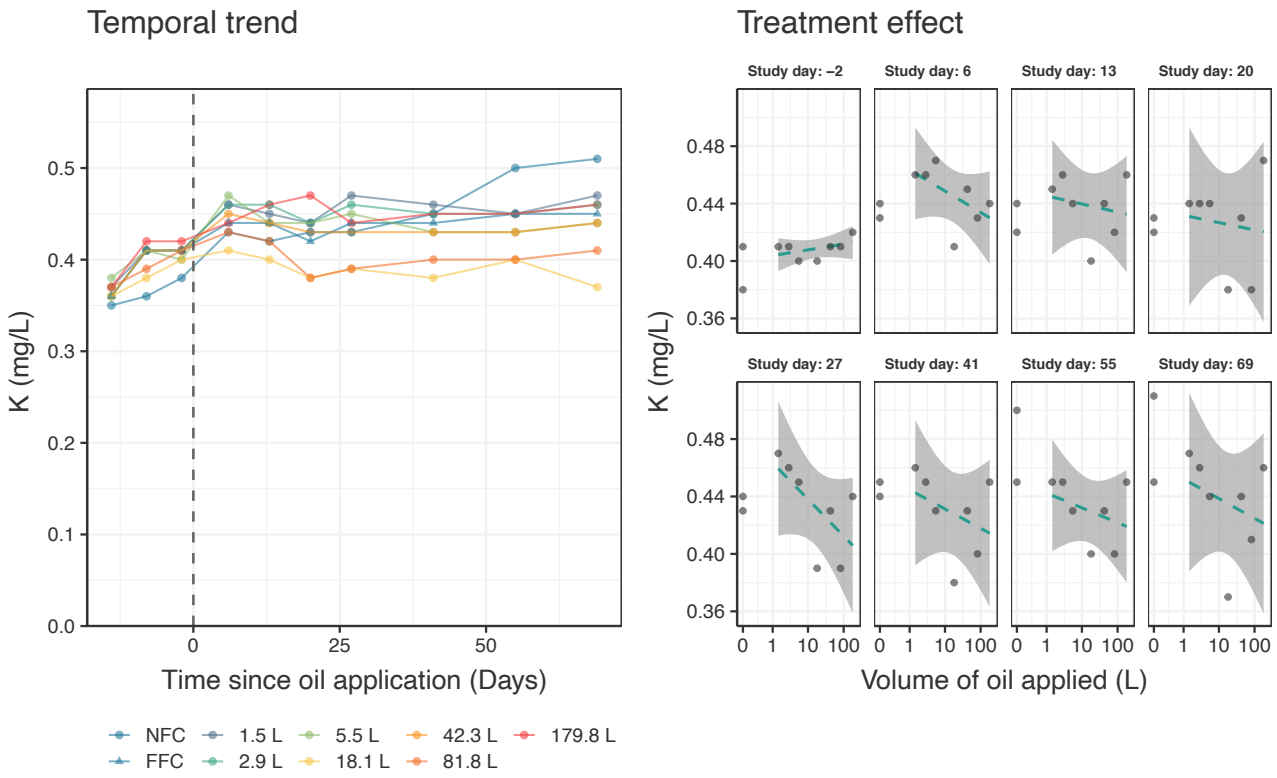

SI Figure 49: Temporal trend of potassium throughout the study (left panel), and sampling-day-specific relation between potassium and applied oil volume for a subset of sampling days (right panel). Dashed vertical line indicates the day of oil addition (day 0)

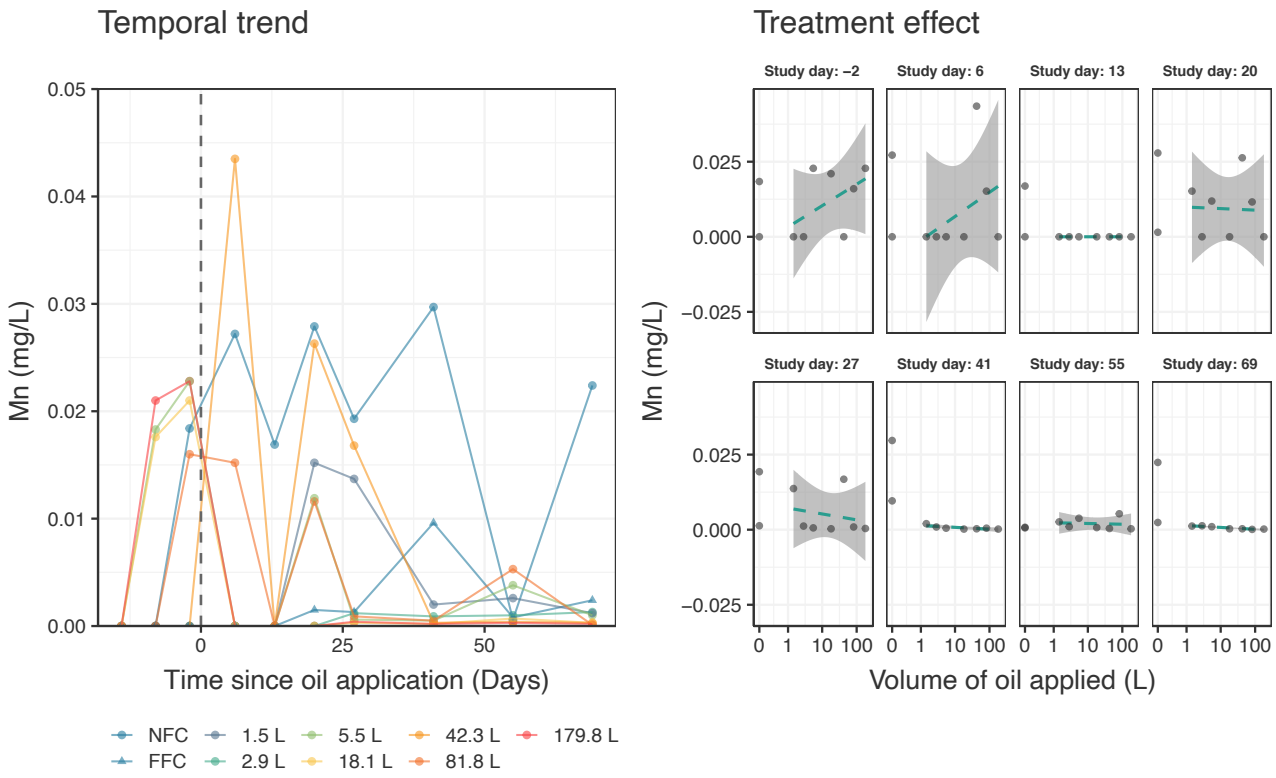

SI Figure 50: Temporal trend of manganese throughout the study (left panel), and sampling-day-specific relation between manganese and applied oil volume for a subset of sampling days (right panel). Dashed vertical line indicates the day of oil addition (day 0)

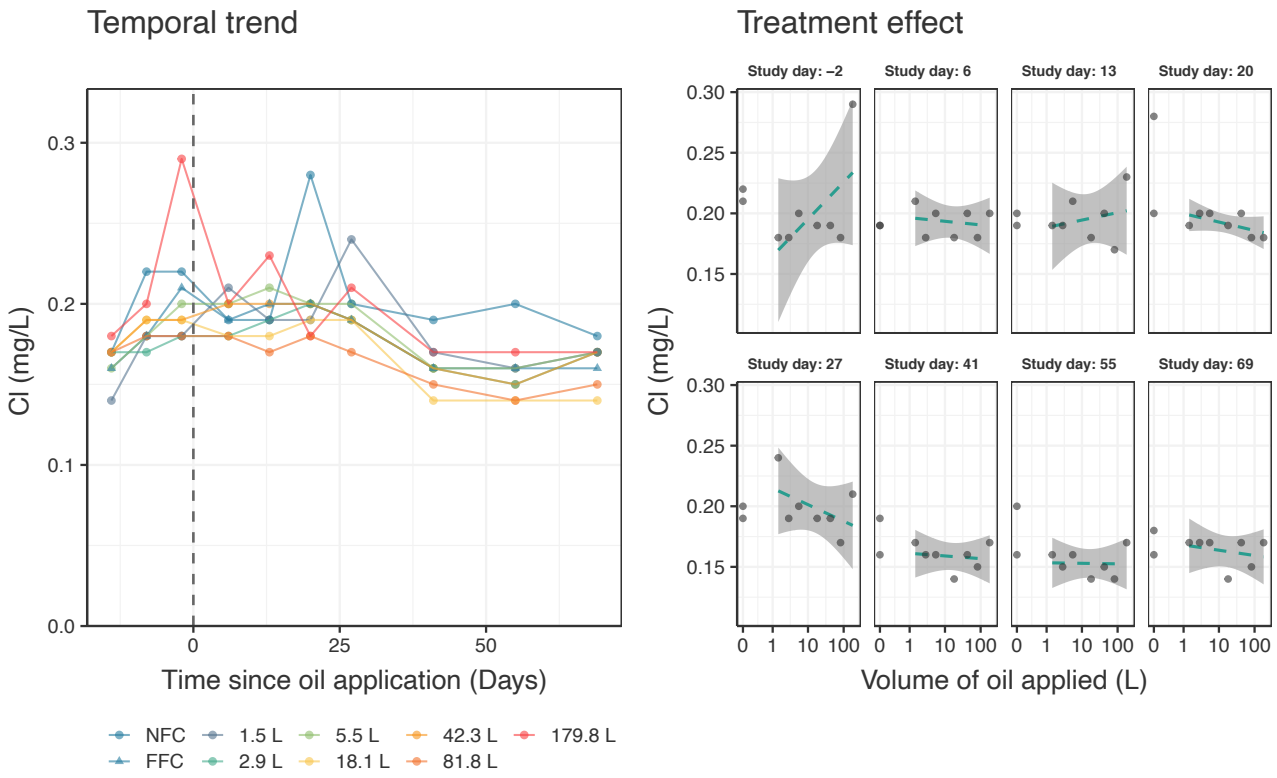

SI Figure 51: Temporal trend of chloride throughout the study (left panel), and sampling-day-specific relation between chloride and applied oil volume for a subset of sampling days (right panel). Dashed vertical line indicates the day of oil addition (day 0)

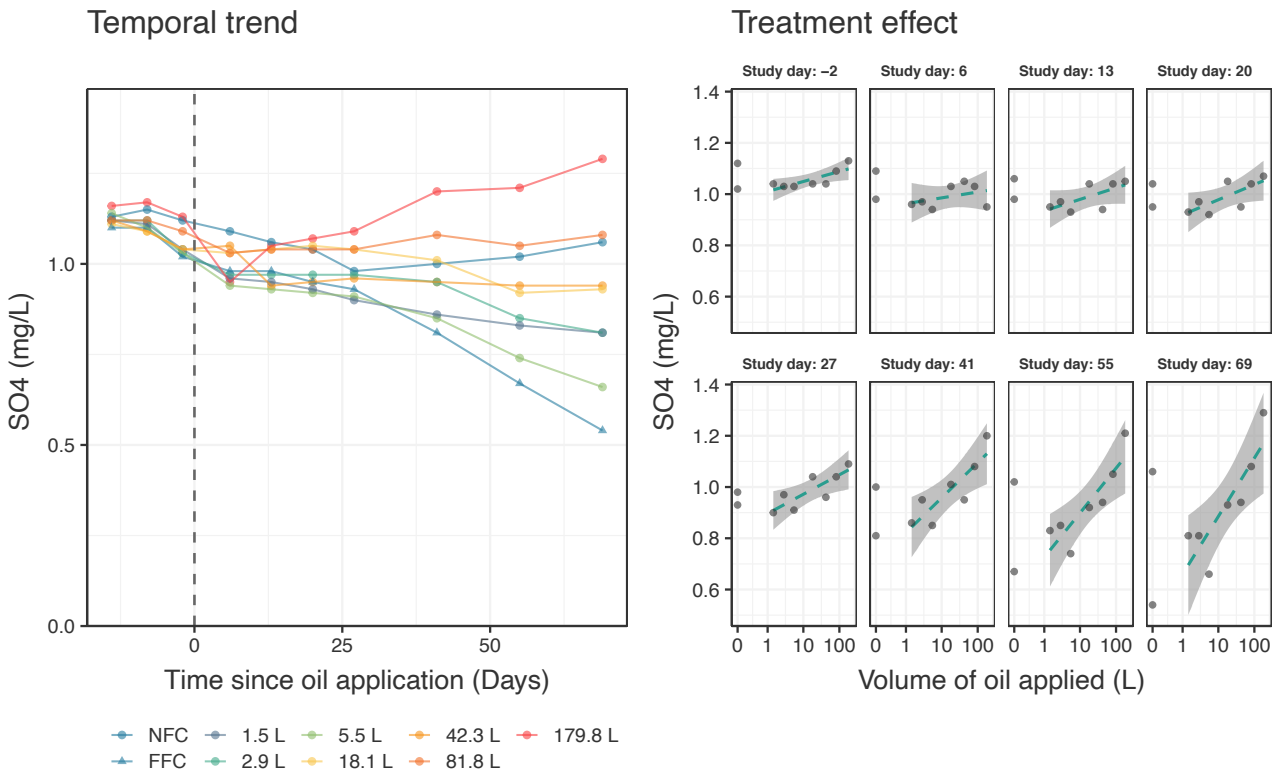

SI Figure 52: Temporal trend of sulphate throughout the study (left panel), and sampling-day-specific relation between sulphate and applied oil volume for a subset of sampling days (right panel). Dashed vertical line indicates the day of oil addition (day 0)

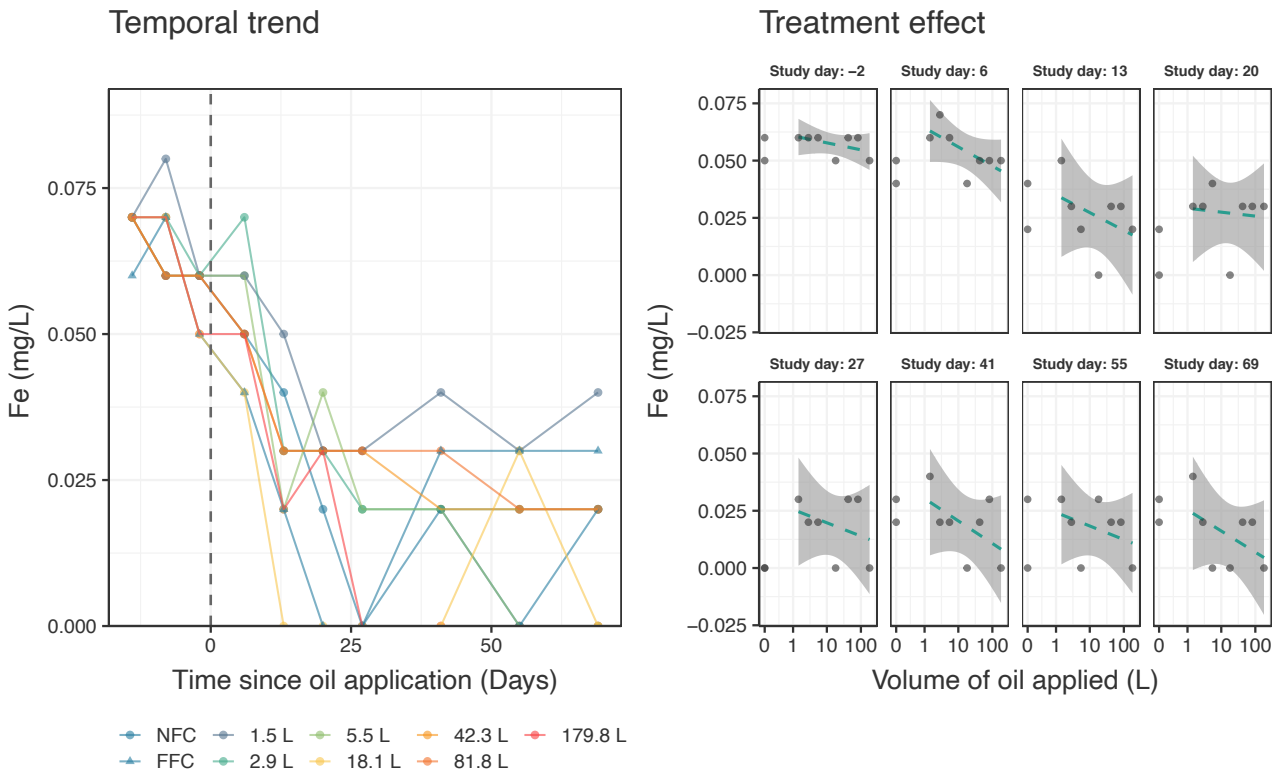

SI Figure 53: Temporal trend of iron throughout the study (left panel), and sampling-day-specific relation between iron and applied oil volume for a subset of sampling days (right panel). Dashed vertical line indicates the day of oil addition (day 0)

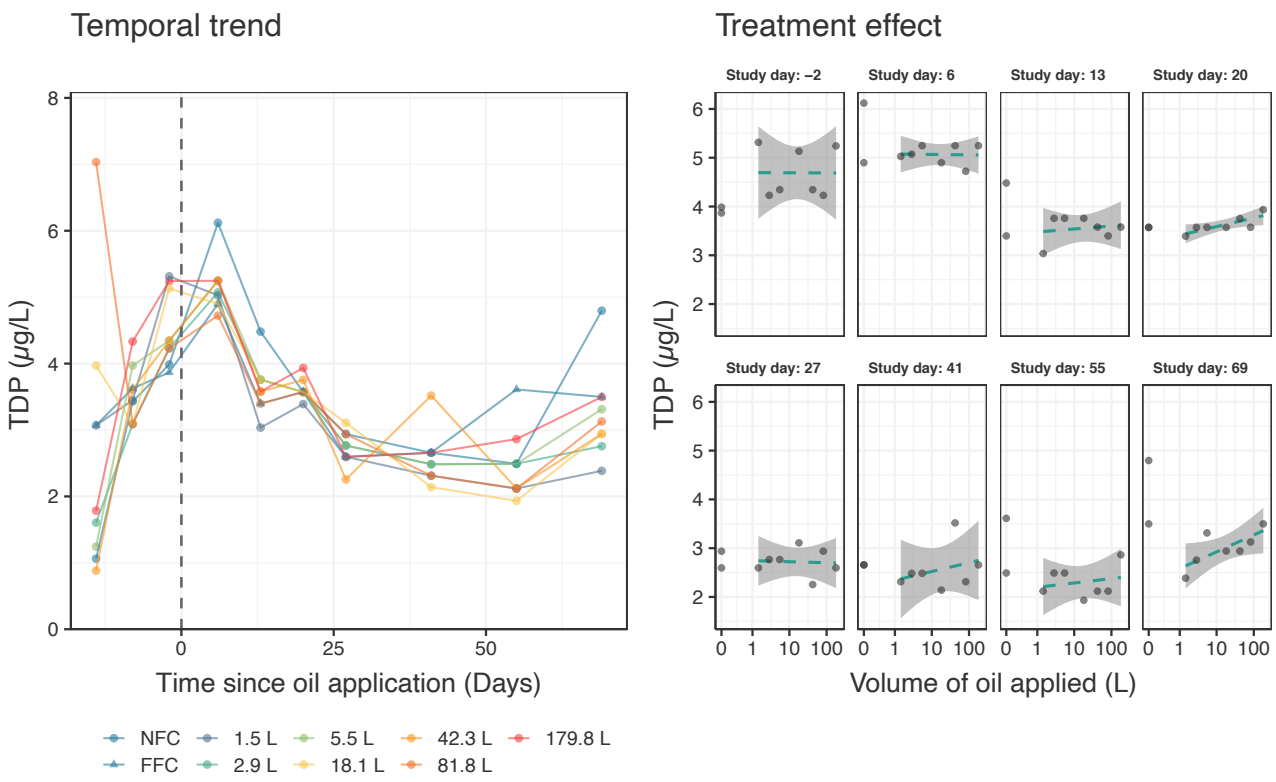

SI Figure 54: Temporal trend of total dissolved phosphorus throughout the study (left panel), and sampling-day-specific relation between total dissolved phosphorus and applied oil volume for a subset of sampling days (right panel). Dashed vertical line indicates the day of oil addition (day 0)

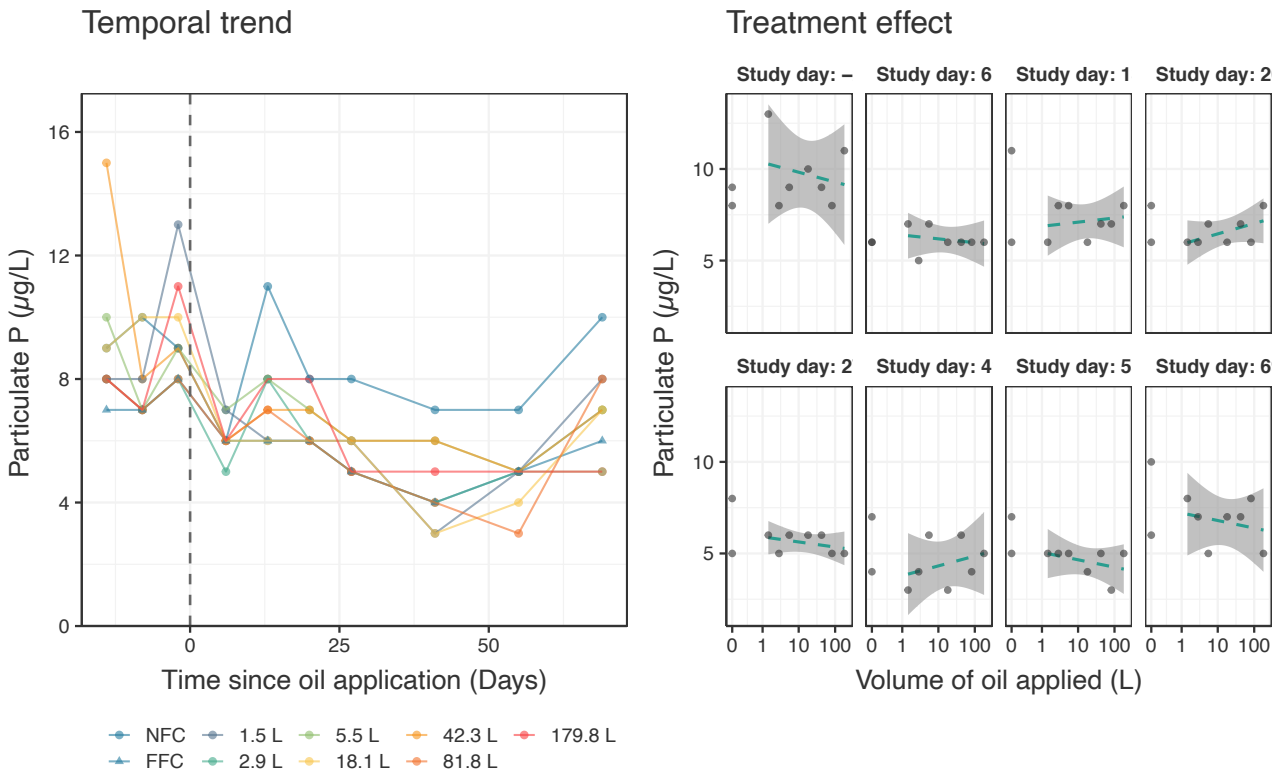

SI Figure 55: Temporal trend of particulate phosphorus throughout the study (left panel), and sampling-day-specific relation between particulate phosphorus and applied oil volume for a subset of sampling days (right panel). Dashed vertical line indicates the day of oil addition (day 0)

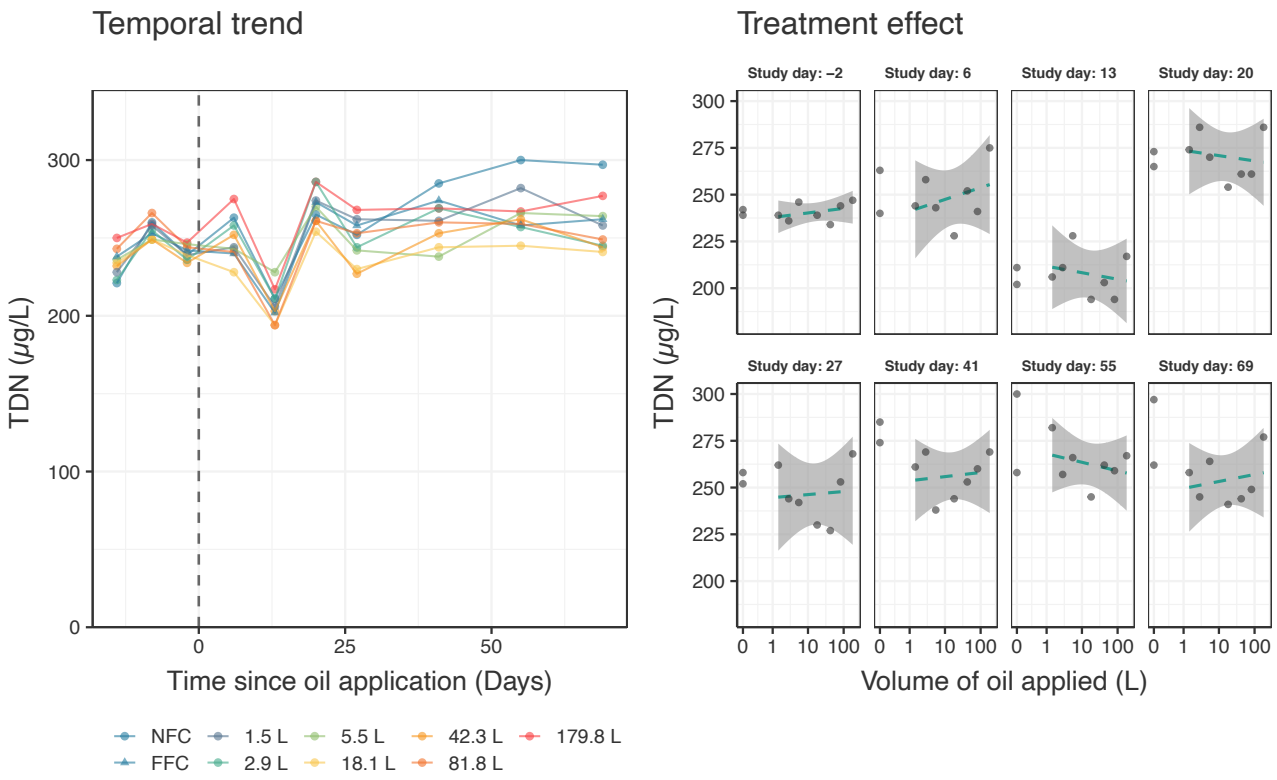

SI Figure 56: Temporal trend of total dissolved nitrogen throughout the study (left panel), and sampling-day-specific relation between total dissolved nitrogen and applied oil volume for a subset of sampling days (right panel). Dashed vertical line indicates the day of oil addition (day 0)

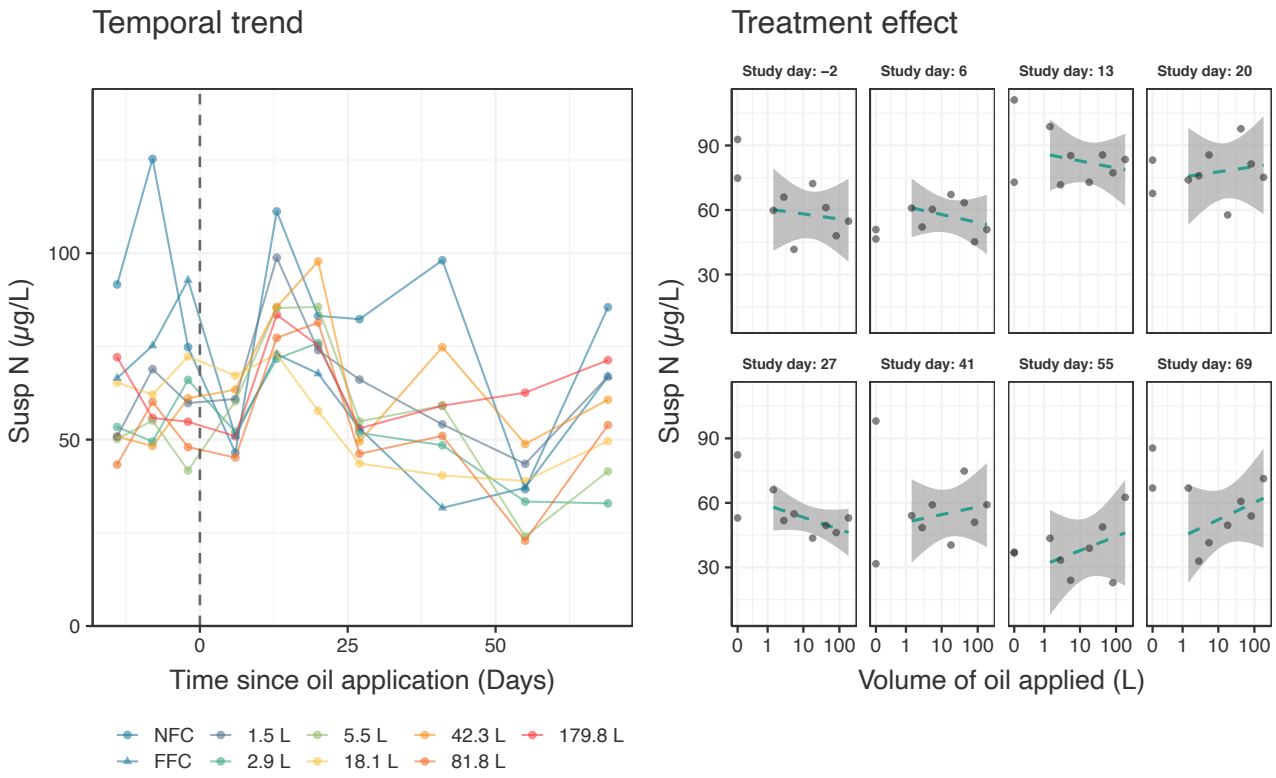

SI Figure 57: Temporal trend of suspended nitrogen throughout the study (left panel), and sampling-day-specific relation between suspended nitrogen and applied oil volume for a subset of sampling days (right panel). Dashed vertical line indicates the day of oil addition (day 0)

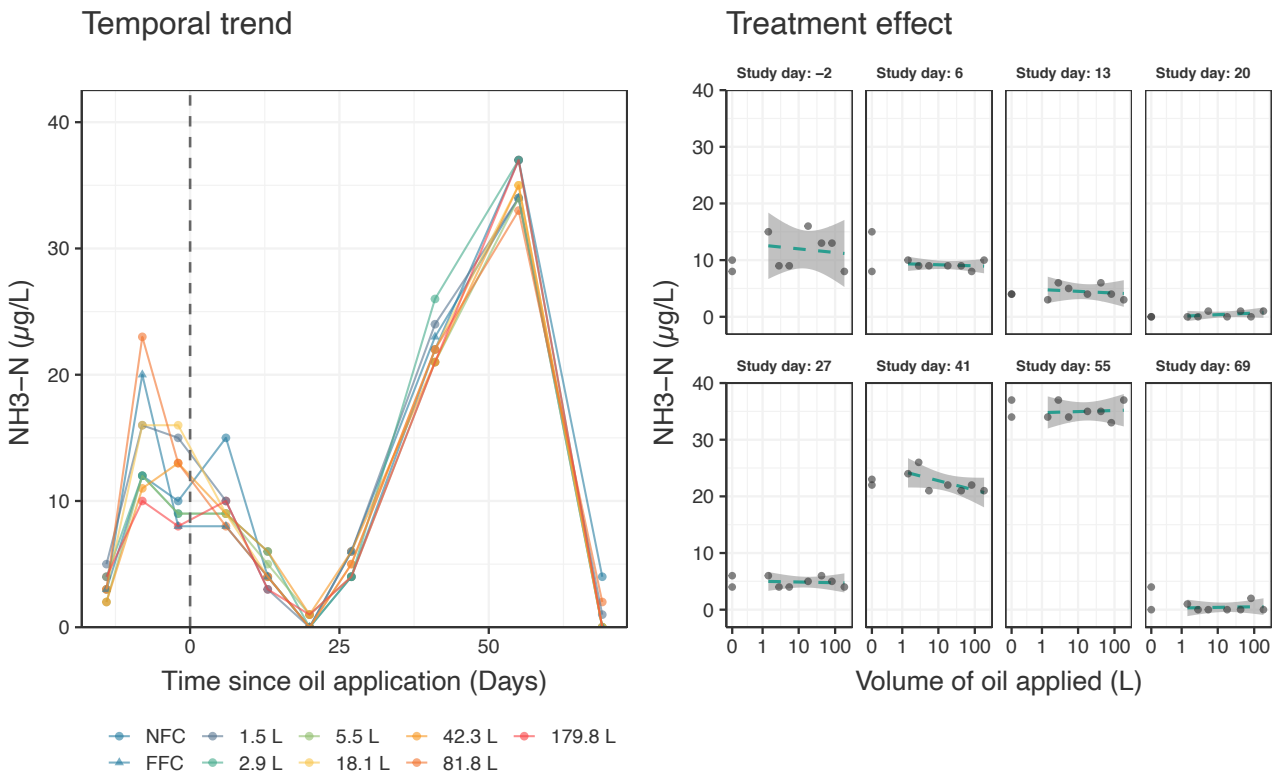

SI Figure 58: Temporal trend of ammonia throughout the study (left panel), and sampling-day-specific relation between ammonia and applied oil volume for a subset of sampling days (right panel). Dashed vertical line indicates the day of oil addition (day 0)

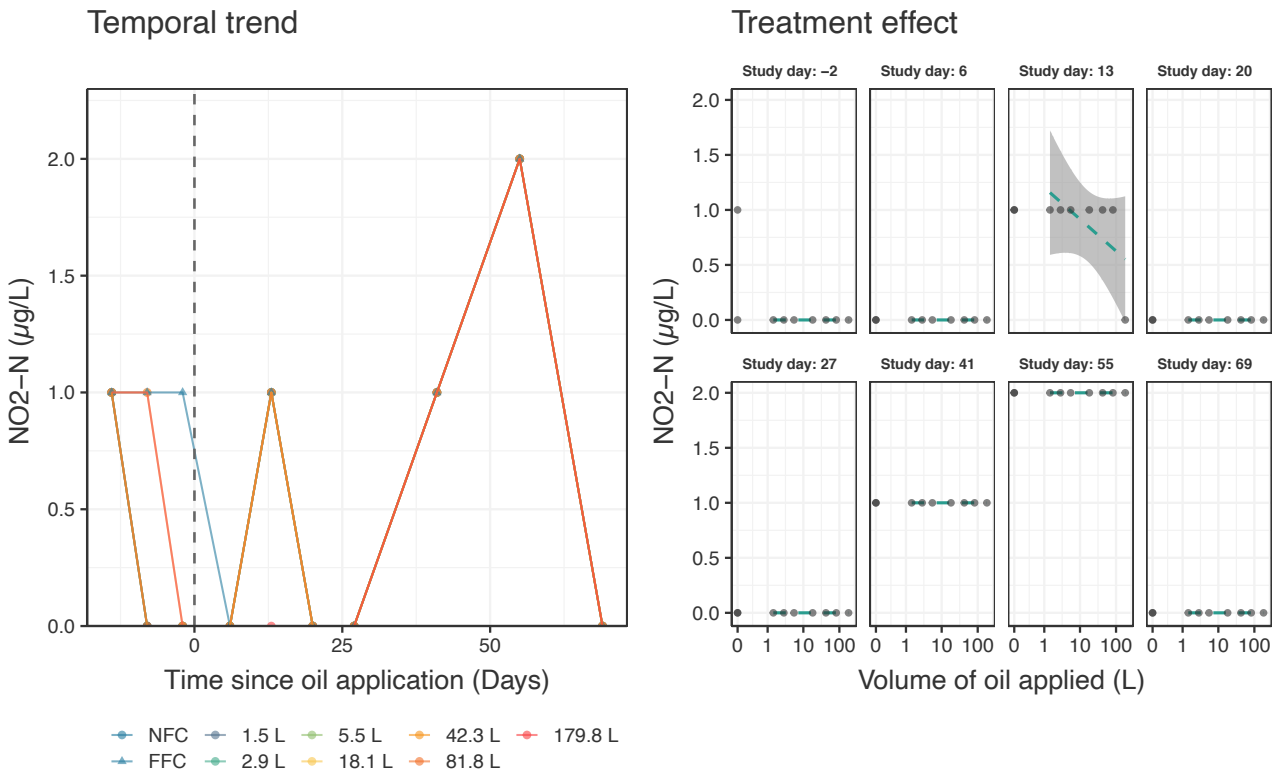

SI Figure 59: Temporal trend of nitrite throughout the study (left panel), and sampling-day-specific relation between nitrite and applied oil volume for a subset of sampling days (right panel). Dashed vertical line indicates the day of oil addition (day 0)

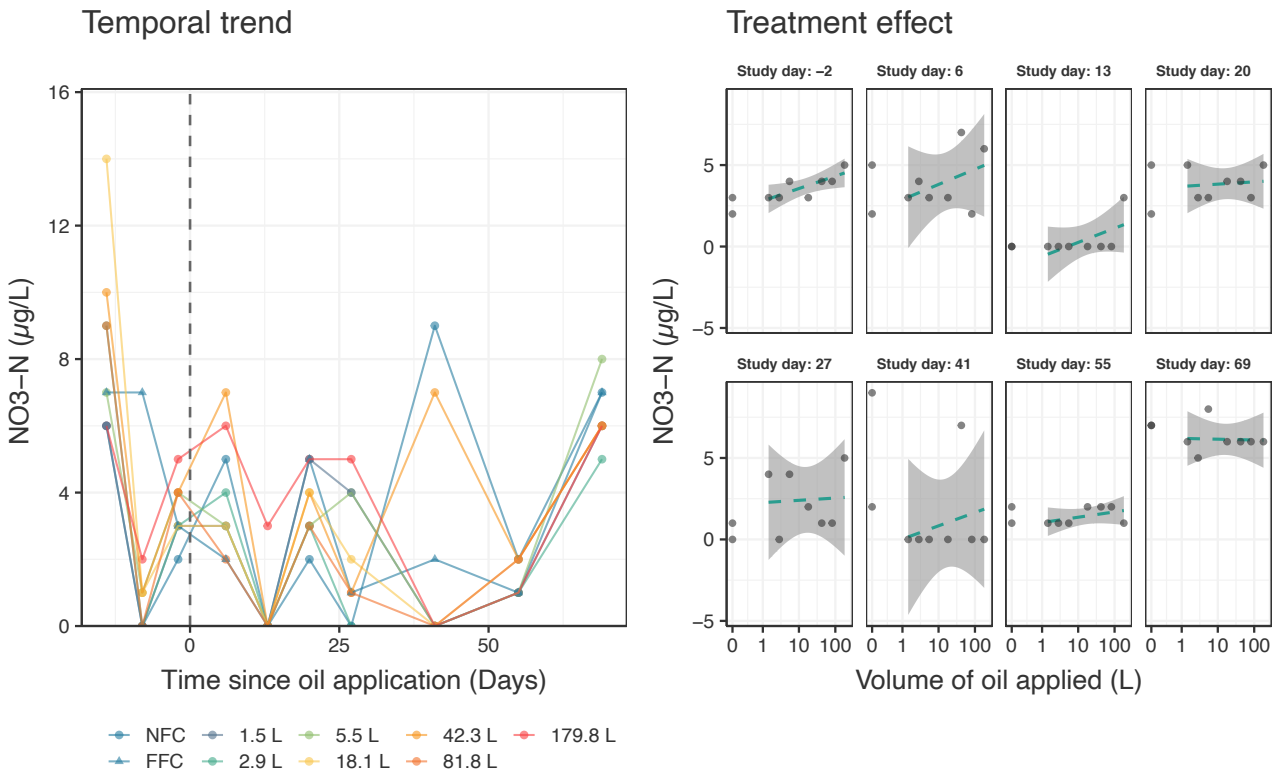

SI Figure 60: Temporal trend of nitrate throughout the study (left panel), and sampling-day-specific relation between nitrate and applied oil volume for a subset of sampling days (right panel). Dashed vertical line indicates the day of oil addition (day 0)

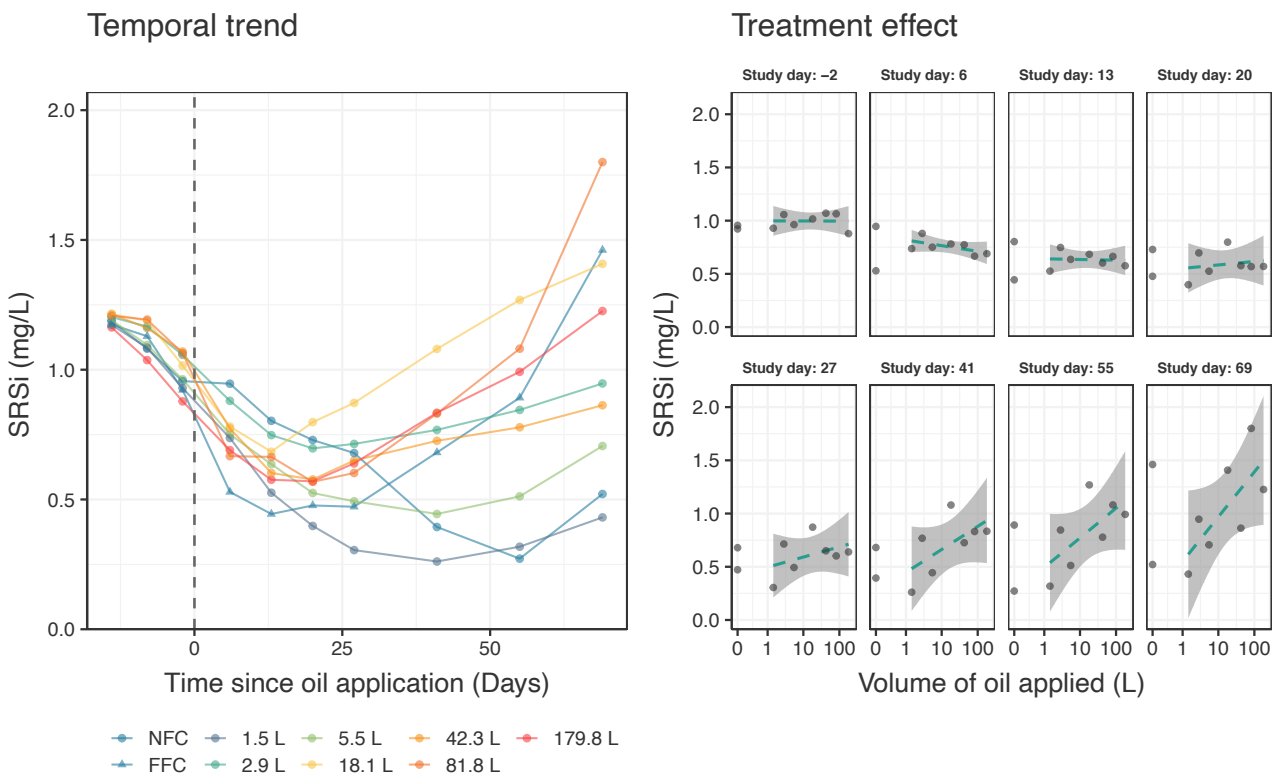

SI Figure 61: Temporal trend of soluble reactive silica throughout the study (left panel), and sampling-day-specific relation between soluble reactive silica and applied oil volume for a subset of sampling days (right panel). Dashed vertical line indicates the day of oil addition (day 0)

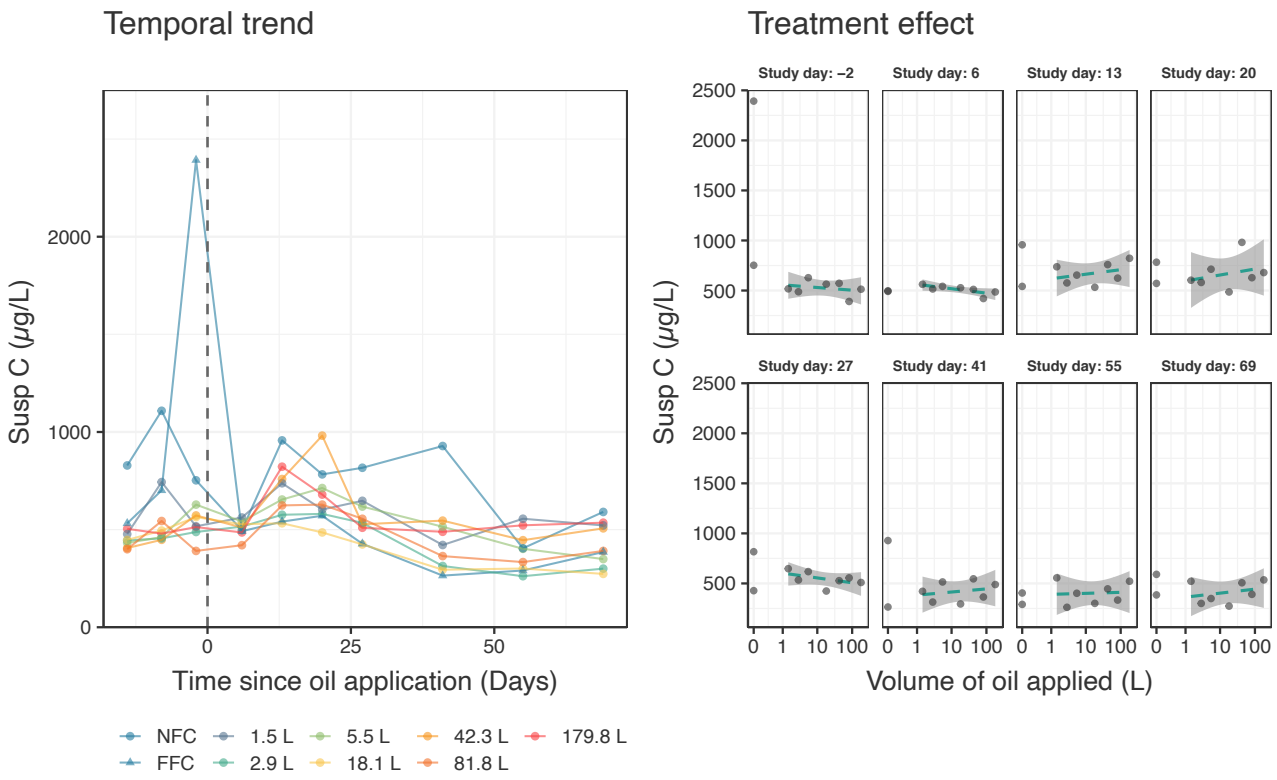

SI Figure 62: Temporal trend of suspended carbon throughout the study (left panel), and sampling-day-specific relation between suspended carbon and applied oil volume for a subset of sampling days (right panel). Dashed vertical line indicates the day of oil addition (day 0)

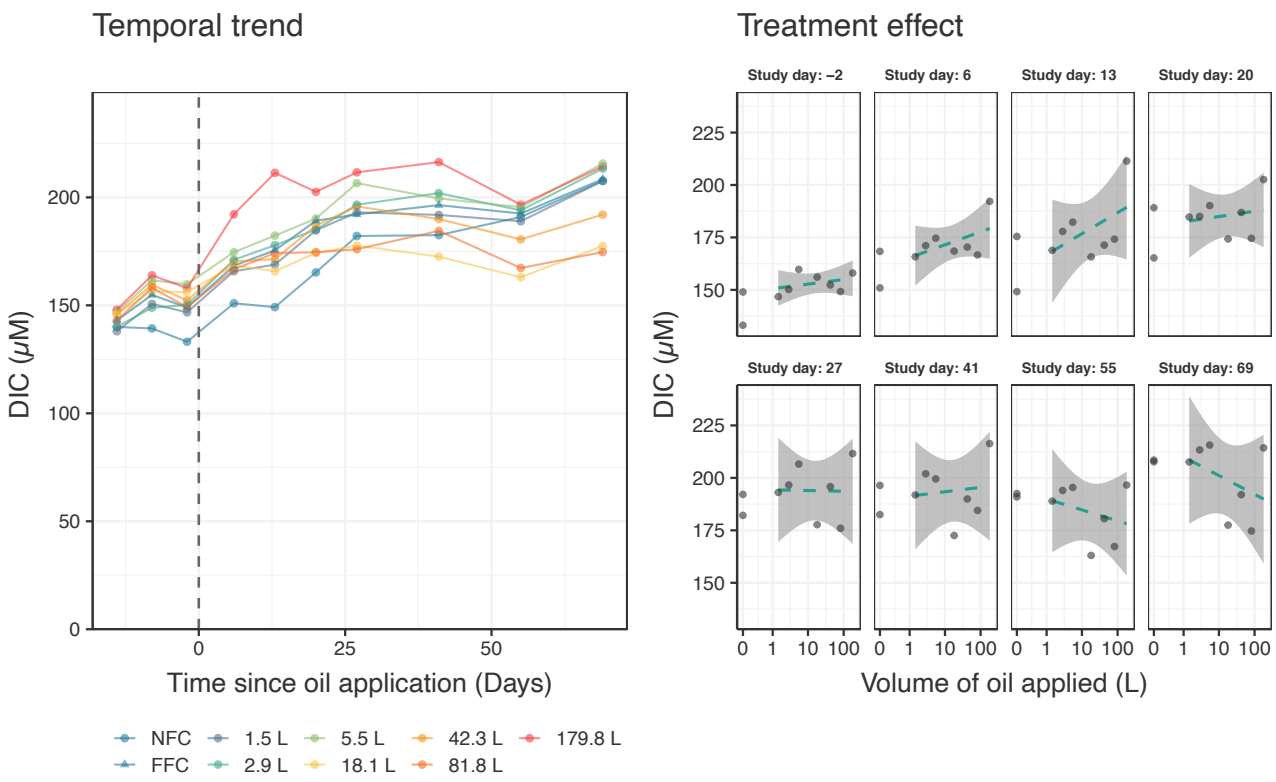

SI Figure 63: Temporal trend of dissolved inorganic carbon throughout the study (left panel), and sampling-day-specific relation between dissolved inorganic carbon and applied oil volume for a subset of sampling days (right panel). Dashed vertical line indicates the day of oil addition (day 0)

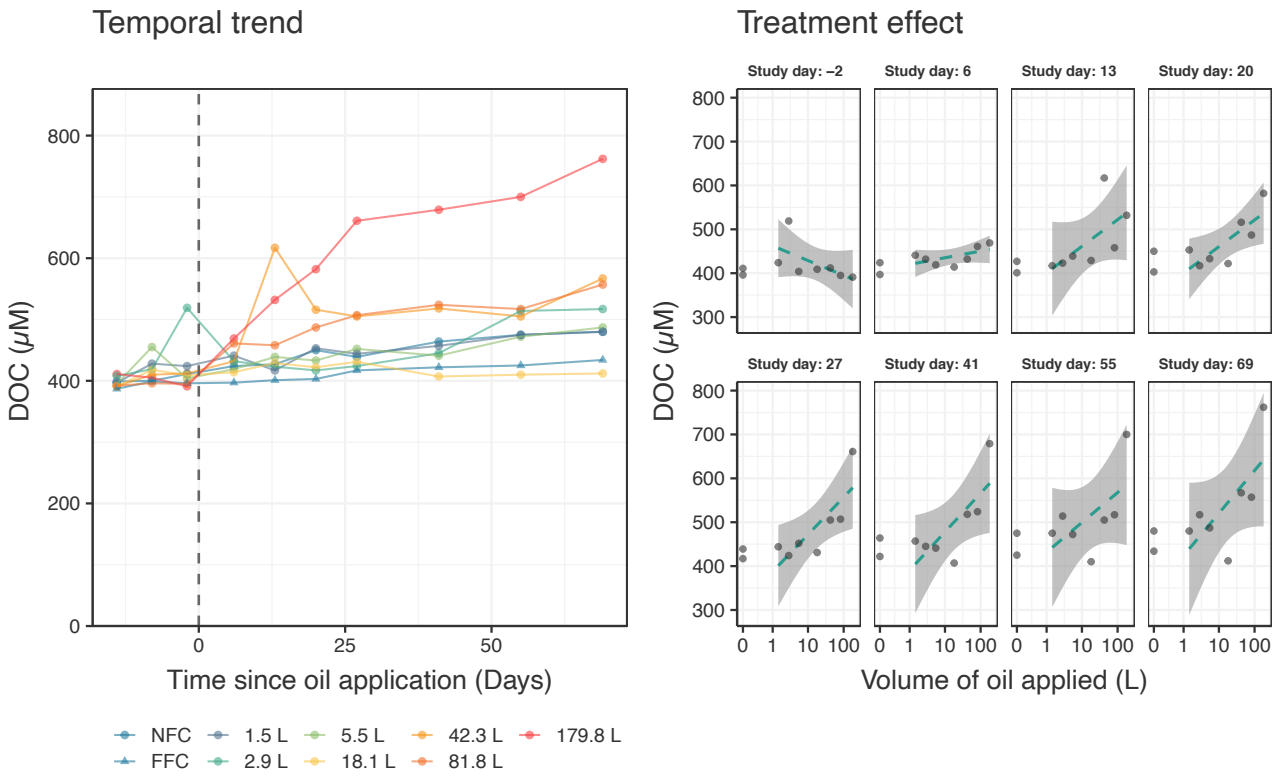

SI Figure 64: Temporal trend of dissolved organic carbon throughout the study (left panel), and sampling-day-specific relation between dissolved organic carbon and applied oil volume for a subset of sampling days (right panel). Dashed vertical line indicates the day of oil addition (day 0)

4 References to the Supplemental Information

Allen RG, Pereira LS, Raes D, Smith M. Crop evapotranspiration-Guidelines for computing crop water requirements-FAO Irrigation and drainage paper 56. Fao, Rome 1998; 300: D05109.

Calmon P, Garnier-Laplace J. Radionuclide fact sheet: Tritium and the environment. Institut de radioprotection et de sûreté nucléaire, France, 2010.

Granger R, Hedstrom N. Modelling hourly rates of evaporation from small lakes. Hydrology and Earth System Sciences 2011; 15: 267-277.

Lucas LL, Unterweger MP. Comprehensive Review and Critical Evaluation of the Half-Life of Tritium. J Res Natl Inst Stand Technol 2000; 105: 541-549.

Michel RL, Jurgens BC, Young MB. Tritium deposition in precipitation in the United States, 1953–2012. US Geological Survey, 2018.

NASA. POWER Data Access Viewer. US National Aeronautics and Space Administration. 2020. https://power.larc.nasa.gov/data-access-viewer/ Accesed: 25/06/2020

R Development Core Team. R: A Language and Environment for Statistical Computing. Vienna, Austria: R Foundation for Statistical Computing, http://www.R-project.org, 2020.

Slota PMA. Evaluation of operational lake evaporation methods in a Canadian Shield landscape. Department of Civil Engineering. Master of Science. University of Manitoba (Canada), Winnipeg, Manitoba, Canada, 2013, pp. 217.

Wickham H. Tidy Data. Journal of Statistical Software; Vol 1, Issue 10 (2014) 2014.

Wickham H, Averick M, Bryan J, Chang W, McGowan LDA, François R, et al. Welcome to the Tidyverse. Journal of Open Source Software 2019; 4: 1686.

Allen RG, Pereira LS, Raes D, Smith M. Crop evapotranspiration-Guidelines for computing crop water requirements-FAO Irrigation and drainage paper 56. Fao, Rome 1998; 300: D05109.

Calmon P, Garnier-Laplace J. Radionuclide fact sheet: Tritium and the environment. Institut de radioprotection et de sûreté nucléaire, France, 2010.

Granger R, Hedstrom N. Modelling hourly rates of evaporation from small lakes. Hydrology and Earth System Sciences 2011; 15: 267-277.

Lucas LL, Unterweger MP. Comprehensive Review and Critical Evaluation of the Half-Life of Tritium. J Res Natl Inst Stand Technol 2000; 105: 541-549.

Michel RL, Jurgens BC, Young MB. Tritium deposition in precipitation in the United States, 1953–2012. US Geological Survey, 2018.

NASA. POWER Data Access Viewer. 2020. US National Aeronautics and Space Administration, 2020.

R Development Core Team. R: A Language and Environment for Statistical Computing. Vienna, Austria: R Foundation for Statistical Computing, http://www.R-project.org, 2020.

Slota PMA. Evaluation of operational lake evaporation methods in a Canadian Shield landscape. Department of Civil Engineering. Master of Science. University of Manitoba (Canada), Winnipeg, Manitoba, Canada, 2013, pp. 217.

Wickham H. Tidy Data. Journal of Statistical Software; Vol 1, Issue 10 (2014) 2014.

Wickham H, Averick M, Bryan J, Chang W, McGowan LDA, François R, et al. Welcome to the Tidyverse. Journal of Open Source Software 2019; 4: 1686.

Allen RG, Pereira LS, Raes D, Smith M. Crop evapotranspiration-Guidelines for computing crop water requirements-FAO Irrigation and drainage paper 56. Fao, Rome 1998; 300: D05109.

Calmon P, Garnier-Laplace J. Radionuclide fact sheet: Tritium and the environment. Institut de radioprotection et de sûreté nucléaire, France, 2010.

Granger R, Hedstrom N. Modelling hourly rates of evaporation from small lakes. Hydrology and Earth System Sciences 2011; 15: 267-277.

Lucas LL, Unterweger MP. Comprehensive Review and Critical Evaluation of the Half-Life of Tritium. J Res Natl Inst Stand Technol 2000; 105: 541-549.

Michel RL, Jurgens BC, Young MB. Tritium deposition in precipitation in the United States, 1953–2012. US Geological Survey, 2018.

NASA. POWER Data Access Viewer. 2020. US National Aeronautics and Space Administration, 2020.

R Development Core Team. R: A Language and Environment for Statistical Computing. Vienna, Austria: R Foundation for Statistical Computing, http://www.R-project.org, 2020.

Slota PMA. Evaluation of operational lake evaporation methods in a Canadian Shield landscape. Department of Civil Engineering. Master of Science. University of Manitoba (Canada), Winnipeg, Manitoba, Canada, 2013, pp. 217.

Wickham H. Tidy Data. Journal of Statistical Software; Vol 1, Issue 10 (2014) 2014.

Wickham H, Averick M, Bryan J, Chang W, McGowan LDA, François R, et al. Welcome to the Tidyverse. Journal of Open Source Software 2019; 4: 1686.

Allen RG, Pereira LS, Raes D, Smith M. Crop evapotranspiration-Guidelines for computing crop water requirements-FAO Irrigation and drainage paper 56. Fao, Rome 1998; 300: D05109.

Granger R, Hedstrom N. Modelling hourly rates of evaporation from small lakes. Hydrology and Earth System Sciences 2011; 15: 267-277.

Lucas LL, Unterweger MP. Comprehensive Review and Critical Evaluation of the Half-Life of Tritium. J Res Natl Inst Stand Technol 2000; 105: 541-549.

Michel RL, Jurgens BC, Young MB. Tritium deposition in precipitation in the United States, 1953–2012. US Geological Survey, 2018.

NASA. POWER Data Access Viewer. 2020. US National Aeronautics and Space Administration, 2020.

R Development Core Team. R: A Language and Environment for Statistical Computing. Vienna, Austria: R Foundation for Statistical Computing, http://www.R-project.org, 2020.

Slota PMA. Evaluation of operational lake evaporation methods in a Canadian Shield landscape. Department of Civil Engineering. Master of Science. University of Manitoba (Canada), Winnipeg, Manitoba, Canada, 2013, pp. 217.

Wickham H. Tidy Data. Journal of Statistical Software; Vol 1, Issue 10 (2014) 2014.

Wickham H, Averick M, Bryan J, Chang W, McGowan LDA, François R, et al. Welcome to the Tidyverse. Journal of Open Source Software 2019; 4: 1686.

Allen RG, Pereira LS, Raes D, Smith M. Crop evapotranspiration-Guidelines for computing crop water requirements-FAO Irrigation and drainage paper 56. Fao, Rome 1998; 300: D05109.

Granger R, Hedstrom N. Modelling hourly rates of evaporation from small lakes. Hydrology and Earth System Sciences 2011; 15: 267-277.

Michel RL, Jurgens BC, Young MB. Tritium deposition in precipitation in the United States, 1953–2012. US Geological Survey, 2018.

NASA. POWER Data Access Viewer. 2020. US National Aeronautics and Space Administration, 2020.

R Development Core Team. R: A Language and Environment for Statistical Computing. Vienna, Austria: R Foundation for Statistical Computing, http://www.R-project.org, 2020.

Slota PMA. Evaluation of operational lake evaporation methods in a Canadian Shield landscape. Department of Civil Engineering. Master of Science. University of Manitoba (Canada), Winnipeg, Manitoba, Canada, 2013, pp. 217.

Wickham H. Tidy Data. Journal of Statistical Software; Vol 1, Issue 10 (2014) 2014.

Wickham H, Averick M, Bryan J, Chang W, McGowan LDA, François R, et al. Welcome to the Tidyverse. Journal of Open Source Software 2019; 4: 1686.

Allen RG, Pereira LS, Raes D, Smith M. Crop evapotranspiration-Guidelines for computing crop water requirements-FAO Irrigation and drainage paper 56. Fao, Rome 1998; 300: D05109.

Granger R, Hedstrom N. Modelling hourly rates of evaporation from small lakes. Hydrology and Earth System Sciences 2011; 15: 267-277.

Michel RL, Jurgens BC, Young MB. Tritium deposition in precipitation in the United States, 1953–2012. US Geological Survey, 2018.

NASA. POWER Data Access Viewer. 2020. US National Aeronautics and Space Administration, 2020.

Slota PMA. Evaluation of operational lake evaporation methods in a Canadian Shield landscape. Department of Civil Engineering. Master of Science. University of Manitoba (Canada), Winnipeg, Manitoba, Canada, 2013, pp. 217.

Allen RG, Pereira LS, Raes D, Smith M. Crop evapotranspiration-Guidelines for computing crop water requirements-FAO Irrigation and drainage paper 56. Fao, Rome 1998; 300: D05109.

Granger R, Hedstrom N. Modelling hourly rates of evaporation from small lakes. Hydrology and Earth System Sciences 2011; 15: 267-277.

Michel RL, Jurgens BC, Young MB. Tritium deposition in precipitation in the United States, 1953–2012. US Geological Survey, 2018.

Slota PMA. Evaluation of operational lake evaporation methods in a Canadian Shield landscape. Department of Civil Engineering. Master of Science. University of Manitoba (Canada), Winnipeg, Manitoba, Canada, 2013, pp. 217.

Michel RL, Jurgens BC, Young MB. Tritium deposition in precipitation in the United States, 1953–2012. US Geological Survey, 2018.